

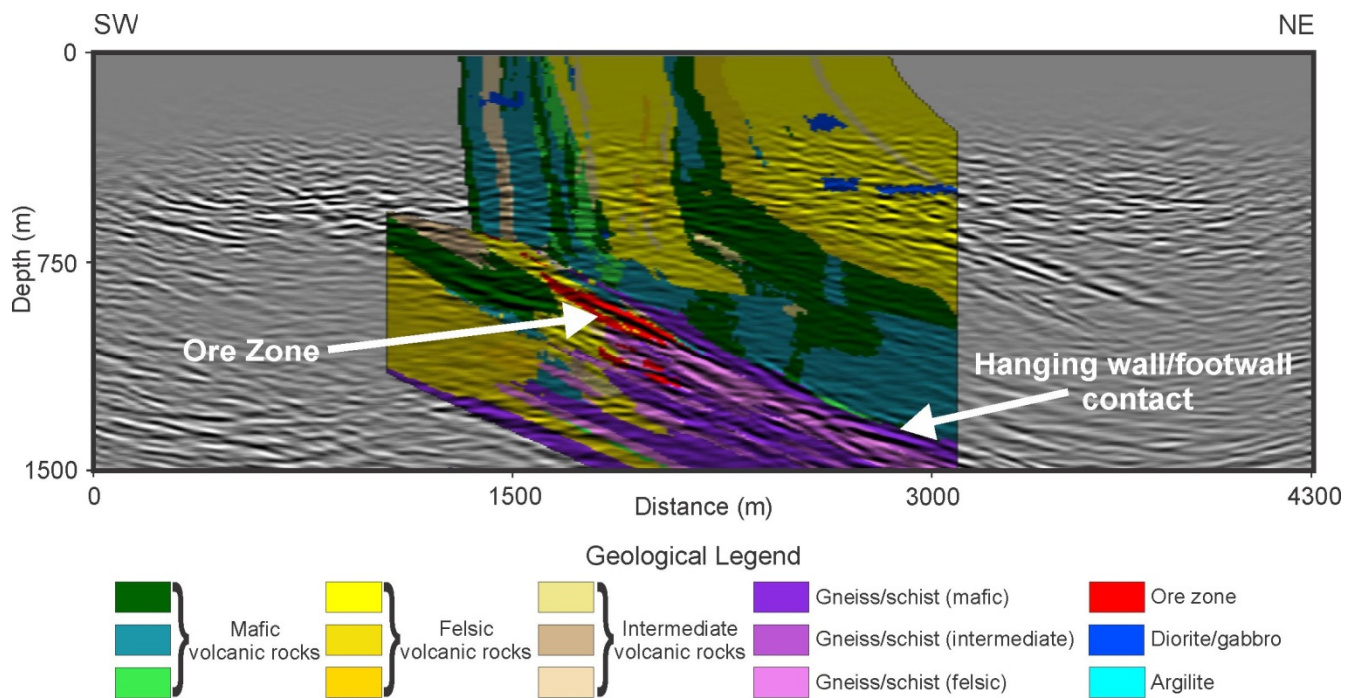


Natural Resources  
Canada

Ressources naturelles  
Canada

## GEOLOGICAL SURVEY OF CANADA OPEN FILE 7863

### Targeted Geoscience Initiative 4: A Synthesis of the Methodology Project at the Lalor VMS Deposit, Manitoba



G. Bellefleur, E. Schetselaar, and J.A. Craven (ed.)

2015

Canada



**GEOLOGICAL SURVEY OF CANADA  
OPEN FILE 7863**

**Targeted Geoscience Initiative 4: A Synthesis of the  
Methodology Project at the Lalor VMS Deposit, Manitoba**

**G. Bellefleur<sup>1</sup>, E. Schetselaar<sup>1</sup>, and J.A. Craven<sup>1</sup> (ed.)**

<sup>1</sup> Geological Survey of Canada, 615 Booth Street, Ottawa, Ontario

**2015**

© Her Majesty the Queen in Right of Canada, as represented by the Minister of Natural Resources Canada, 2015

doi:10.4095/296303

This publication is available for free download through GEOSCAN (<http://geoscan.nrcan.gc.ca/>).

**Recommended citation**

Bellefleur, G., Schetselaar, E., and Craven, J.A. (ed.), 2015. Targeted Geoscience Initiative 4: A Synthesis of the Methodology Project at the Lalor VMS Deposit, Manitoba; Geological Survey of Canada, Open File 7863, 50 p. doi:10.4095/296303

Publications in this series have not been edited; they are released as submitted by the author.

# TARGETED GEOSCIENCE INITIATIVE 4: A SYNTHESIS OF THE METHODOLOGY PROJECT AT THE LALOR VMS DEPOSIT, MANITOBA

*Edited by  
Gilles Bellefleur, Ernst Schetselaar, and Jim Craven*

<b>THE TGI-4 METHODOLOGY PROJECT AT LALOR: AN INTRODUCTION</b> GILLES BELLEFLEUR, ERNST SCHETSelaar, AND JIM CRAVEN .....	1
<b>GEOLOGICAL BACKGROUND</b> ERNST SCHETSelaar AND GILLES BELLEFLEUR.....	4
<b>3D GEOLOGICAL MODELLING</b> ERNST SCHETSelaar.....	10
<b>PHYSICAL ROCK PROPERTIES OF HOST ROCKS AND SULPHIDE MINERALIZATION AT LALOR</b> GILLES BELLEFLEUR AND ERNST SCHETSelaar .....	13
<b>ACQUISITION, PROCESSING AND INTERPRETATION OF THE LALOR 3C-3D SEISMIC DATA</b> GILLES BELLEFLEUR, ERNST SCHETSelaar, AND DON WHITE.....	16
<b>PASSIVE SEISMIC INTERFEROMETRY OVER THE LALOR LAKE AREA</b> SAEID CHERAGHI, JIM CRAVEN, AND GILLES BELLEFLEUR .....	23
<b>MODE-CONVERTED VMS ORE LENS REFLECTIONS IN VERTICAL SEISMIC PROFILES AND 3D FINITE DIFFERENCE MODELING FROM FLIN FLON, MANITOBA, CANADA</b> DAVE MELANSON, DON WHITE, CLAIRE SAMSON, GILLES BELLEFLEUR, ERNST SCHETSelaar, AND DOUG SCHMITT .....	27
<b>ACQUISITION, PROCESSING, AND INTERPRETATION OF GRAVITY DRILL HOLE DATA</b> ERNST SCHETSelaar AND PEJMAN SHAMSIPOUR .....	32
<b>3D STOCHASTIC INVERSION OF POTENTIAL FIELD DATA USING STRUCTURAL GEOLOGIC CONSTRAINTS</b> PEJMAN SHAMSIPOUR AND ERNST SCHETSelaar .....	38
<b>SUMMARY OF RESULTS AND IMPLICATIONS FOR EXPLORATION</b> GILLES BELLEFLEUR, ERNST SCHETSelaar, AND JIM CRAVEN .....	41
<b>ACKNOWLEDGMENTS</b> .....	43
<b>REFERENCES</b> .....	44

## TGI-4 METHODOLOGY PROJECT AT LALOR: AN INTRODUCTION

GILLES BELLEFLEUR<sup>1</sup>, ERNST SCHETSelaar<sup>1</sup>, AND JIM CRAVEN<sup>1</sup>

<sup>1</sup> Geological Survey of Canada, 615 Booth Street, Ottawa, Ontario, K1A 0E9

During the winters of 2013 and 2014, the Geological Survey of Canada conducted novel geophysical surveys over the Lalor volcanogenic massive sulphide (VMS) deposit located in Manitoba (Figure 1) to test and develop approaches leading to effective exploration of deep deposits. The geophysical data were acquired as part of the methodology project of the phase 4 of the Targeted Geoscience Initiative (TGI-4), a project that aimed to develop and improve methods for deep mineral exploration and provide a better understanding of ore systems. In addition to the acquisition and interpretation of geophysical data, a 3D common-earth model (i.e., a 3D geological grid model with inter-consistent lithofacies, litho-geochemistry, and physical rock properties) was constructed to gain a better understanding of data inter-dependencies and unravel geophysical responses caused by mineralization and hydrothermal alteration from responses produced by host rock contacts. The common-earth modelling approach greatly benefited from a rich catalog of existing geological, geochemical, and geophysical data including extensive drill-core and borehole logs available at Lalor. The 3D common-earth model provides excellent constraints on geophysical data interpretation near the deposit whereas geophysical data allows tracing the continuation of key contacts away from areas with borehole control.

The Lalor deposit was discovered in 2007 by Hudbay Minerals and is one of the largest base metal deposits (25 Mt) within the Flin Flon Greenstone Belt. The deposit was intact at the time of geophysical data acquisition and provided an ideal test bed to assess the response of the host rocks, zones of sulphide mineralization, and hydrothermal alteration. Aspects of the geology that pose a challenge to effective use of geophysical methods at Lalor include the presence of both massive and disseminated mineralized zones, their association with an extensive hydrothermal alteration system, and post-volcanic metamorphism that significantly modified the mineralogy of the alteration zones in some areas near the deposit. In addition to defining the response of the ore deposit, other important objectives of this study included the determination of the lateral continuity of the highly prospective hanging wall-footwall contact, the definition of the geometry of the footwall rocks and integration of the geophysical data with detailed three-dimensional geological information. Geophysical data acquired by the TGI-4 program to address those issues at Lalor include (Figure 1):

- 16 km<sup>2</sup> 3-component 3D seismic data.
- 3D passive seismic data.
- Borehole gravity measurements in five boreholes.
- Collocated geochemical and petrophysical measurements on 137 rock samples.

Borehole seismic data, although not acquired at Lalor, were also studied during this project using Vertical Seismic Profiling (VSP) data previously acquired near the Flin Flon 777 mine. Results from the VSP data were also analyzed in a 3D common-earth model framework established during an earlier phase of the Targeted Geoscience Initiative. Each geophysical method above is evaluated as a stand-alone technology and as an element in an integrated workflow. All geophysical data (3D active-source seismic, 2D and 3D passive seismic, borehole gravity and petrophysical measurements on core samples) were acquired by the TGI-4 Methodology project. Other geological information including geological logs and geochemical analysis, and most of the petrophysical data were provided to the TGI-4 methodology project by Hudbay.

This Open File summarizes the results of eight papers published or in the process of being published in peer-reviewed journals and written as part of the TGI-4 methodology project. The intent here is not to reproduce the papers, but rather synthesize the key results and their impacts for exploration. Topics include 3D common-earth modelling of geological, geochemical and petrophysical data; analysis of physical rock properties; acquisition, processing and interpretation of active-source, passive seismic data, and borehole gravity data and a new method for the constrained inversion of potential field data using gradient constraints from strike-dip measurements and 3D seismic data. Readers can find further details for each topic in the original papers listed below (name in bold indicates member of the TGI-4 methodology project). The list also comprises technical papers describing methods that were critical to obtain results at various stage of the project, but that are not exhaustively discussed in this Open File:

**Bellefleur, G., Schetselaar, E., White, D., Miah, K.,** and Dueck, P., 3D seismic imaging of the Lalor volcanogenic deposit, Manitoba, Canada. *Geophysical Prospecting* (in press).

**Cheraghi, S., Craven, J., and Bellefleur, G.,** Feasibility of seismic interferometry method in mineral exploration: A test study in Lalor Lake VMS mining area, Manitoba, Canada. *Geophysical Prospecting* (in press).

Górszczyk, A., Malinowski, M., and **Bellefleur, G.,** Application of 2D curvelet transform for denoising 3D seismic data acquired in hardrock environment. *Geophysical Prospecting* (in press).

**Hillier, M.J., Schetselaar, E.M., de Kemp, E.A.,** Perron, G. 2014. Three-Dimensional Modelling of Geological Surfaces Using Generalized Interpolation with Radial Basis Functions. *Mathematical Geosciences*, 46 (8), pp. 955-956.

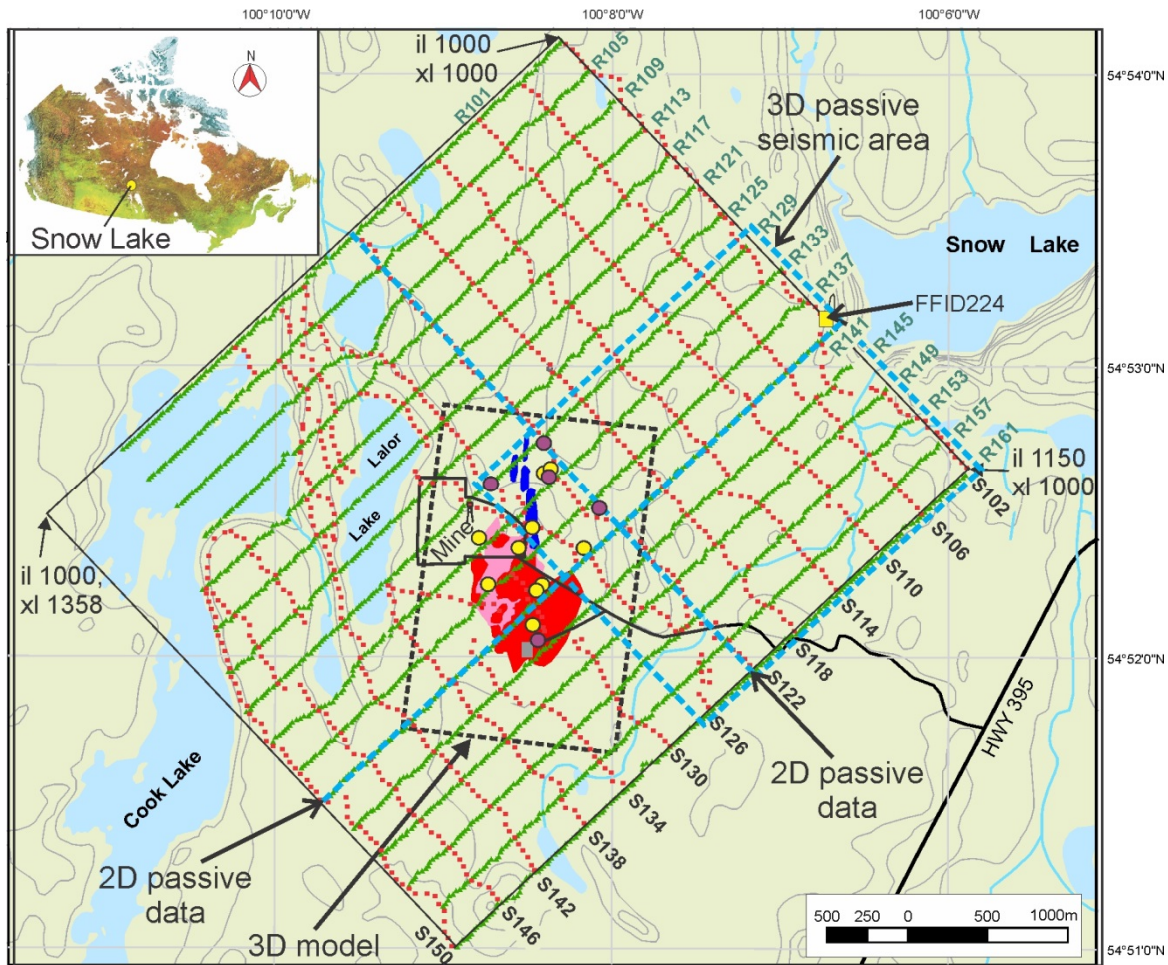


**Figure 1.** Location map of the 3D-3C Lalor active-source seismic survey. Receiver locations are shown as green triangles whereas shot points are shown as red dots. The mine site area and main road are shown in black (polygon for the mine site). The surface projection of the zinc, gold, and gold-copper zones are shown in red, pink, and blue, respectively. The outline of the 3D geological model used for the interpretation of the data is also shown (rectangle with dashed black line). Polygon with blue dashed line indicates the survey area for the 3D passive seismic experiment. Dashed lines in blue correspond to 2D passive seismic profiles. The yellow dots are the collar locations of drillholes with both geochemistry and wireline logging data used in the physical rock property analysis. Dots in purple indicate boreholes used for the downhole gravity measurements. Inlines (il) and crosslines (xl) for the final 3D seismic volume are indicated. FFID 224 is the location of a shot gather shown in Figure 9.

Marcotte, D., **Shamsipour, P.**, Coutant, O., Chouteau, M. 2014  
 Inversion of potential fields on nodes for large grids (2014)  
 Journal of Applied Geophysics, 110, pp. 90-97.

**Melanson, D.M., White, D.J., Samson, C., Bellefleur, G., Schetselaar, E.,** and Schmitt, D.R., Mode-converted VMS ore lens reflections in vertical seismic profiles from Flin Flon, Manitoba, Canada. Geophysical Prospecting (in press).

**Schetselaar, E. and Shamsipour, P.**, Interpretation of Borehole Gravity Data of the Lalor Volcanogenic Massive Sulphide deposit, Snow Lake, Manitoba, Canada, Interpretation (submitted to Interpretation).

**Shamsipour, P., Schetselaar, E., Bellefleur, G.,** and Marcotte, D., 2014. 3D stochastic inversion of potential field data using structural geologic constraints. Journal of Applied Geophysics, 111, 173-182.

In this Open File, we first briefly review the geology of the deposit and provide some details on the methodology used to construct the 3D common-earth model of the Lalor deposit and how this model was used to guide and support the interpretation of the geophysical data. Then, we review the physical rock properties of host rocks and ore zones and present the acquisition, processing and interpretation of both the active-source 3D seismic data and passive seismic data. We also show a comprehensive analysis of the VSP data acquired near the Flin Flon 777 VMS deposit. We then present progress made in potential field methodology by discussing the acquisition parameters, processing and interpretation of the borehole gravity survey conducted in five boreholes surrounding the Lalor deposit. An innovative inversion method taking advantage of constraints from seismic or geological data in boreholes is introduced. Finally, we summarize the key results of this project and highlight their significance for exploration of deep-seated

deposit. Although this study is site- and commodity-specific, the common-earth modelling approach and the various methods developed herein are recommended to be adopted for exploration elsewhere and are easily adaptable to other deposit types.

## GEOLOGICAL BACKGROUND

ERNST SCHETSelaar<sup>1</sup> AND GILLES BELLEFLEUR<sup>1</sup>

<sup>1</sup> Geological Survey of Canada, 615 Booth Street, Ottawa, Ontario, K1A 0E9

### INTRODUCTION

The Lalor volcanogenic massive sulphide deposit is located near Snow Lake, Manitoba, about 700 km north of Winnipeg and lies within the Snow Lake arc assemblage of the Paleoproterozoic Flin Flon Greenstone Belt in the juvenile part of the Trans-Hudson orogen (Figure 2 inset). The Flin Flon Greenstone Belt is composed of an accretionary collage of 1.92-1.88 Ga arc, back-arc and ocean floor assemblages, 1.87-1.84 Ga successor arc plutonic suites and 1.85-1.83 Ga clastic sedimentary sequences that amalgamated to form distinct tectonostratigraphic assemblages during ocean closure and collision with the Archean Hearne, Sask and Superior cratons between ca. 1.92 Ga and 1.80 Ga (Corrigan et al., 2009 and references therein, Figure 2).

metamorphosed at lower to middle almandine-amphibolite facies seventy-five million years after the formation of the volcanic arc assemblage (David *et al.*, 1996; Bailes and Galley, 1999). The Lalor area also comprises extensive synvolcanic to successor-arc felsic and mafic intrusive rocks (Figure 3).

The Chisel sequence has been subdivided into the Lower and Upper subsequences (Bailes and Galley, 2007, Figure 4) forming respectively the footwall and hanging wall of a structural contact 10-200 m above the sulphide ore lenses of Zn-rich VMS deposits (Chisel, Chisel North, Ghost, Lost and Lalor, Figures 3 and 5.). This contact has been tentatively interpreted as a thrust fault on the basis of contrasting litho-geochemical trace element signatures of its hanging wall and footwall sequences, an abrupt change in

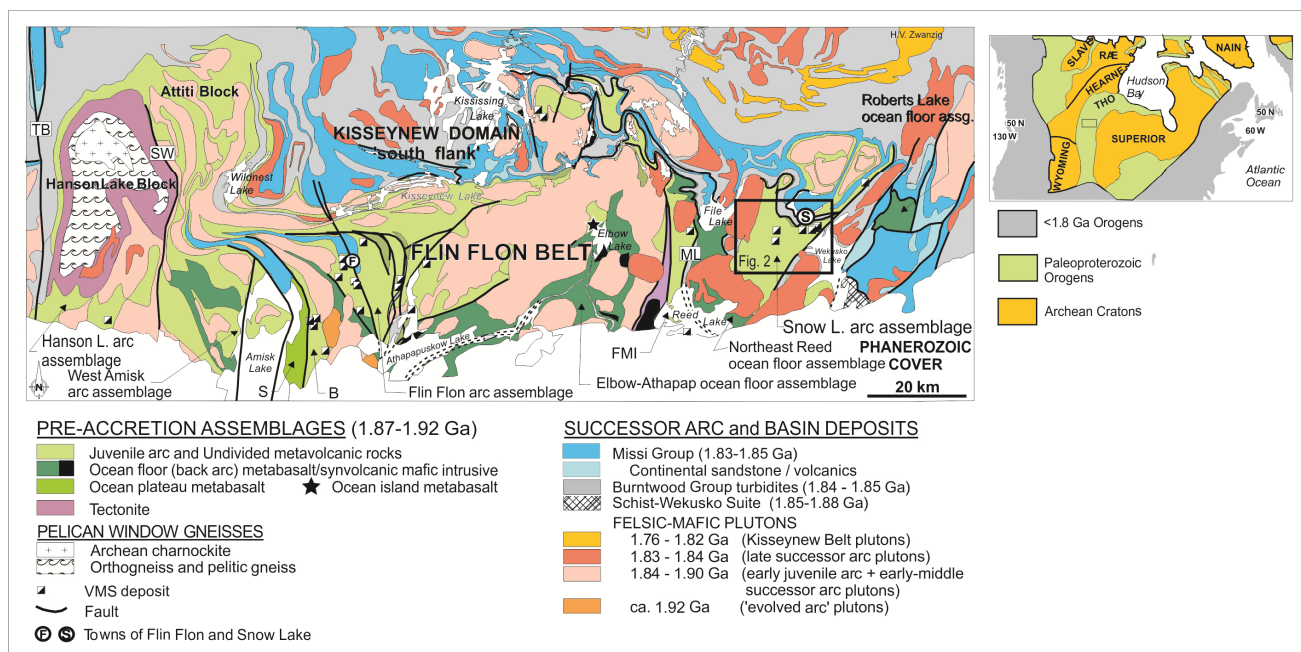
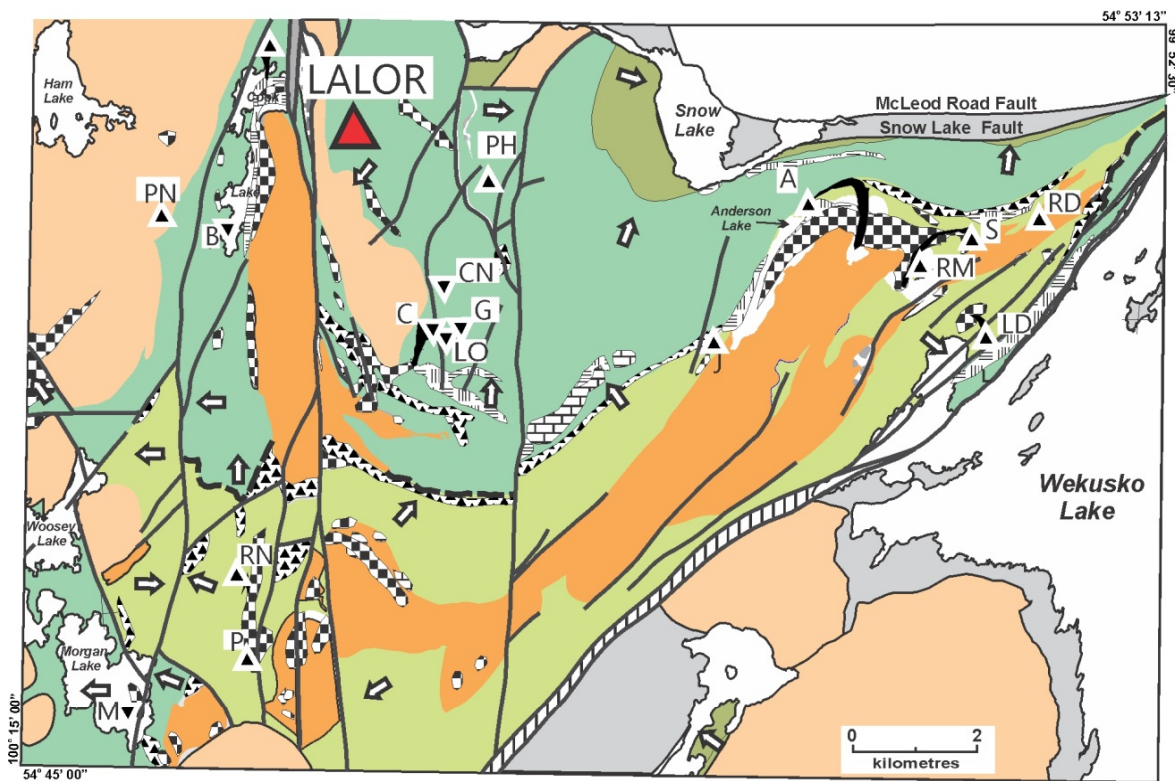


**Figure 2.** Tectonic assemblage map of the Flin Flon Belt (after Galley et al., 2007 and references therein), illustrating the tectonostratigraphic assemblages, the location of the various accretionary assemblages, and major mineral deposits. B=Birch Lake assemblage; FMI=Fourmile Island assemblage; ML=Morton Lake fault zone; S=Sandy Bay assemblage; TB=Tabernor fault zone. Rectangle outlines portion of the Snow Lake arc assemblage shown in Figure 3.

The 1.89 Ga Snow Lake arc assemblage, located in the eastern part of the Flin Flon greenstone belt (Figure 2) is a 20 km wide and 6 km thick stratigraphic section that comprises three volcanic successions (Bailes and Galley, 1999) displaying a geodynamic evolution from a primitive arc (Anderson sequence to the South) to a mature arc (Chisel sequence) to an arc-rift (Snow Creek sequence to the Northeast) setting. The three successions of the Snow Lake assemblage are dominated by fold-thrust style tectonics (Kraus and Williams, 2000) and were

dip and opposing facing directions (Bailes et al., 2013), although elsewhere (in outcrops near the Chisel Lake and Ghost Lake VMS deposits) it is considered to be conformable (Engelbert, 2014a). Detailed chemostratigraphic observations of the Chisel sequence at the Lalor deposit, confirms the contrasting litho-geochemical signatures of the volcanic and volcanoclastic rocks below and above the Chisel-Lalor contact with calc-alkaline affinities in the Lower Chisel subsequence and transitional to tholeiitic magmatic affinities in the Upper Chisel subsequence (Caté et al. 2014a).

GEOLOGICAL BACKGROUND



**ALTERED ROCKS (METAMORPHOSED AT 1.82-1.81 GA)**

-  Alteration pipes and completely altered rocks
-  Chlorite+garnet+biotite-rich rocks ± staurolite ± actinolite
-  Amphibole-rich rocks ± garnet
-  Epidote-rich rocks
-  Quartz+plagioclase-rich rocks ± epidote ± actinolite (derived from a mafic protolith)

**> 1.88 GA SYNVOLCANIC INTRUSIVE ROCKS**



▲ ▼ Massive sulphide deposit (Cu-Zn, Zn-Pb-Cu)

**> 1.88 GA SUPRACRUSTAL ROCKS**

-  Arc rift supracrustal rocks (Snow Creek Sequence)
-  Mature arc supracrusta rocks (Chisel Sequence)
-  Primitive arc supracrustal rocks (Anderson Sequence)

**ROCKS POSTDATING ALTERATION**

-  < 1.84-1.83 Intrusive rocks
-  1.85-1.84 Ga Burntwood Group greywacke

**SYMBOLS**

-  Facing direction of strata
-  Berry Creek Fault Zone
-  Fault (early kinematic, late kinematic)

**Figure 3.** Generalized geological map of the Snow Lake arc assemblage, including large-scale metamorphosed hydrothermal alteration zones, and volcanogenic massive sulphide deposits and major occurrences. A=Anderson; B=Bomber zone; C=Chisel Lake; CN=Chisel North; G=Ghost; J=Joannie zone; LA=Lalor; LO=Lost; LD=Linda zone; M=Morgan Lake zone; P=Pot Lake zone; PH=Photo Lake; PN=Pen zone; RD=Rod; RM=Ram Zone; RN=Raindrop zone; S=Stall Lake. Modified from Bailes and Galley (1999).

GEOLOGICAL BACKGROUND

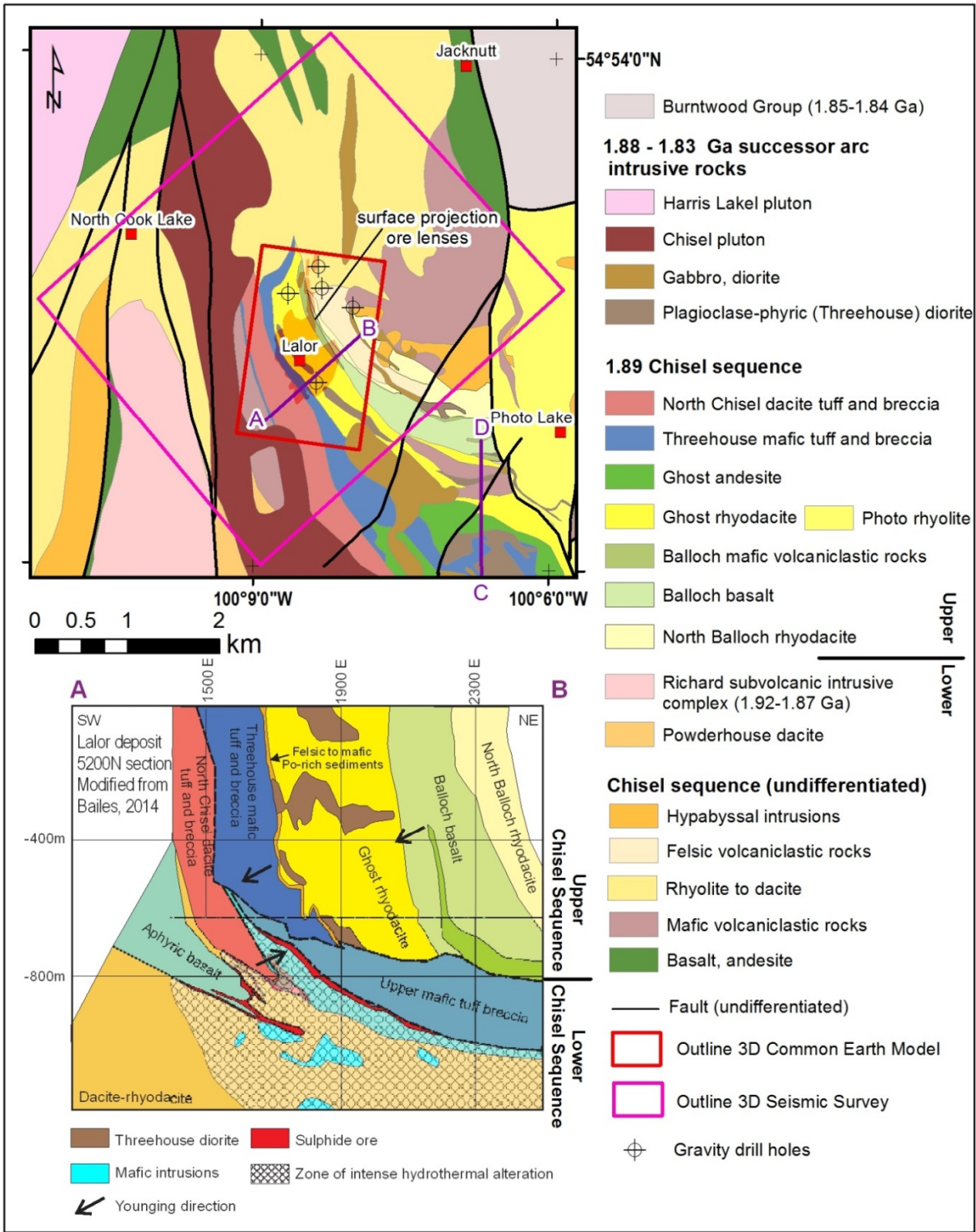


**Figure 4.** Geological map of the Lalor deposit with outlines of the 3D seismic survey and 3D Common Earth Model and SW-NE oriented cross section of the Lalor deposit (after Bailes, 2014). Interpreted structural contacts (thicker black lines) are compiled after Bailes (2014a) Caté et al. (2014b) and Engelbert et al. (2014b). Line C-D refers to cross section after Bailes, 2012 shown in Figure 6.

**Table 1.** Chemical associations, corresponding metamorphic mineral assemblages and settings of the Lalor hydrothermal alteration system from Caté *et al.* (2013).

<b>Geochemical association</b>	<b>Dominant metamorphic minerals</b>	<b>Occurrence / setting</b>
K	Muscovite, biotite, kyanite, sillimanite, quartz	Footwall of base metal-rich upper massive sulphide ore lenses
K-Fe-Mg	Biotite, kyanite, sillimanite, staurolite ± garnet, pyrite, quartz	Footwall hydrothermal alteration zone
Mg-Fe	Mg-Fe amphiboles, chlorite, cordierite, garnet, staurolite, quartz ± talc	Footwall hydrothermal alteration zone
Mg-Ca	Mg-chlorite, Ca-amphiboles, carbonates, Ca-plagioclase, biotite, quartz and talc	Heterogeneously distributed in proximal footwall of Lalor ore lenses
Ca	Ca-amphiboles, epidote, grossular	Footwall, hanging wall, Upper Chisel sequence; overprints other alteration assemblages

A large subconcordant hydrothermal alteration system developed in the footwall of the Zn-rich VMS deposit closely associated in space and time to the magmatic evolution of the Richards subvolcanic intrusion (Bailes, 2014b, Figure 4). Disconformable alteration zones that can be traced up section to the Chisel, Chisel North and the Lalor deposits are rooted within it (Bailes, 2014b). The footwall hydrothermal alteration in the Lower Chisel subsequence evolved in two stages. The first produced semi-conformable zone of albitization, silicification and epidotization 1-2 km below the deposit that is spatially associated with synvolcanic dykes and intrusions (Bailes *et al.*, 2013). The second produced sub-concordant zones of intense hydrothermal alteration in the immediate footwall of the massive sulphide deposits (Bailes *et al.*, 2013) that after metamorphism to the amphibolite facies (Gagné *et al.* 2011) transformed volcanic and volcanoclastic rocks of mafic to felsic composition into schist and gneiss rich in large aluminosilicate porphyroblasts of garnet, staurolite, cordierite, kyanite and anthophyllite (Caté *et al.* 2013; 2015). Alteration in close proximity to the sulphide ore zones at Lalor also includes pervasive zones of finely disseminated sulphides (pyrite, pyrrhotite, sphalerite, chalcopyrite, and galena) associated with carbonate, tremolite, talc and chlorite-rich rocks (Bailes *et al.*, 2013; Caté *et al.*, 2013). Five distinct chemical associations, each corresponding to distinct metamorphic mineral assemblages can be distinguished in the hydrothermal alteration system of the Lalor deposit, reflecting lithogeochemical variations of the protoliths hydrothermal alteration and metasomatism

during subsequent metamorphic crystallization (Table 1; Caté *et al.*, 2013; 2015; Mercier-Langevin *et al.*, 2014).

The hosting rock units and the ore lenses of the Lalor deposit were affected by polyphase ductile deformation. The main foliation is a  $S_2$  penetrative mineral shape to gneissic fabric with local evidence of transposition of  $F_1$  isoclinal folds (Bailes *et al.*, 2013; Caté *et al.* 2014; Engelbert *et al.*, 2014).  $F_2$  folds are also isoclinal, verge towards South and involve the upper massive sulphide ore lenses. The  $F_2$  folds were refolded by open N-NE upright  $F_3$  folds locally resulting in Type 1 (Ramsay, 1967) fold interference patterns (Caté *et al.* 2014b). The limbs of these fold structures are locally attenuated by shear zones often displaying boudinage of competent rock units and quartz-carbonate veins with both normal and thrust sense of displacement. The upper massive sulphide ore and sub-concordant zone of intensely hydrothermally-altered rocks and massive sulphide ore (lens 10) were brought up in a southwestward direction against a succession of relatively weakly altered volcanic and volcanoclastic rocks (Bailes *et al.* 2013; Caté *et al.* 2013, Figure 2). This moderately steeply NE-dipping structure is subparallel to  $S_2$  and interpreted as a high-strain transposition zone (Caté *et al.* 2014b) that accommodated ductile shear and possibly attenuated earlier  $F_2$  S-verging isoclinal fold structures involving thin ore lenses with which it appears to be aligned deeper down the footwall.

# Lalor Development

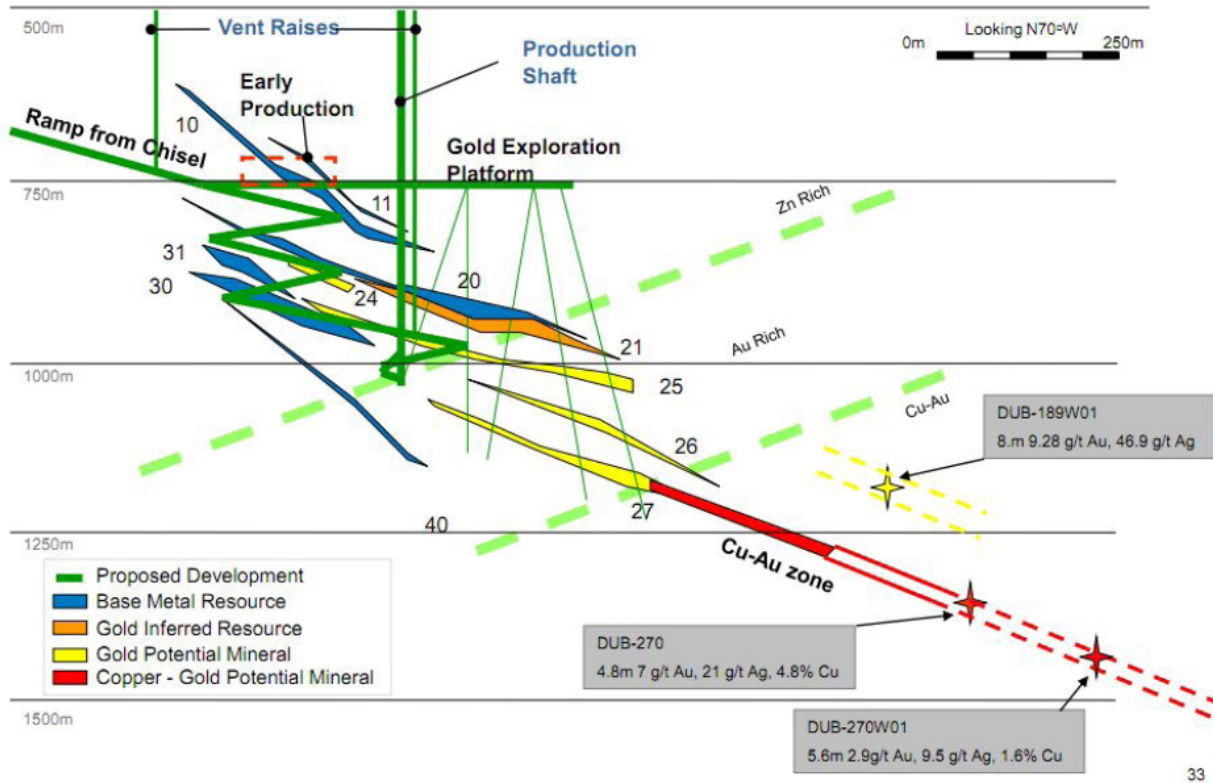


**Figure 5.** Vertical section of the Lalor deposit from HudBay internal reports showing Zn-rich, Au-rich and Cu-Au rich mineralized zones.

The tectonic setting of the Lalor deposit, including the nature of the Chisel-Lalor contact has, up to date, not been fully resolved. The abrupt transition from steeply NE-dipping units in its hanging wall to shallowly N-NE dipping units in its footwall in combination with opposing facing directions at Lalor (Bailes *et al.*, 2013, Figure 2) strongly suggest that the Chisel-Lalor break is a tectonic contact. Moreover, a sharp contact between rhyodacite of the Upper Chisel subsequence and mafic volcanoclastic rocks of the Lower Chisel subsequence overprinted by  $S_2$  has been observed in drill core (Caté *et al.* 2014b) that further corroborates this interpretation and suggests fault activity during early stages of deformation. The Chisel-Lalor contact cannot be traced further west of the previously-described NE-dipping fault that juxtaposes intensely-altered rocks (Lalor volcanic succession: Caté *et al.*, 2014) against unaltered to weakly-altered volcanic rocks (western volcanic succession: Caté *et al.*, 2014). Instead, weakly altered intermediate volcanic and volcanoclastic rocks can be correlated to the North Chisel dacite tuff and breccia exposed at surface on their similar trace element geochemical signatures (Bailes, 2014a). A ductile shear zone defining the contact between the Chisel dacite tuff and Threehouse mafic volcanoclastic unit observed in outcrop

(Engelbert *et al.* 2014b) has been linked to shear zone fabrics in mafic volcanic clastic rocks above the upper massive sulphide ore zone in the subsurface (Engelbert *et al.*, 2014b, Figure 2). This inferred structure would provide a feasible explanation for the truncation of the Chisel-Lalor contact at depth and be consistent in orientation and kinematics with the NE dipping fault that locally defines the footwall of the intensely hydrothermally-altered rocks a greater depth.

The Lalor deposit consists of 12 mineralized zones starting at a vertical depth of 570 m and extending down to approximately 1160 m. As of January 2014, the Lalor deposit has a proven and probable reserve estimate of 15 Mt grading 6.7% Zn, 0.63% Cu, 2.01 g/t Au and 23 g/t Ag, and inferred resource estimate of 10 Mt with 2.5% Zn, 1.03% Cu, 4.23 g/t Au and 28 g/t Ag. The mineralization zones trend to the northwest and have dips between 10° and 30° to the NNE. They are generally thin (average thickness is less than 12 m) and vary in size and grade. The deposit comprises six zinc-rich and six gold-rich zones (Carter *et al.*, 2012; Duff *et al.*, 2015, Figure 5). The zinc-rich zones (zones 10, 11, 20, 30, 31, and 40; see Figure 6 for location) account for approximately 15 Mt of the 25 Mt of the

**GEOLOGICAL BACKGROUND**

deposit. The zinc-rich zones are the largest and also shallowest of the deposit and generally comprise near-massive to massive sulphide mineralization. Sulphides in the zinc-rich zones dominantly consist of pyrite crystals and sphalerite interstitial to the pyrite. The deposit also includes six gold-rich zones (zones 21, 24, 25, 26, 27, and 28) generally found below the zinc zones in the footwall rocks. However, some of the gold zones (zones 21, 25, and 26) overlap and cut through the zinc zones (Carter *et al.*, 2102; Caté *et al.*, 2015, Duff *et al.*, 2015). The gold zones (including 8.8 Mt at 4.6 g/t Au: Caté *et al.*, 2015; Duff *et al.*, 2015) tend to be disseminated with some stringers of sulphide mineralization. These zones contain a low amount of iron sulphide, typically less than 4-5%. One of the gold zones (zone 27) is also associated with higher copper grades (average grade of 4.64% Cu for this zone) and is referred to as the gold-copper zone. The continuation of the gold-copper mineralization found in the deeper part of deposit remains an active and open exploration target at greater depths.

across its faulted parts and (ii) the observation that the contact is conformable elsewhere (Engelbert 2014a). Although more work is required to fully unravel its tectonic significance, a possible explanation is that the Upper and Lower Chisel volcanic sequences were initially juxtaposed along early (pre-D<sub>1</sub>) brittle extensional faults that were cut and partly reactivated by ductile thrust faults (post-D<sub>1</sub>) during a later stage of the deformation history. This tentatively-inferred inversion is not only consistent with the lack of structural repeats and overall upward younging direction of the volcanic sequences of the Snow Lake assemblage, but also with diachronous excision of Upper Chisel units along the Chisel-Lalor contact with progressive widening of a stratigraphic gap towards the S-SW that is depicted on a regional NS-oriented cross section (Bailes *et al.* 2013, Figure 6) as well as the local cross section of the Lalor deposit (Figure 4). The conformable stratigraphic contacts between the Upper and Lower Chisel subsequences would in this model be preserved where normal faults cut down the section to lower stratigraphic levels (not shown on

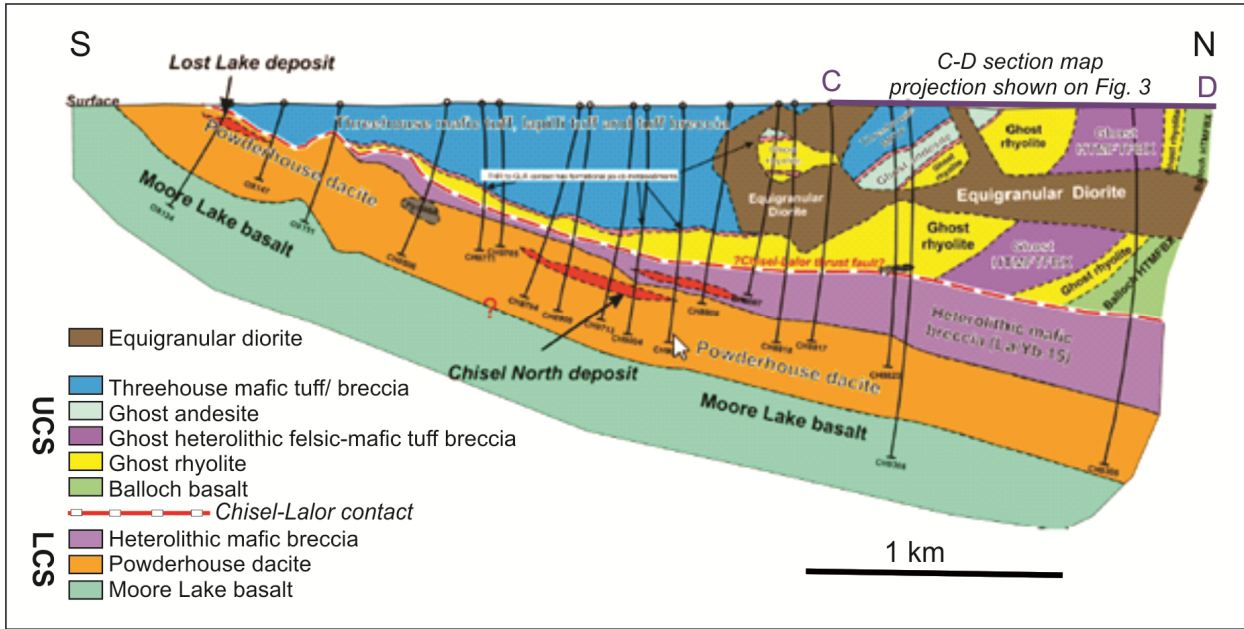


**Figure 6.** NS-oriented cross section after Bailes, 2012 (see for location segment C-D, Figure 4). Note how the spatial relationship between the hanging wall and footwall of the Chisel-Lalor contact is consistent with an interpretation of extensional faulting in which Upper Chisel Sequence units have been excised along the Chisel-Lalor contact with progressive widening of a stratigraphic gap towards the south. A similar relationship is evident on the NE-SW-oriented cross section of the Lalor deposit (Figure 4).

**THE CHISEL-LALOR CONTACT**

The interpretation of the nature and regional significance of the Chisel-Lalor contact has important implications for understanding the distribution and structural setting of the Zn-rich VMS mineralization hosted in the Chisel sequence, including the Lalor deposit. Although its origin is still subject to debate (Bailes, 2014b; Cate *et al.* 2014b; Engelbert *et al.* 2014b), one of the preferred interpretations has considered the contact to be a shallow N-dipping thrust fault (Bailes *et al.*, 2013). This interpretation is, however, inconsistent with: (i) the lack of repeated volcanic units

Figure 4 and Figure 6) although to date no such faulting relationships have been established.

### 3D GEOLOGICAL MODELLING

ERNST SCHETSelaar<sup>1</sup>

<sup>1</sup> Geological Survey of Canada, 615 Booth Street, Ottawa, Ontario, K1A 0E9

Over 220 exploration and delineation boreholes totaling 195 linear km were used to build a detailed 3D geological model of the Lalor deposit that guided the interpretation of the 3D seismic data (Figure 9). Recent in-mine drill holes that focused on the ore zones were also used as 3D modeling constraints. The model covers an area of 2050 m by 1330 m around the drill-delineated ore lenses and extends down to a depth of 1500 m (see Figure 1 for outline of the 3D model). The various steps of the work flow for creating the 3D geological model are shown in Figure 7.

First, 3D geological surfaces, representing the contacts between the main lithostratigraphic units, were built (1 in Figure 7). These surfaces define the contacts between the hanging wall and footwall lithostratigraphic units of the Lalor deposit. Constraints used for modelling them included: (i) lithostratigraphic unit contacts extracted from the 1:20 000 scale geological map (Bailes and Galley, 2007) (ii) lithostratigraphic markers defined in a selected set of 17

reference drill holes (Bailes, unpublished report, 2013b) (iii) lithofacies intervals encoded from the detailed log descriptions of all the drill holes and (iv) bedding orientations restored from drill core angles between the drill core axis and intersected bedding (Figure 7). The sulphide ore lenses provided additional ‘soft’ constraints for validating and refining the footwall-hanging wall contact and the Chisel-Lalor structural break.

Second, a curvilinear grid model was built from the 3D geological surfaces using the structural knowledge-unified approach SKUA<sup>®</sup> (Mallet, 2004; 2 in Figure 7). This approach benefits from using a coordinate transformation (the UVT transform) that enables to condition stochastic grid modelling of categorical and continuous properties by the geometry of the host rock geological structure (Figure 8; Schetselaar, 2013). The 3D-modelled geological surfaces provided a complete partitioning of the volume of interest, yielding a total of 7 lithostratigraphic units (Figure 7).

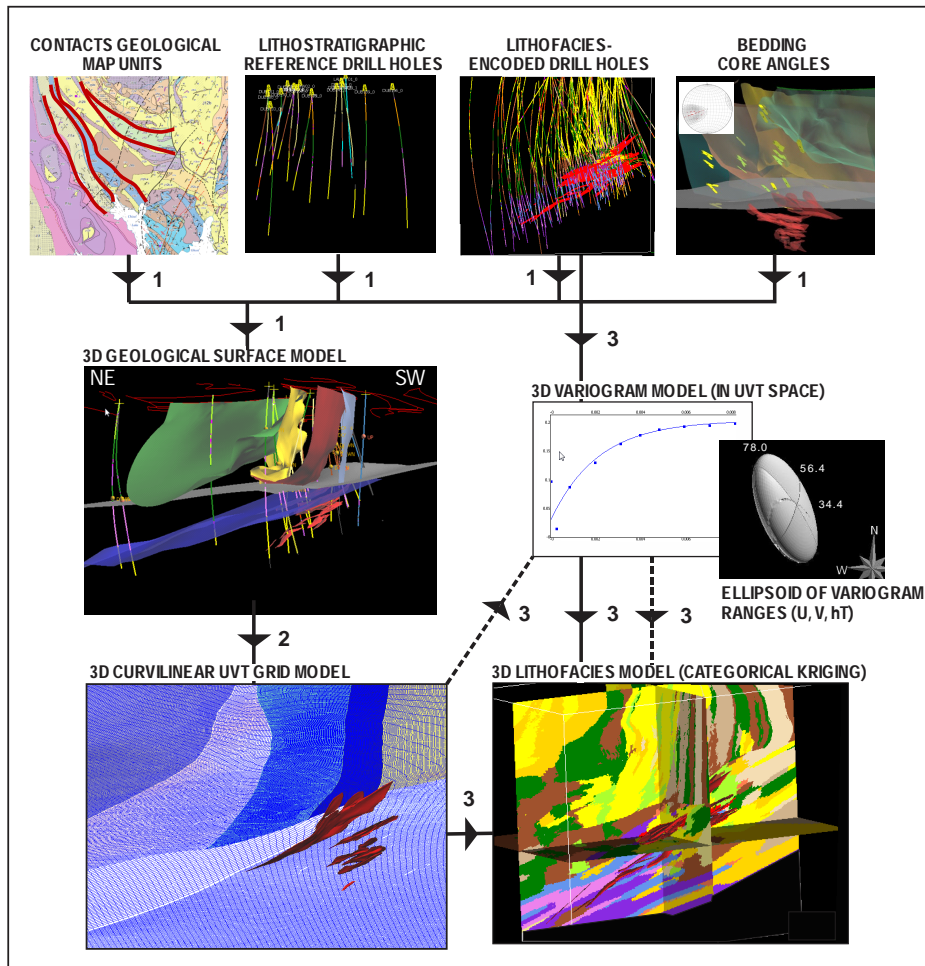


**Figure 7.** Work flow for building a 3D geologic surface and lithofacies grid model of the Lalor deposit. Numbers refer to the various processing steps discussed in the text.

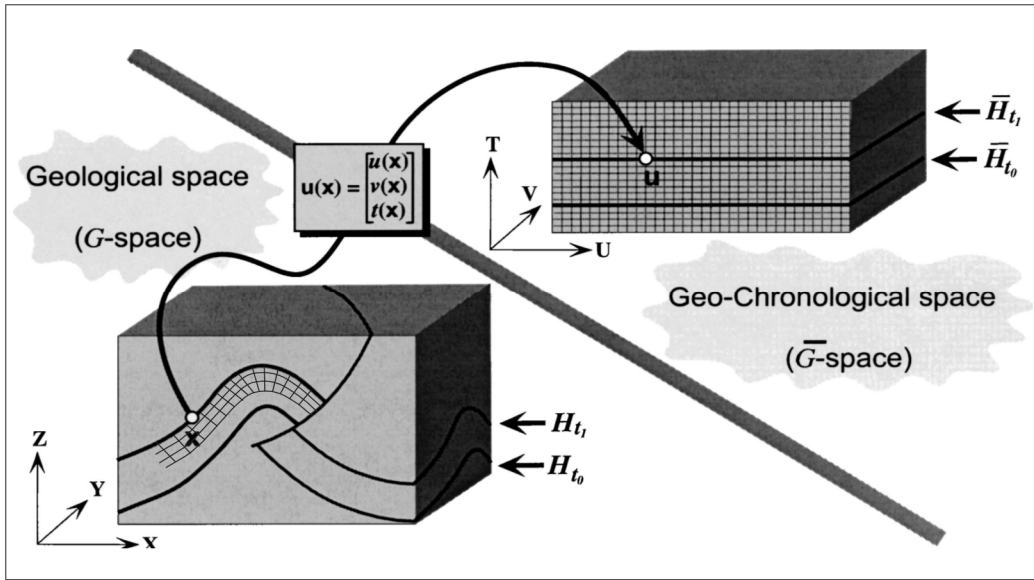


**Figure 8.** Transformation between Geological and Geochronological spaces to facilitate numerical grid modelling in complex geological settings (after Mallet, 2004). The faulted-curvilinear grid in Geological space becomes a Cartesian grid in geochronological space after applying the UVT transform, in which UV represent paleogeographic coordinates parallel to stratification and T represents geologic time normal to stratification. Since points of equal geologic time are by definition on a horizontal plane, the UVT transform ‘flattens’ out fold and fault structures, which facilitates stochastic modelling of continuous and categorical properties. The modelled-properties are mapped back on the curvilinear grid in geological space using the inverse UVT transform (Mallet, 2004).

Because the lithostratigraphic units could not be correlated across the Chisel-Lalor break, this contact was considered an angular unconformity in the topological encoding of the modelling work flow. This provided the best solution for honouring the distinct lithostratigraphic sequences in the footwall and hanging wall of the deposit, even though this contact is most likely of tectonic origin (Bailes *et al.*, 2013).

Third, class labels from a total of 15 lithofacies classes was mapped on the cells of the curvilinear grid by applying categorical kriging on a point set sampled at a spacing of 2 m along the lithofacies-encoded drill hole intervals (3 in Figure 7). This 15-fold lithofacies classification was based on the immobile Zr/TiO<sub>2</sub> immobile element ratio computed from drill hole lithochemochemistry, subdividing the samples into lithofacies of mafic, intermediate or felsic composition.

**Table 2.** Lithofacies classification for 3D modelling of the Lalor deposit based on Zr/TiO<sub>2</sub> immobile element ratio and textural and fabric observables in drill core.

Main lithofacies group	Zr/TiO <sub>2</sub>	Nr	CODE	Description
COHERENT VOLCANIC ROCKS	<=0.013	1	MAFVR	mafic volcanic rocks (basalt, andesite)
	> 0.013 & < 0.019	2	INTVR	intermediate volcanic rocks (dacite)
	>= 0.019	3	FELVR	felsic volcanic. rocks (rhyolite, rhyodacite)
COARSE-GRAINED VOLCANICLASTIC ROCKS (FRAGMENTALS)	<=0.013	4	VCLCM	mafic coarse-gr volcanicl. rocks (fragmentals)
	> 0.013 & < 0.019	5	VCLCI	interm. coarse-gr volcanicl. rocks (fragmentals)
	>= 0.019	6	VCLCF	felsic coarse-gr volcanicl. rocks (fragmentals)
FINE-GRAINED VOLCANICLASTIC ROCKS (LAPILLI TUFF / TUFF)	<=0.013	7	VCLFM	mafic fine-gr volcanicl. rocks (tuff/lapilli tuff)
	> 0.013 & < 0.019	8	VCLFI	interm. fine-gr volcanicl. rocks (tuff/lapilli tuff)
	>= 0.019	9	VCLFF	felsic. fine-gr volcanicl. rocks (tuff/lapilli tuff)
GNEISS /SCHIST (UNRECOGNIZABLE PROTOLITHS)	<= 0.013	10	GNSCHM	gneiss/schist mafic protolith
	> 0.013 & < 0.019	11	GNSCHI	gneiss/schist mafic protolith
	>= 0.019	12	GNSCHF	gneiss/schist mafic protolith
REMAINING LITHOFACIES CLASSES		13	ORE	sulphide ore
		14	ARG	Argillite
		15	DIO	feldspar-phyric diorite/gabbro

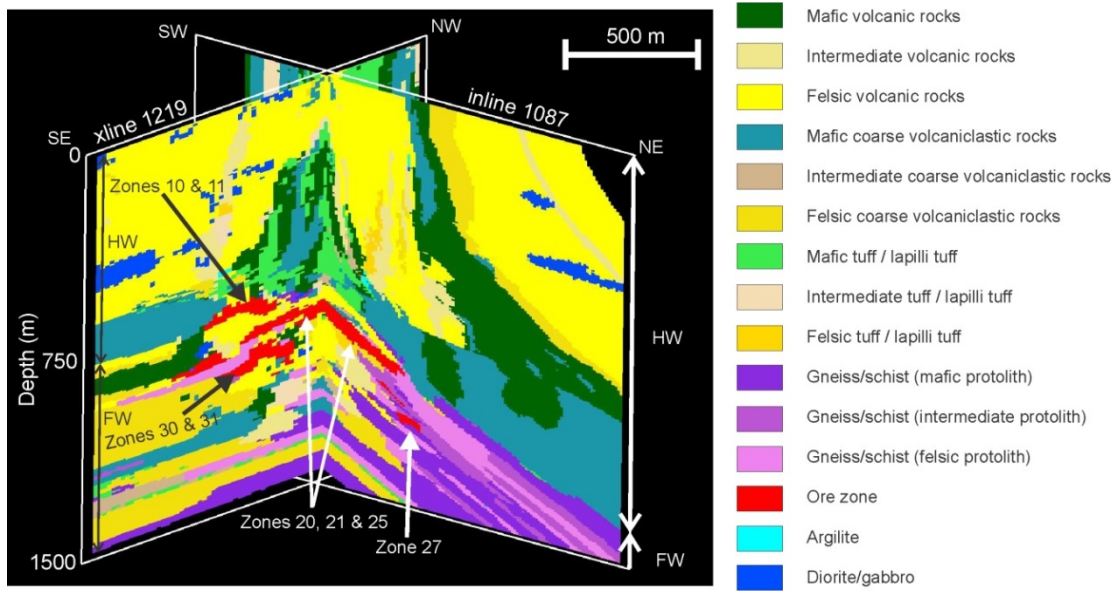


**Figure 9.** Perspective view to the west of the 3D litho-geological model used to constrain and support the interpretation of the 3D seismic data. The outline of the 3D model relative to the 3D seismic data is shown in Figure 1. Hanging wall units are steep especially above the ore zones. The least altered footwall rocks are shown in green and yellow whereas the most altered footwall rocks are in pink-to-purple tones. The two sections, which correspond to inline 1087 and crossline 1219 of the 3D seismic volume, provide a good overview of the main ore zones of the Lalor deposit. HW=hanging wall; FW=footwall.

Further subdivision of these three categories using fabric and textural descriptive attributes of drill core, resulted in the total of 15 lithofacies classes (Table 2). To support variable structural anisotropy in the distribution of each lithofacies unit, 3D variograms were estimated for each of the 15 lithofacies classes in the point set using an exponential variogram model.

Fourteen of the fifteen lithology classes were interpolated in UVT space using ordinary categorical kriging on grid cells of 20 m parallel to and 5 m normal to the stratigraphic layering to honour the geological structure of the footwall and hanging wall of the deposit. Only lithofacies class 15: mafic intrusive rocks (diorite and gabbro) which are often sub-horizontal and intrude the general structure, were kriged in a Cartesian coordinate system. Finally, all 15 interpolated lithofacies classes were resampled to a Cartesian voxel model with cubic grid cells to facilitate integration with the 3D seismic data (Figure 9). The lithofacies model is relatively accurate in the immediate vicinity of the boreholes but less reliable near the edges or at greater depth (i.e., near 1500 m) where the distribution of boreholes is sparse. An extensive overview on the 3D lithofacies grid modeling method can be found in Schetselaar (2013).

Figure 9 presents two cross-sections through the 3D lithofacies model which reveal the geological complexity of the area. Rocks forming the hanging wall are generally steeply-dipping near the surface but have shallower dips close to the contact with footwall rocks, particularly in the northeastern part of the model. Footwall rocks are everywhere moderately-dipping to the northeast. Footwall rocks with the most intense hydrothermal alteration (pink

and purple units in Figure 9) were classified using the characteristics of the protolith rather than their actual metamorphic description (i.e., gneiss and schist). The protolith signatures were determined from the ratio of immobile elements ( $Zr/TiO_2$ ) obtained from geochemical analysis available for cores from almost all boreholes (Floyd and Winchester, 1977; Caté *et al.*, 2013). This approach was used to help define the characteristics of the host rocks prior to metamorphism. This approach was not used for the footwall rocks towards the southwest which are also altered but not intensely enough to mask their volcanic origin (units in yellow and green in Figure 9). The model suggests an interfingered lateral transition between the most to least altered footwall rocks (Figure 9). Alternatively, a fold structure associated with a fault could explain the juxtaposition of moderately and highly altered footwall rocks (Caté *et al.*, 2014; Schetselaar and Shamsipour, 2015). Also note that many units in this model have a limited lateral extent and are discontinuous which complicates their imaging with seismic methods. Figure 9 also shows sulphide bodies (red) corresponding to five zinc zones (zones 10, 11, 20, 30, and 31), and three gold zones (zone 21, 25, and the gold-copper zone 27). In the 3D model, the ore zones are defined from the economical envelope used for the planning of the mine and therefore exclude non-economical mineralized intersections logged in several boreholes. Ore zones close to each other or overlapping are generally grouped as one zone in the model.

# PHYSICAL ROCK PROPERTIES OF HOST ROCKS AND SULPHIDE MINERALIZATION AT LALOR

GILLES BELLEFLEUR<sup>1</sup> AND ERNST SCHETSelaar<sup>1</sup>

<sup>1</sup> Geological Survey of Canada, 615 Booth Street, Ottawa, Ontario, K1A 0E9

## INTRODUCTION

An analysis of physical rock properties was conducted to assess the main response of the ore zones and host rocks at Lalor on seismic data, including possible effects of alteration and post-sulphide metamorphism. For this analysis, we used wireline logging data acquired in boreholes located close to or intersecting the deposit and measurements (Vp, Vs, and density) made on 45 core samples. The implication of this petrophysical analysis for seismic reflectivity is discussed below in terms of both host rocks and sulphide mineralization.

more qualitative approach using visual core descriptions, especially in the most altered part of the footwall. Also shown on Figure 10 are ellipsoids determined from principal component analysis and representing the mean and scaled eigenvectors of the covariance matrix of the distribution of each lithological unit. The major and minor axes of the ellipsoids correspond to one standard deviation. Given the relatively large spread of data points for some of the lithological units, the results presented below are based mostly on the ellipsoids from the principal component analysis.

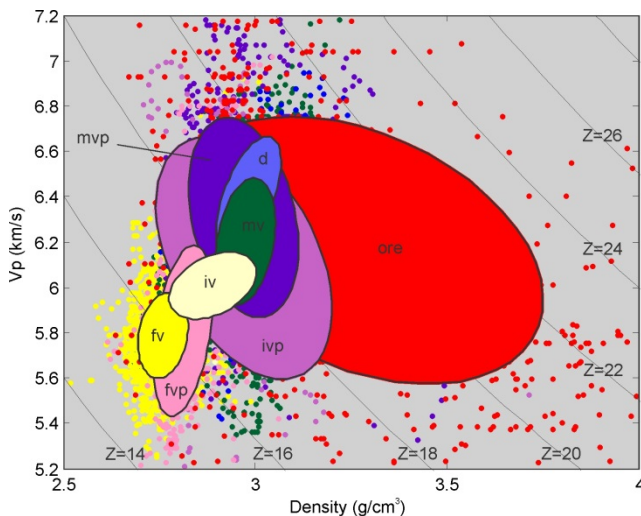


**Figure 10.** P-wave velocity and density of the main lithological units intersected in ten boreholes (see Figure 1 for collar locations). Units include felsic volcanic rocks (fv), intermediate volcanic rocks (iv), mafic volcanic rocks (mv), diorite (d), felsic volcanic protolith (fvp), intermediate volcanic protolith (ivp), mafic volcanic protolith (mvp), and ore. Lines of constant acoustic impedances (Z) are also shown. The ellipsoids are defined from the principal component analysis of each lithological unit with the minor and major axes representing one standard deviation from the mean.

## PROPERTIES OF HOST ROCKS

Figure 10 shows the P-wave velocity and density from the logging data acquired in ten boreholes (DUB183, DUB185W03, DUB186, DUB189, DUB191, DUB195W05, DUB202, DUB209, DUB245, and DUB253). Those boreholes contain both wireline logging data and geochemical data which allowed the classification of the most altered footwall rocks according to their protolith. For the petrophysical analysis, we only selected wireline logging data located near geochemical sample points (i.e., within a maximum distance of 1.5 m from a geochemical data point). The geochemical data were used to determine the protolith (i.e. rock type of origin). This quantitative approach based on geochemistry was preferred over the

The physical rock properties at Lalor are in general agreement with properties obtained elsewhere in the Flin Flon Belt (Fowler *et al.*, 2005; White *et al.*, 2012) or in other volcanogenic massive sulphide mining camps (Salisbury *et al.*, 2003; Malehmir *et al.*, 2013). Similar to many volcanogenic massive sulphide mining camps, the contrast of acoustic impedances between felsic and mafic volcanic rocks is generally sufficient to generate reflections (see Salisbury *et al.*, 2003). The contrast of acoustic impedance indicated by the separation between the ellipsoids corresponding to these units (fv and mv on Figure 10) is sufficiently large to produce prominent reflections (i.e., a reflection coefficient of 7.3% using mean values of ellipsoids on Figure 10). Volcanic rocks of intermediate composition (iv on Figure 10) have acoustic impedances between felsic and mafic volcanic rocks suggesting that contacts between iv and either fv or mv may not generate prominent reflections (i.e., a reflection coefficient less than 4.2% using mean values of ellipsoids on Figure 10). Diorites (d in Figure 10) have high acoustic impedances similar to mafic volcanic rocks, suggesting that they may generate reflections when in contact with felsic volcanic rocks (i.e., a reflection coefficient of 8.8% using mean values of ellipsoids on Figure 10). Those estimated reflection coefficients are representative of most contacts in the hanging wall and in the least altered part of the footwall (i.e., footwall units in yellow and green on Figure 5). In the footwall, the physical properties of the most altered rocks (units in pink to purple on Figure 5) are controlled by the composition of their protolith. Similar to the contacts between mafic and felsic rocks in the hanging wall, rocks with a mafic protolith (mvp ellipse on Figure 10) will generate a strong reflection when in contact with rocks with a felsic protolith (fvp ellipse on Figure 10). In this case, the mean values of ellipsoids on Figure 10 suggest a reflection coefficient of 6.9%. Rocks with intermediate protolith cover a wide range of P-wave velocity and density (see ivp on Figure 10) but they are generally closer to the ellipse of rocks with mafic protolith. In fact, the mean values of rocks with intermediate and mafic protolith are relatively similar, suggesting that intermediate-felsic protolith contacts may also produce detectable reflections (i.e., a re-

flection coefficient of 5.5% using mean values of ellipses on Figure 10). For the most altered footwall rocks, we also compared the physical rock properties of both protoliths (felsic and mafic) and their metamorphosed equivalents (gneiss and schist). Figure 11 shows the distribution of Vp/Vs and acoustic impedance for gneiss and schist (Figure 11a) and for felsic and mafic protoliths (Figure 11b). Gneiss and schist cannot be distinguished on the basis of acoustic impedances (Figure 11a) whereas protoliths of mafic and felsic composition have slightly overlapping but yet separated acoustic impedances (Figure 11b; see also fvp and mvp on Figure 10). This confirms that contacts between protoliths of felsic and mafic volcanic origin may generate reflections whereas a juxtaposition of gneiss and schist

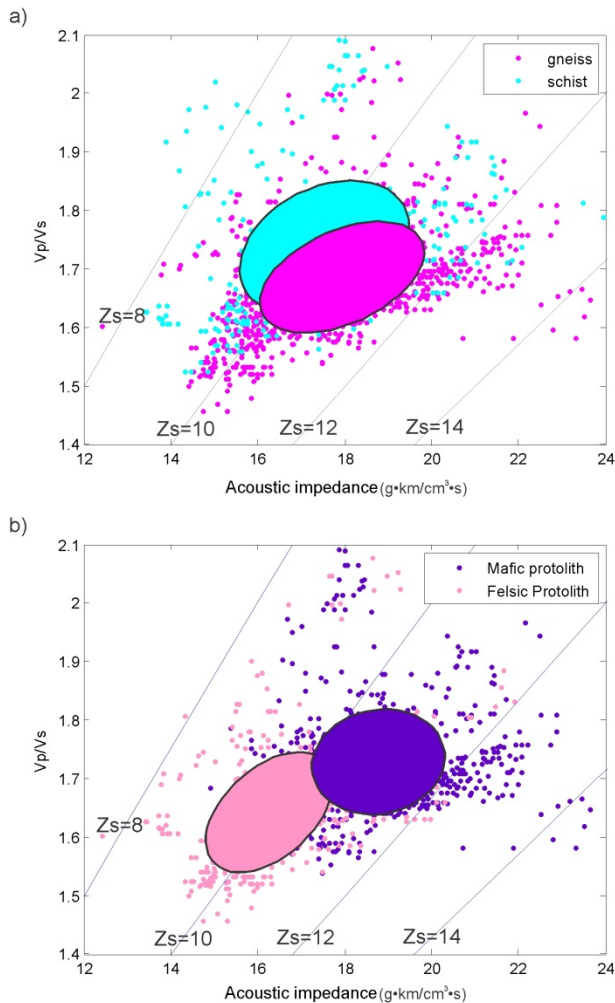


**Figure 11.** Physical rock property of (a) schist and gneiss (b) felsic and mafic protolith in ten boreholes (see Figure 1 for collar locations). The same logging data is used for (a) and (b) but categorization relies on geological description in (a) and protolith defined from Zr/TiO<sub>2</sub> in (b). Schist and gneiss have a similar range of acoustic impedance but are slightly separated along the Vp/Vs axis. Felsic and mafic protoliths although partly overlapping, show different ranges of acoustic impedance possibly explaining many reflections in the most altered part of the footwall. Lines of constant elastic impedances (Zs) are also shown on this figure.

might not. It is important to note that each of the felsic and mafic protoliths are found in both gneiss and schist. Figure 11 also shows a moderate separation between gneiss and schist and mafic-felsic protoliths with respect to Vp/Vs. The Vp/Vs separation between schist and gneiss (Figure 11a) is possibly related to well-developed foliation (anisotropy) in the schist. However, no anisotropy measurements are available to confirm this hypothesis. The cause of the Vp/Vs separation between mafic and felsic protoliths is still ambiguous but could be related to compositional variations.

### REFLECTIVITY OF ORE

As shown in Figure 10, the mineralized zones cover a wide range of acoustic impedances suggesting that ore zones with various compositions have different physical rock properties and/or ore intervals also include weakly mineralized rocks. As part of their core-logging procedure, Hudbay Minerals divided the mineralized intersections into 9 classes representing rocks with minor indication of mineralization to solid massive sulphides. All mineralized intersections in boreholes including non-economical intervals followed this classification. Although mostly qualitative, this classification provides a means to assess the physical rock properties of various ore classes of the deposit and estimate their potential reflectivity against host rocks or against ore with different composition. Figure 12 shows the P-wave velocities and density for the nine ore classes. All 12 boreholes with logging data at Lalor were used in Figure 12. Near-solid to solid sulphide (R62 in Figure 12) and near-solid sulphide (R63 in Figure 12) intersections generally have higher densities which result in higher acoustic impedances. The solid massive sulphides (R61 in Figure 12) span across a wide range of impedances mostly related to changes in density and includes some values typical of non-mineralized host rocks. Those values suggest that some of the intervals identified as solid massive sulphides also included sub-intervals with weak or no mineralization. Many logging data points from the solid sulphide class (R61) have high impedances and overlap with the near-solid and near-solid-to-solid sulphides but generally have lower P-wave velocity typical of sphalerite (see Salisbury *et al.*, 2003). Other mineralized classes are associated with stringer of sulphides and disseminated mineralization and have significantly lower acoustic impedances, some very similar to impedances of host rocks (R64 to R69 in Figure 12). In general, density is the primary property allowing discrimination between near-solid to solid sulphides (R61 to R63) and stringers and disseminated sulphides (R64 to R69). Density measurements on samples from both zinc and gold zones conducted as part of the resource evaluation by Hudbay Minerals also confirm this trend. Density for the zinc zones ranges from 2.66 to 4.75 g/cm<sup>3</sup> with an average of 3.59 g/cm<sup>3</sup> (Carter *et al.*, 2012). In comparison, the disseminated gold zones have an average of 2.84 g/cm<sup>3</sup> with values ranging between 2.72 to 3.79 g/cm<sup>3</sup>.

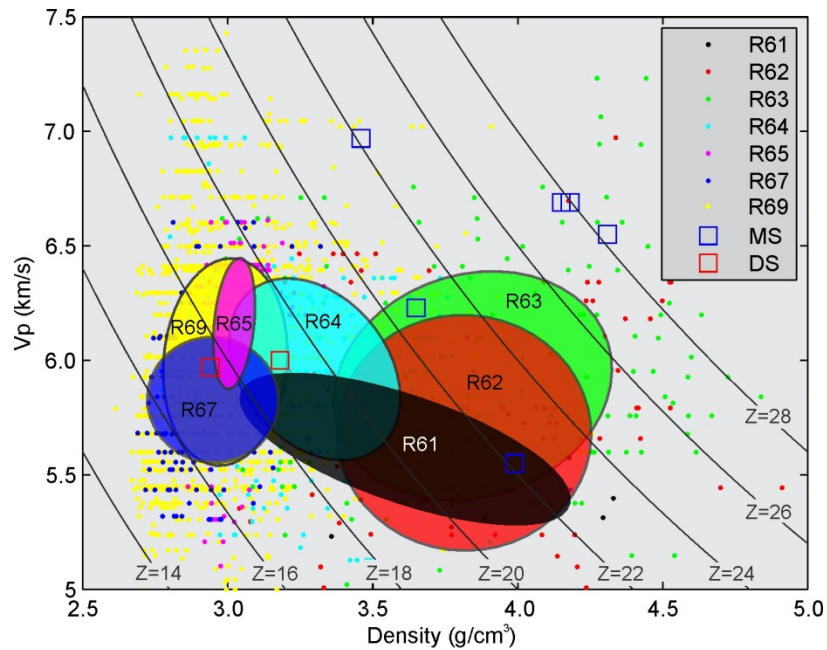


**Figure 12.** P-wave velocity ( $V_p$ ) and density for the various ore classes identified during the geological logging of the cores. R61: solid sulphides; R62: near solid to solid sulphides; R63: near solid sulphides; R64: disseminated to near solid sulphides; R65: disseminated sulphides; R66: well-mineralized to disseminated sulphides; R67: well-mineralized intersection; R68: cherty ore zone; R69: mineralized intersection. Squares represent measurements on core samples from massive (MS) and disseminated (DS) sulphides. P-wave velocity measurements on samples in this figure were done at 80 MPa.

A total of 1957 and 1455 density measurements were made for the zinc and gold zones, respectively. Physical rock property measurements ( $V_p$ ,  $V_s$ , and density) made on massive and disseminated sulphide rock samples show similar results (see squares on Figure 12). In this case, massive sulphide core samples are from pyrite-rich intersections which also have high P-wave velocity (Figure 12).

These results (Figure 12) and comparison with Figure 10 confirm that reflections can be expected from near-solid to solid sulphides when juxtaposed against any rock units in the Lalor area. However, most of the disseminated sulphide zones which constitute an economically important part of the deposit (i.e., the gold and gold-copper zones) will generate weak to very weak reflections or no detectable reflections. This is even more likely when the generally smaller size of the gold-rich zones is considered. Similar to electromagnetic methods which tend to respond well to solid sulphides, seismic methods can only directly reveal the shallower semi-massive-to-massive sulphide zones of the Lalor deposit. However, given the close proximity of some ore zones, their small thickness, and possible interference with lithological contacts near the ore zones, it is also possible that some reflections might be indirectly associated with some disseminated zones (see section on the interpretation of the Lalor 3C-3D seismic data).

## CONCLUSIONS

Physical rock properties show that zinc-rich massive sulphide zones which are associated with pyrite have high acoustic impedances that are sufficient to produce prominent reflections when juxtaposed against any host rocks. The disseminated gold-rich zones which constitute an economically significant part of the deposit cannot be imaged directly with seismic reflection methods. Physical rock properties also show that contacts between felsic and mafic volcanic rocks regardless of the intensity of hydrothermal alteration and metamorphism are the most likely cause of reflections in this area.

# ACQUISITION, PROCESSING AND INTERPRETATION OF THE LALOR 3C-3D SEISMIC DATA

GILLES BELLEFLEUR<sup>1</sup>, ERNST SCHETSelaar<sup>1</sup>, AND DON WHITE<sup>1</sup>

<sup>1</sup> Geological Survey of Canada, 615 Booth Street, Ottawa, Ontario, K1A 0E9

## INTRODUCTION

During the winter of 2013, the Geological Survey of Canada acquired a 16 km<sup>2</sup> 3-component 3D seismic data set over the Lalor volcanogenic massive sulphide deposit located in Manitoba, Canada (Figure 1) to assess the reflectivity of the ore and further validate the potential of 3D reflection seismic methods for deep mineral exploration. In this section, we present the main field acquisition and processing parameters. Results presented here based on only P-wave processing of the data recorded on the vertical component of the receivers. Finally, we analyze and interpret the main reflections associated with the hanging wall, ore zones, and footwall, and use this information to provide guidelines for the exploration of similarly metamorphosed massive sulphide deposits.

## DATA ACQUISITION AND PROCESSING

The 3D active-source seismic survey covers an area of approximately 16 km<sup>2</sup> that includes 908 shot points and 2685 receiver stations (Figure 1). The 16 receiver lines were oriented SW-NE and are almost parallel to the dip direction of the ore zones and footwall rocks near the deposit. The 15 shot lines were generally orthogonal to the receiver lines with many shot points located northeast of the deposit to provide sufficient ore zone illumination from the down-dip direction. Shot and receiver lines locally deviated from planned location to adjust for difficult terrain (e.g., steep hills, cliffs). Deviations were more significant logistically for shot lines which provided access for the track-mounted drill rigs used for the shot holes. The area between Lalor Lake and Cook Lake was particularly challenging for shot lines (Figure 1). No shots were fired close to existing mining infrastructure including the main mine area and ventilation raise, or over lakes (Figure 1). Energy sources were 0.5 kg of explosives loaded in 5 m deep holes that were tamped with bentonite and cuttings from the drilling. Digital multi-component accelerometers deployed at 2685 stations were kept live for the entire survey (i.e., one receiver patch was used) and provided a total of 8055 traces per shot gather. The generally cold temperatures during the 3D acquisition (generally below minus 20° C during the acquisition phase in March 2013) resulted in solidly frozen near-surface conditions, which allowed excellent ground-to-geophone coupling. Table 3 shows the main acquisition parameters used for the 3D seismic data acquisition.

The quality of the raw shot gathers ranges from poor to excellent with most shot gathers generally having good signal-to-noise ratio and clear first arrivals at large offsets (up to 4 km). Many of the poor-quality shot gathers are located in areas with muskeg that strongly reduces the shot

coupling and attenuates seismic waves. Figure 13a shows a typical raw shot gather recorded on receiver lines 133 to 141 (Figure 1 for location). Direct, refracted P-waves, S-waves, and surface waves are the most prominent arrivals on the shot gather. Weak and mostly discontinuous reflections are occasionally identified on raw shot gathers. Much of the surface wave energy on the shot gather is characterized by frequencies typically below 45 Hz. The best shot gathers have signal at frequencies up to 250 Hz whereas signal on poor-quality shot gathers only reaches 100 Hz. However, average shot records have high amplitudes (i.e., within 10 dB of the maximum amplitude) at frequencies ranging between 150-200 Hz.

**Table 3.** Acquisition parameters for the 3D-3C Lalor seismic survey.

Sensor/accelerometer	Sercel 428/DSU3 (3C)
Traces/record	3 x 2685
Sample interval	1 ms
Sample /trace	4001
Anti-alias filter	400 Hz
Source type/ Source depth	0.5 kg explosive / 5m
No. of shots	908
Source spacing/line spacing	50 m/ 365 m
Receiver spacing/line spacing	25 m/ 250 m
No. of source/receiver lines	15/16
Patch	All live
Survey area	16 km <sup>2</sup>

The final seismic images presented in this paper were obtained using a prestack dip-moveout (DMO) and poststack time migration processing flow. Such a processing flow is particularly effective and often produces superior results to images obtained with prestack-time migration for seismic data acquired in crystalline rock environments (Milkereit *et al.*, 1996; Adam *et al.*, 2003; White *et al.*, 2012). The stacked DMO volumes also preserve diffractions that may originate from smaller ore bodies, edges or larger massive sulphide lenses (Malehmir and Bellefleur, 2009). At Lalor, results from this approach produced generally more continuous reflections with significantly less short and discontinuous reflections than did a trial prestack-time migration processing flow. The number of short and discontinuous reflections is particularly significant in the shallow part of the prestack-time migrated volume and the great majority could not be reconciled with observed geological features

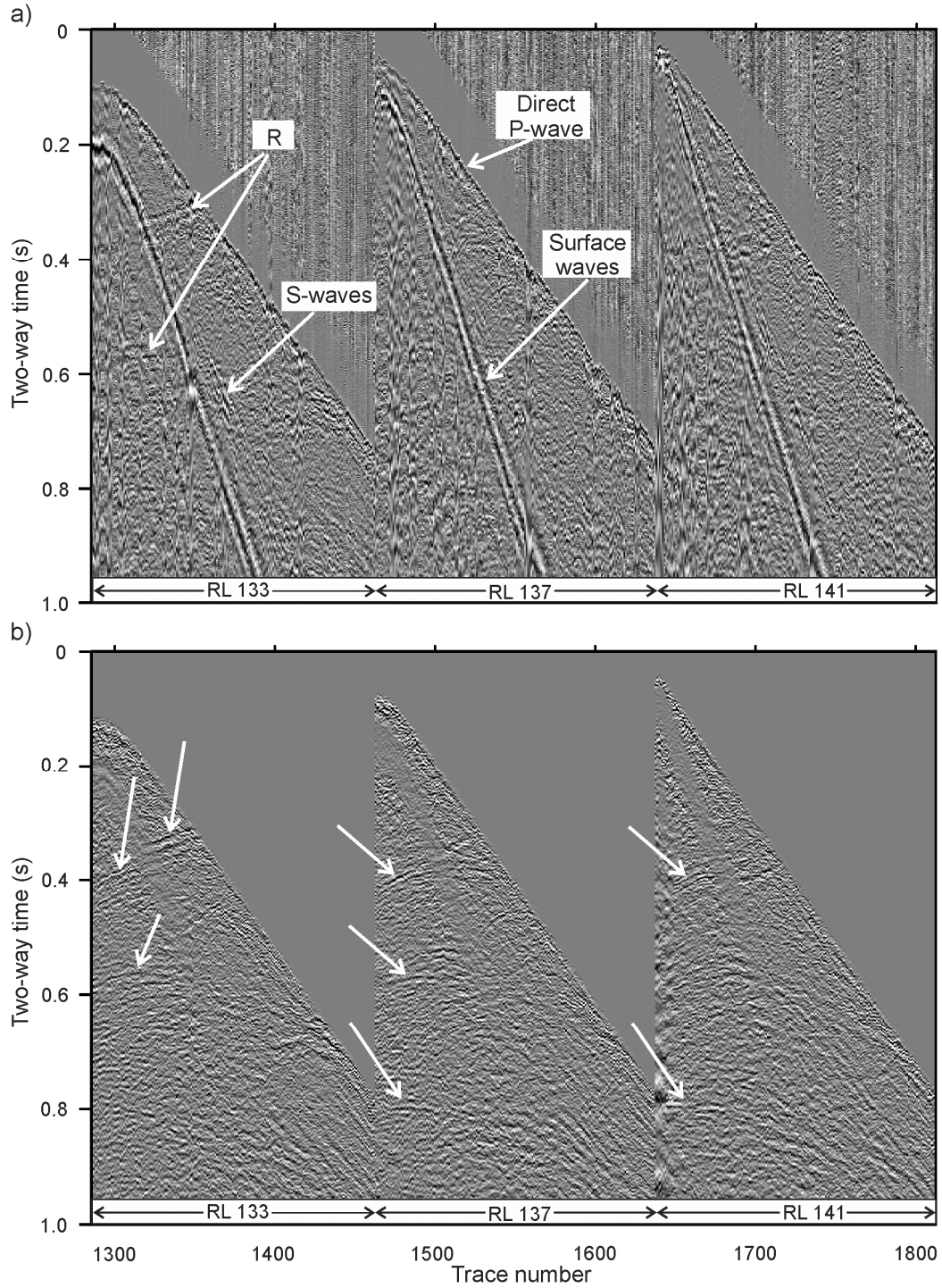


**Figure 13.** (a) Example of a good quality raw vertical-component shot gather (FFID 224; see Figure 1 for location) on three receiver lines. (b) Same shot gather after some processing (refraction static corrections, coherent noise attenuation and surface-consistent deconvolution). Arrows point to a few reflections (R in a).

**Table 4.** Processing parameters for the prestack DMO poststack migration flow.

Step	Parameters
1.	Geometry assignment and 3D Binning, CDP Bin size 12.5 m x 25.0 m
2.	Trace editing
3.	Trace balancing (2 second window)
4.	Spherical divergence correction
5.	Refraction static corrections, datum = 330 m, $V_r = 5900$ m/s
6.	Spiking deconvolution 80 ms filter length
7.	F-k filter on shot and receiver gathers to attenuate surface and refracted arrivals
8.	Air wave removal
9.	Band pass filter 5-35-175-225 Hz
10.	Automatic Gain Control, 500 ms window length
11.	Velocity analysis (iterative)
12.	Surface-consistent residual statics, max shift 15 ms, window 200-1500 ms (iterative)
13.	Normal moveout correction
14.	Dip moveout correction – 3D integral method (iterative - 3 loops)
15.	CDP trim statics, max shift 8 ms
16.	Stacking
17.	3D Kirchhoff poststack time migration
18.	Automatic Gain Control, 300 ms window length
19.	Band pass filter 10-35-160-190 Hz
20.	Curvelet denoising

near the deposit. However, both processing approaches revealed the stronger and most continuous reflections. Results from the prestack-time migration processing flow can be found in Bellefleur and White (2014). Table 4 shows the detailed sequence and parameters used to process the vertical-component of the Lalor 3D data presented in this paper (prestack DMO-poststack migration processing flow).

Of the pre-processing steps (see Table 4), trace editing and coherent noise attenuation were particularly important steps. Noisy traces with no clear first arrivals and weak traces contaminated with occasional mining noise were removed during trace editing. When present, the strong mining noise typically formed sequences of coherent hyperbolic arrivals randomly distributed in time, including before the first arrivals. The apexes of the hyperbolic events were always located at receiver stations near the main mining area. Traces with such noise were removed from the data. The main underground explosions occurred twice a day at times communicated by the mine personnel and were avoided by temporarily stopping recording during data acquisition.

Approximately 6.5% (162429 traces) of the traces were eliminated during trace editing. Refracted shear-waves and surface waves were attenuated with 2D filtering in the frequency-wavenumber domain combined with a bandpass filter (5-35-175-225 Hz). Some refracted S-waves still remained after these steps and were further attenuated using median filters that followed a linear moveout velocity of

3200 m/s. Refraction and elevation static corrections were instrumental in improving the continuity of reflections in shot gathers (Figure 13b). The 3D refraction static corrections were determined from over 1.2 million picked arrivals. An automatic picking algorithm combined with manual inspection and adjustments were used to pick the first arrivals. Receiver refraction statics varied from -6 ms to 46 ms with most receivers being within the -3 to 7 ms range. The largest receiver static corrections were located over Cook Lake (Figure 1). Shot statics were generally smaller and ranged between -4 and 21 ms with a mean of 3 ms.

The pre-processed data were then sorted into common depth point gathers using a bin size of 12.5 m by 25 m in the inline and crossline directions, respectively. Nominal fold reached a maximum of 170 in the centre of the 3D grid. Three iterative loops of NMO-DMO were used to update the velocity models. Residual static corrections were included in the last two NMO-DMO loops. A 3D Kirchhoff poststack time migration was applied to the final DMO stack volume. Post-migration filtering included an automatic gain control (300 ms window), bandpass filter (10-35-160-190 Hz), and curvelet denoising. Curvelet denoising provided a higher signal-to-noise ratio than did F-XY deconvolution which is often applied as a post-migration filter (Górszczyk *et al.*, 2015). The final time-migrated volume was converted to depth using a constant velocity of 5900 m/s and then integrated with the 3D geological model. This velocity is supported by borehole logging data, particularly in the hanging wall and produced the most satisfactory tie with borehole data (see Bellefleur *et al.*, 2015).

## DATA INTERPRETATION

### *Hanging Wall Reflections*

The final seismic data are compared with the geological model in Figures 10 and 12. The hanging wall is generally devoid of reflections mostly due to the near-vertical orientation of strata in the hanging wall. This is especially the case above the deposit where reflections are generally short and weak, and have no obvious correlation with lithological units (Figures 10 and 12). Some weak shallowly-dipping reflections are observed towards the northeast end of the model (H1 to H3 on Figure 14) where hanging wall units have shallower dips in the 3D geological model. Reflection H2 on Figure 14 is located at the contact between mafic volcanic and mafic volcanoclastic rocks. The mafic volcanoclastic unit just above the hanging wall- footwall contact has relatively high density values that could potentially explain the reflections even though such an increase in density is not associated with a clear reflection on the synthetic trace (see Bellefleur *et al.*, 2015). Reflections H1 and H3 are observed within a felsic or mafic volcanic unit and cannot be explained due to lack of borehole constraints near the northeastern edge of the model. Some short sub-horizontal

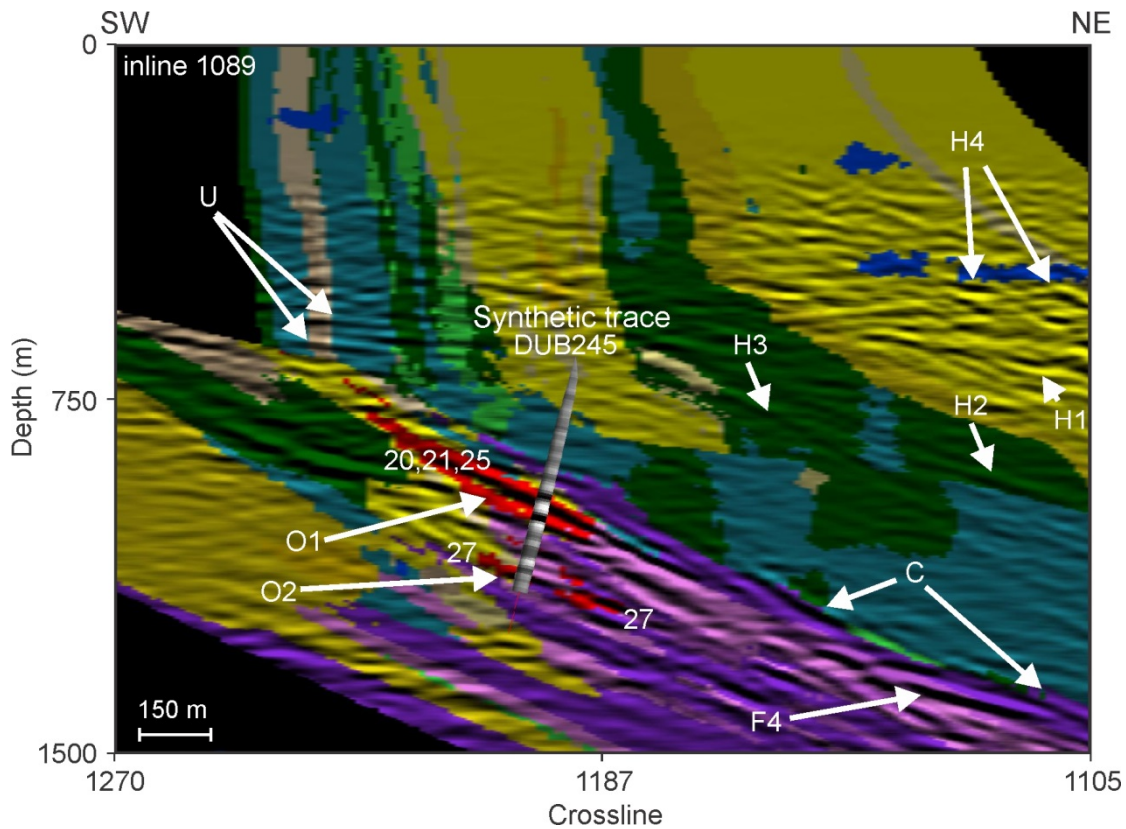


**Figure 14.** Inline 1089 from the final migrated seismic volume with the geological model overlain on top of the seismic section. See text for details on interpretation. Legend for geology as in Figure 5. The labels are referred to in the text. Ore zones 20, 21, 25, and 27 are also shown.

reflections are locally correlated with diorite intrusions (H4 on Figure 14). However, not all diorites intersected in boreholes have reflections associated with them (see other diorites in Figure 14). Overall, hanging wall reflections are not particularly significant in the area of the 3D model.

Some reflections with moderate amplitudes are observed further to the northeast outside the limits of the 3D geological model (Figures 11 and 12). The dip of these reflections is generally shallow (approximately 25°) and similar to the dip of reflections in the footwall. Whereas the exact cause for these reflections cannot be precisely assessed due to lack of borehole control, the surface geological map and the projection of lithological unit from the model help to define their nature. In particular, reflection H5 (Figure 15) is associated with or coincides with the continuity of a contact between felsic and mafic volcanic rocks. Reflection H2 shown in Figure 14 also continues to the northeast on inline 1098 (Figure 16a). Reflections H6 and H7 are observed in the northeast part of the seismic volume (Figures 11 and 12). Reflection H6 is interpreted as the continuity of a felsic-mafic contact between the Balloch basalt and North-Balloch rhydacite (see Figure 16). If true, then reflection H7 appears to coincide with the top of the North-Balloch rhydacite. Detailed surface geological maps indicate the presence of a mafic volcanoclastic unit northeast of the North-Balloch rhydacite (Bailes *et al.*, 2013). The contact between this

unit and the North-Balloch rhydacite may explain reflection H7.

Reflectivity along the hanging wall-footwall contact depends on the composition of units juxtaposed at the interface, footwall alteration, and the presence of mineralization, all of which vary spatially. On inline 1089 (Figure 14), this contact has no clear seismic signature with only a few short reflections being locally observed (event C on Figure 14). On the time slice, there are no clear reflections associated with the contact (Figure 15). However, the contact is clear and continuous on an east-west section (C on Figure 16b) where mafic units in the hanging wall are juxtaposed with felsic units in the footwall. The contact is also locally observed on inline 1098 (C on Figure 16a).

#### **Ore Zones Reflections**

Whereas physical properties alone suggest an easy distinction between semi- to massive sulphides and host rocks, the reality is complicated by the close proximity of several mineralized zones and their generally small thickness. For instance, clear reflections are observed at the location of the shallower ore zones on inline 1089 (O1 on Figure 14). Three ore zones (20, 21, and 25) are all comprised in the shallowest ore interval shown in red in the model and indicated by O1 on Figure 14. The reflections

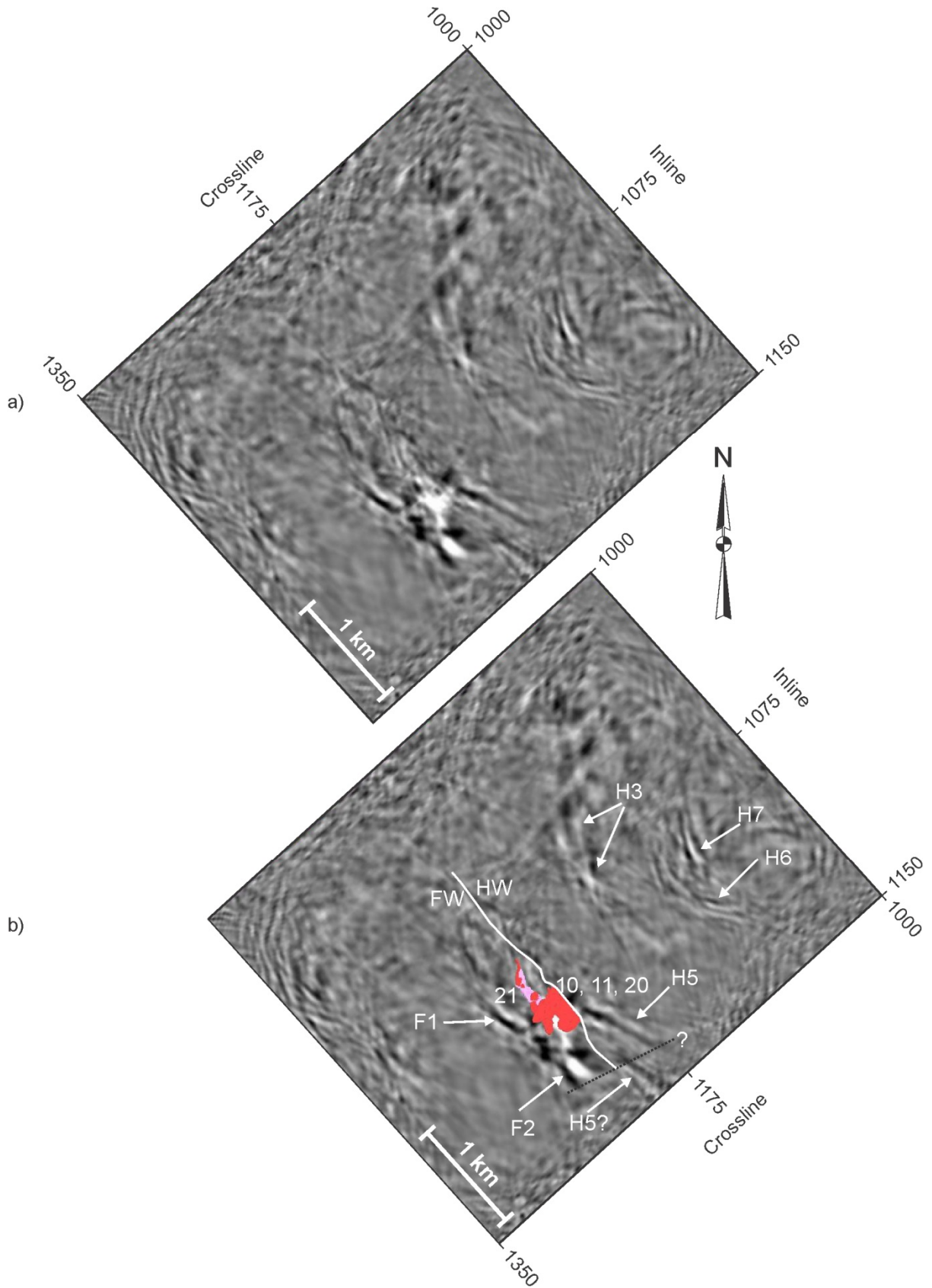


**Figure 15.** (a) Time slice at 283 ms (approximately 835 m depth) showing a strong amplitude anomaly at the location of the massive sulphide ore zones. (b) Same as (a) with interpretation. Ore zones 10, 11, 20 and 21 are shown in (b). Black dashed line indicates a possible fault.

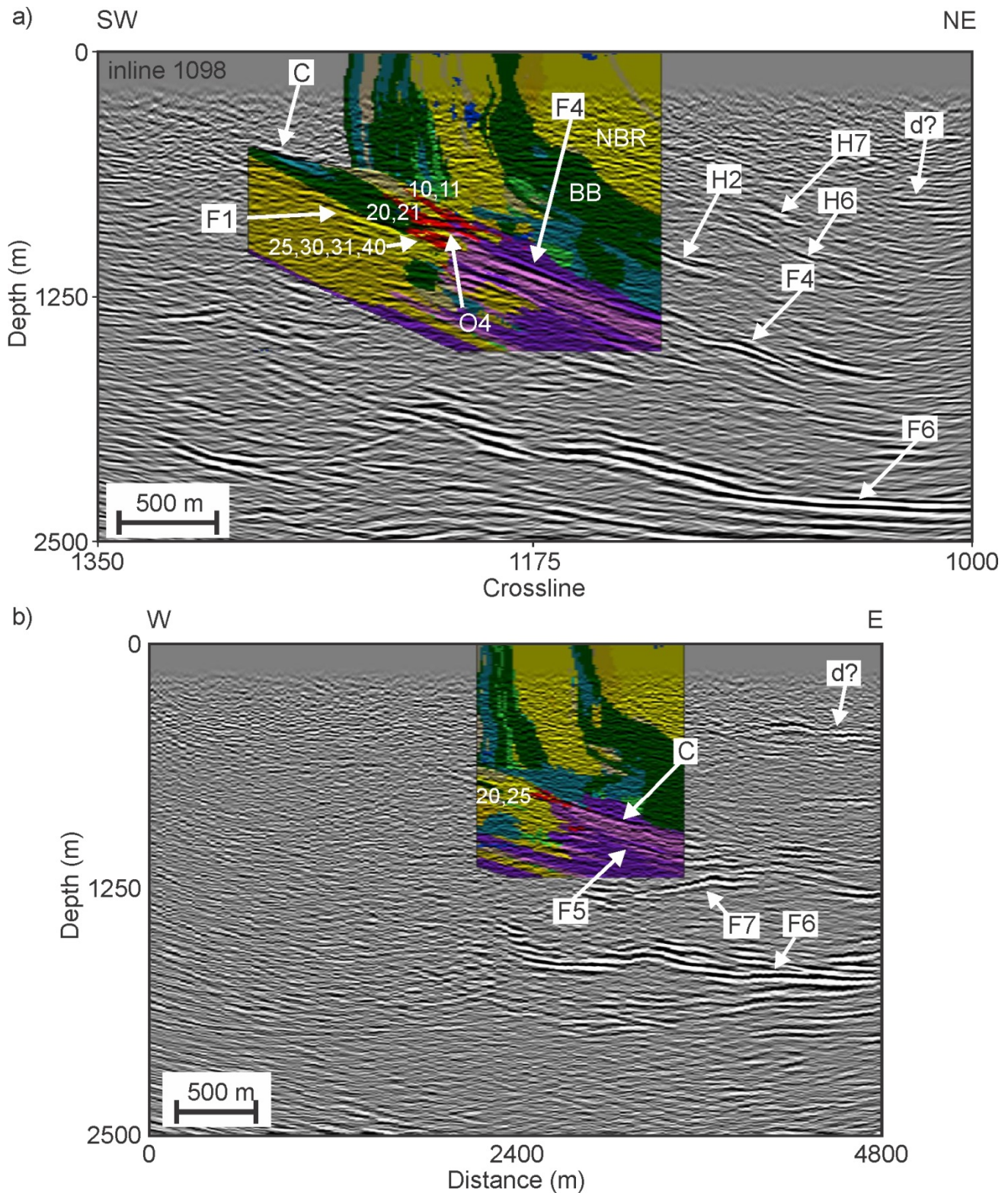


**Figure 16.** (a) SW-NE section (inline 1098) from the final seismic volume with geological information from the 3D model. (b) E-W section from the final seismic volume. The location of this E-W section is shown in Figure 1. See text for interpretation of events identified in (a) and (b). Legend for geology as in Figure 5. Post-migration curvelet denoising is not applied on these sections. Location of the cross-section is shown in Figure 1. Ore zones 10, 11, 20, 21, 25, 30, 31, and 40 are shown in (a). Ore zones 20 and 25 are shown in (b). BB: Balloch basalt; NBR: North-Balloch Rhyodacite.

result from the combination of the response of the shallow ore zone (zone 20) and contacts between felsic volcanic rocks and mafic protoliths above and below the ore zones (see also Bellefleur *et al.*, 2015). This combined effect is also observed on a time slice at 283 ms which correspond to a depth of approximately 835 m (Figure 15). The particularly strong localized amplitude anomaly on this time slice coincides with several ore zones (zones 10, 11, 20, and 21). The amplitude anomaly is clear and would have been identified as a potential target if the data would have been acquired as part of an exploration program. The deeper ore zone intersected in DUB245 (gold-copper zone 27) is indirectly associated with a reflection located at the contact between felsic and mafic protoliths (O2 on Figure 14). This reflection follows the felsic-mafic protolith contact on either side of zone 27. Other reflections are associated with ore zones elsewhere in the final seismic volume but those are not as strong as reflection O1 (see O3 and O4 on Figures 10 and 12). A series of sub-horizontal reflections coincide with ore zones 10, 20, 30, 31, and 40 on inline 1098 (Figure 16). The disseminated gold zones and gold-copper zone 27 have no clear reflections associated with them.

### **Footwall Reflections**

In general, the number and strength of reflections are significantly higher in the footwall and especially in the intensely altered zone. On Figure 14, the less altered rocks in the immediate footwall are in general southwest of the main ore zones (units in yellow and green) whereas the most altered footwall rocks are southeast of the deposit (units shown in pink to purple). The strongest reflections in the least altered part of the footwall correspond to contacts between felsic and mafic volcanic rocks. Reflections from such contacts are observed on the time slice (F1 and F2 on Figure 15), and on inline 1098 (F1 on Figure 16a). Reflections in the most altered part of footwall are relatively continuous and can be tracked over significant distances, mostly to the northeast in the down-dip direction. These reflections coincide primarily with contacts between rocks with felsic and mafic protoliths. The correspondence between strong footwall reflections and felsic-mafic protolith contacts is clear in Figures 10 and 12 (see F4 and F5 on those figures). Figure 16b shows a strong sub-horizontal reflection just below the limit of the geological model (F7 on Figure 16b). This reflection merges with the felsic-mafic protolith reflection F4 approximately 500 m east of the area with geological information. The nature of this strong reflection cannot be established due to the lack of boreholes, but we speculate that it marks the bottom of the mafic protolith unit located above (F5 on Figure 16 is at the top of this mafic protolith unit). If so, the lithological unit below F7 would have a felsic composition or felsic origin (i.e., felsic protolith). At greater depths, the footwall is characterized by numerous reflections generally dipping to the northeast on most inlines (see F6 on Figure 16). The most continuous are located near the base of the Lower Chisel sequence near the contact with the Anderson sequence. Given their strength and excellent continuity,

these reflections are likely of lithological origin but their exact nature still needs to be determined. Possibilities include the contact between the Chisel and Anderson sequences, a conformable mafic intrusion, and the continuation at depth of the synvolcanic Richard Lake pluton located west-to-southwest of the survey area. Based on the similarities in geometry of most footwall reflections (see Figure 16a), we infer that the deeper reflections F6 were conformably deformed with the shallower footwall units. For instance, the pinch out of the mafic protolith unit (i.e., intersection of F7 and C on Figure 16b) occurs in an area where reflection F6 is shallower (also compare the depth of F6 in Figure 16a and b). If this interpretation is valid, then the general architecture of the deeper reflection F6 can help identify areas where the hanging wall-footwall contact is shallower and within mining depths.

### **CONCLUSIONS**

Processing of the data following a prestack DMO poststack migration approach revealed some strong reflections associated with the zinc-rich massive sulphide zones. The most prominent reflection from the ore results from the interference of thin and closely-spaced massive sulphide zones and felsic-mafic volcanic rock contacts above and below the mineralization. Other weaker reflections are also associated with zinc-rich zones but no clear reflections can be attributed to the disseminated gold zones. Contacts between metamorphosed rocks with felsic and mafic protoliths in the most altered part of the footwall also produce prominent and continuous reflections. The shallowest of these reflections can be used as a proxy for the hanging wall-footwall contact which is only locally observed on the seismic data. At depth, a series of strong and continuous reflections provide indications on the general geometry of the volcanic sequences in the area of the 3D seismic survey and can help to identify areas where the hanging wall-footwall contact is shallower and within mining depth range.

## PASSIVE SEISMIC INTERFEROMETRY OVER THE LALOR LAKE AREA

SAEID CHERAGHI<sup>1</sup>, JIM CRAVEN<sup>1</sup>, AND GILLES BELLEFLEUR<sup>1</sup>

<sup>1</sup> *Geological Survey of Canada, 615 Booth Street, Ottawa, Ontario, K1A 0E9*

### INTERFEROMETRY BACKGROUND

A number of studies have shown that an active mine site is a source of seismic energy due to both direct noise sources such as underground explosions and indirect sources such as mining induced seismicity (e.g. Snelling *et al.*, 2013). We suggest the reverberations from these noise sources can be processed in such a manner that they appear as if they were generated from sources located on the surface instead. As such, this ‘virtual’ data can theoretically replace data obtained from a traditional, far more expensive, active source seismic survey. The specialized processing required is termed interferometry as we seek to cancel out (via interference) the reverberations from below the surface, leaving behind only those from the surface itself. Important to our proof-of-concept is the validation of the technique against other, similar, methods. The new survey technique is evaluated against the information obtainable from a 3D active source collected in the same area.

In terms of theoretical developments, the importance of the paper by Claerbout (1968) cannot be overstated. Claerbout demonstrated that the reflection response of a layered medium was exactly equivalent to the autocorrelation of the measured response. Wapenaar (2004) and Wapenaar *et al.* (2002, 2004) demonstrated that Claerbout’s layered earth conjecture was applicable to arbitrary 3D inhomogeneous acoustic or elastic media. This theory holds for both impulsive and white-noise sources, in addition to situations where the ambient noise sources are either at depth or the surface. Draganov *et al.* (2007, 2009) provides the earliest use of interferometry to uncover body waves for exploration. Dragonov *et al.* (2013) provides a thorough overview of recent work on the recovery of body wave reflectivity using interferometry.

In addition to the study by Snelling *et al.* (2013), a recent study by Boltz *et al.* (2014) indicated close to 200 events related to mining induced seismicity in a two week period alone at an active mine in Utah and detected over 1800 events in a 2 km<sup>2</sup> area over an eight month period. Valley *et al.* (2012) looked at the harmonic content of noise sources in an active mine and found a broad spectrum (0.00001 Hz to 1000 Hz) with significant power spectral amplitudes at the higher frequencies associated with body waves. Further, we speculate that surface waves at remote mines (where surface wave sources such as traffic or coastlines are not generally a problem for active source surveys) are minimal. The actual underground workings at Lalor are not known to the authors at this time; however, during the course of our survey we were informed that a number of drills were active in the subsurface for exploration and ore extraction purposes. In addition, a number of significant detonations (at least two) were occurring daily to sink the main shaft

over 1 m per day and to aid in exploration and mining. Taken together, we speculate that noise sources in the vicinity of an active mine such as Lalor may be potential sources for an interferometry survey and afford a reasonable chance to extract body waves from the ambient noise.

A few other requirements regarding the theoretical developments should be pointed out as we cannot address them at this time. The recording measurements should be in the far field of the sources. A smoothly varying medium must surround the noise-source boundary. The noise sources must illuminate the observation points with equal strength from all directions. And finally, there must exist at least two uncorrelated noise sources per wavelength (for a general inhomogeneous medium). Given that the acquisition and medium parameters of the Lalor interferometry survey are uncertain with respect to these requirements, it is nonetheless worthwhile to investigate the utility of interferometry for mineral exploration to minimize costs and field logistics. A 3D-3C active source seismic survey involves considerable amount of survey planning and permitting. At Lalor, 2.74 m wide shot lines were permitted, surveyed and eventually cut using heavy equipment to enable the shot hole drilling trucks to traverse the lines. A number of these costly issues can be avoided if a technique can be found that provides similar images, but only utilizes receivers.

### PASSIVE SEISMIC INTERFEROMETRY AT LALOR

The purpose of this study was to test and evaluate a new method of seismic exploration for ore deposits. VMS deposits are good targets for seismic surveys due to their anomalous body wave velocity and density of metallic minerals (sulphides). Whilst a number of studies have indicated that 3D seismic surveys similar to those acquired for oil and gas exploration would be a useful complement to the exploration strategy of any resource company, high cost of acquisition and processing, relatively few case studies and difficulties integrating results into an exploration program have prevented widespread adoption of the technique (see for example, Cheraghi *et al.*, 2012). A key factor inhibiting industry reception to seismic is the cost related to the deployment of seismic energy sources such as explosives or Vibroseis which can be both costly and difficult to permit and survey. We seek to develop a new exploration methodology that does not require the deployment of specific energy sources at the surface, but instead utilizes the natural or man-made (ambient) noise sources either nearby or far from the survey area to perform the same or similar role.

To test the feasibility of passive seismic interferometry to image ore deposits in the crystalline rock environment

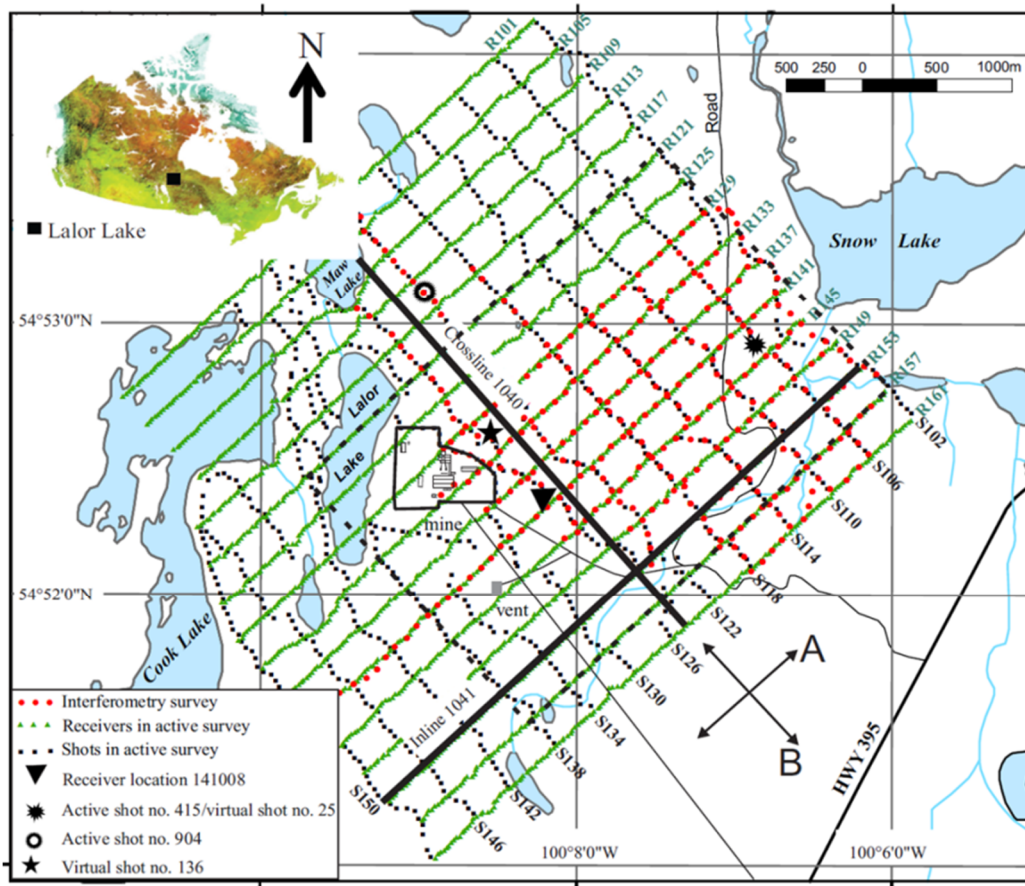


**Figure 17.** Map of the Lalor mining area showing shots (e.g., S102, S106, S110, ...) and receiver lines (R101, R105, R109, ...) of the active-source 3D seismic survey. The passive survey (red dots on Figure 1) was also acquired along the same lines, but covers a smaller area. The primary mine area and ventilation shaft are also shown in the figure. Direction A (southwest to northeast) and direction B (southeast to northwest) is shown on the figure. The DMO stacked sections along inline 1041 and crossline 1040 of the both active and passive surveys are shown in this paper. The dashed rectangle shows the outline of the 3D DMO stacked cube of the passive survey. Inline 1041 and crossline 1040 from the passive survey do not extend beyond this rectangle. Inset shows Canada map and the Lalor Lake area.

approximately 300 hours of ambient noise data were recorded on a grid of receivers over the Lalor mine, Canada, done in March 2013 immediately prior to the acquisition of a dynamite 3D seismic survey over the same area (see Figure 17). The active survey was acquired near the end of the ambient noise acquisition; therefore, it did not interfere with ambient noise measurements. Receiver stations of the passive survey are located along 9 parallel lines trending southwest to northeast (direction A, see Figure 17) and 7 parallel lines trending in the southeast to northwest direction (direction B, see Figure 17). Directions A and B coincide with the receiver and shot lines of the active survey, respectively (see Figure 17). The station spacing along each passive seismic line is about 100 m whereas the spacing between two successive lines is 360 m and 400 m for directions A and B, respectively. The passive survey covers an area of about 4 km<sup>2</sup> which corresponds to the northeast quadrant of the active survey. Table 5 shows the acquisition parameters for the passive survey.

The Lalor Lake deposit is located far from any densely populated areas and coast lines which are usually good

sources of ambient noise. The Town of Snow Lake (population of 800) located approximately 8 km northeast of the survey area is the closest settlement. The nearest large town (> 5000 people) is Flin Flon, 215 km west of the Lalor

**Table 5.** Acquisition parameters of ambient noise measurements in Lalor Lake area.

Instrument	OYO Geospace Seismic Recorder (GSR) units set to record for one month
No. of receivers	336
Sampling interval	2 ms
Direction A station spacing/line spacing	100 m/360 m
Direction B station spacing/line spacing	100 m/400 m
Geophone type/geophone frequency	Vertical component/10 Hz
Measuring area	4 km <sup>2</sup>
Total measuring time	~300 hours

**Table 6.** Processing steps applied to the retrieved shot gathers of the Lalor Lake area.

1.	Elevation corrections and set up geometry (the elevation datum is considered 310 m)
2.	Picking theoretical line of first arrivals based on the coordinates of virtual shots and receivers and considering velocity of 5.9 km/s.
3.	Top mute: 20 ms after the theoretical line of first arrivals.
4.	Apply median filter to remove potential surface and shear waves (at velocities of 2.5 & 3 km/s)
5.	Sorting to CDP domain
6.	Trace balancing
7.	Velocity analysis in 5-8.5 km/s range(iterative)
8.	Residual static correction
9.	DMO corrections (5.5-6.5 km/s)
10.	Stack
11.	FX-deconvolution

Lake deposit (see Figure 18). Access to the mine is along a gravel road with generally little traffic. The nearest railroad is 65 km southeast of the Lalor Lake deposit and the area is not an active zone in terms of earthquakes. The only significant activities likely generating seismic noise are underground drilling, blasting, and hauling of minerals associated with the ongoing exploration and exploitation of the deposit (see Figure 17 for the mine location).

Ambient noise was continuously recorded in SEG-D format at each receiver location of the study area for a period of 300 hours. Subsequently, noise records were divided into one hour panels for a total of 300 panels of one hour per receiver location. To better investigate the ambient noise content, we analysed the RMS amplitude for each hourly panel along all lines in directions A and B (see Figure 17 for the directions). The RMS amplitude investigation shows that underground explosions which mainly occur near 6 am and 6 pm are dramatically changing the energy level along each receiver line. Other hours are quiet or only few activities happen. Power spectral density is also calculated for frequencies between 1 and 250 Hz (the Nyquist frequency for the 2 ms sampling rate in the survey) for hourly data along the survey lines. The calculated power demonstrates that the frequency range of about 2-35 Hz contains the highest level of energy for the entire noise recording time. The noise panels were also visually inspected after the application of a 2-35 Hz band-pass filter. Some noise panels show groups of weak steeply-dipping events with high apparent velocities (about 6 km/s) and also some hyperbolic events with apparent velocity of about 4 km/s. Both the steeply-dipping and hyperbolic events could result from surface or body waves. Due to the general quietness at surface in the Lalor area and the relatively fast apparent velocity of the events, we favour body waves

related to deep mining activity. The beamforming analysis over the grid of receivers provides in the frequency ranges of 1-3 Hz, 10-13 Hz, and 23-25 Hz shows evidence of both low velocity surface waves (velocity less than 3 km/s) originating from the northeast and higher velocity body waves (velocity higher than 3.2 km/s) from the mine. Our interpretation is consistent with the two main sources of ambient noise in the area, namely the underground mining activities and human activities in Snow Lake (8 km northeast of the area).

To create virtual shot gathers from ambient noise, a Green's function is retrieved between each pair of receiver locations by calculating of cross-correlation. The cross-correlated noise produces a Green's function at positive and negative time lags, corresponding to the causal and acausal parts of the Green's functions. Prior to cross-correlation, the noise energy in each panel was filtered to preserve the frequency content between 2-35 Hz. This frequency bandwidth was chosen based on power spectral density calculation, visual inspection of the noise panels, and the beamforming analysis discussed earlier. All traces of each panel were subsequently normalized by applying a trace-by-trace process to ensure that energy from all subsurface sources was equally weighted. For each hourly noise panel, the cross-correlation is calculated for each possible pair of receiver locations (i.e., 336 receiver locations in the area representing about 110000 calculations/panel for a total of 33 million calculations done over all 300 noise panels). For one panel, the cross-correlation of noise at a specific receiver with noise at other receiver locations forms a virtual shot gather, as if a shot was acquired at that specific receiver location. The final virtual shot gathers were obtained by summing the causal and acausal parts of the cross-correlated signal at each receiver pair, and then by summing virtual gathers from all panels. The decision to sum the causal and acausal parts of the signal is based on the beamforming analysis which demonstrates noise sources from different directions. A total of 336 virtual shot gathers were generated following this procedure. The virtual shot gathers were processed following a conventional seismic processing flow to evaluate the applicability of the ambient noise interferometry for seismic imaging in crystalline rocks. Because of the complex structures in the study area and the absence of clear reflected waves in the virtual shot gathers, interpretation of the seismic section is challenging. We applied both 2D and 3D processing approaches. In both cases, processing focused on the imaging of high-velocity reflections (with moveout velocities >5 km/s) typical of body-waves propagating in crystalline rock environments. Table 6 shows the key steps of the 2D and 3D processing of the virtual shot gathers. The steps were kept as close as possible to the processing flow used for the active data.

The availability of the coincident active-source 3D data provides an opportunity to compare the passive processing results directly with the active source data. However, the bandwidths of the sections derived using the two ap-

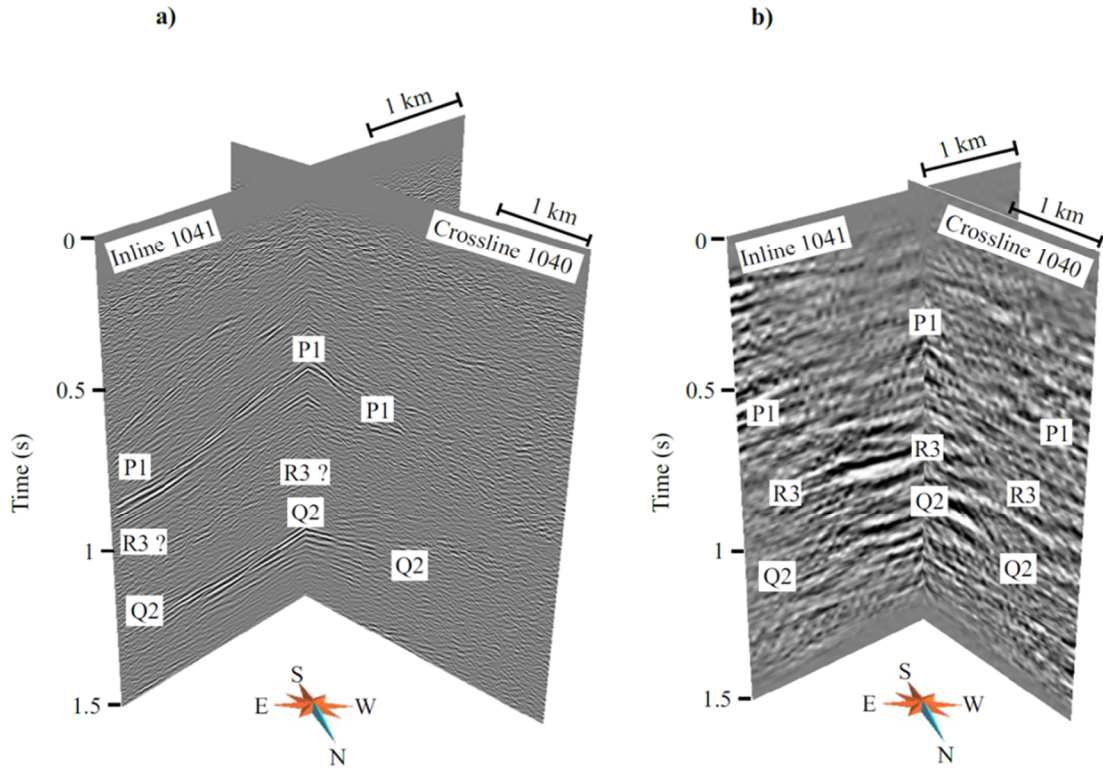


**Figure 18.** The DMO stacked sections along inline 1041, crossline 1040 (see Figure 17 for the locations). (a) The active-source survey. (b) The passive interferometry survey. Note that the minimum frequency in (a) is 30 Hz. See text for interpretation of P1, Q2, and R3 reflections.

proaches differ as frequencies less than 30 Hz are filtered out of the active P-wave data while the highest frequency in the passive data is 35 Hz. The passive 3D DMO stacked cube covers a smaller area than the active 3D DMO stacked cube and mostly has lower image quality (see Figure 17 for the location of the passive survey DMO stacked cube). A comparison of the 3D processed images along inline 1041 and crossline 1040 of both surveys is shown in Figure 18. Reflections P1 and Q2 are imaged in both inline and crossline directions of the active survey image (Figure 18a). Reflection P1 is a coherent and continuous moderately-dipping reflection in the inline direction of the active survey whereas it is shorter (only about 1 km long) and has shallower dip in the crossline direction (Figure 18a). Only the shallowly-dipping parts of P1 are imaged with the passive seismic survey (Figure 18b). In particular, parts of P1 near the end of inline 1041 and close to the intersection with crossline 1040 are imaged (see Figure 18b). P1 appears to extend further in the crossline direction of the passive cube. However, this part of P1 is not observed on the active seismic data. The dip of P1 on the passive crossline (Figure 18b) is also very close to the dip observed on the active data (Figure 18a). Reflection Q2 is imaged as a subhorizontal reflection in inline and crossline directions of the active and passive survey images (Figure 18). Q2 shows higher amplitude in Figure 2b at intersection of the inline and crossline at 1.25 s. Reflection R3 is a high amplitude reflection between P1 and Q2 near 0.75-1 s of the passive survey image (Figure 18b). R3 is mostly sub-horizontal on inline

1041 but has a slight dip to the northwest on crossline 1040. In comparison, R3 is not clearly imaged on the active seismic cube (Figure 18a).

### CONCLUSIONS

Ambient noise acquired over the Lalor Lake mining area has provided an opportunity to test passive seismic interferometry over a complex crystalline rock environment. The underground mining activity and human activity at the Town of Snow Lake are the main sources of the ambient noise. The recorded ambient noise from these noise sources comprises both surface and body waves. Estimated Green's function obtained by cross-correlating of the recorded noise between all possible pair of receivers forms the virtual shot gathers used in this survey. Comparison of the 3D processing results of the passive and active survey images is encouraging. In general, results of the passive survey show fewer reflections. However, best results for 3D passive processing were obtained for subhorizontal reflections.

# MODE-CONVERTED VMS ORE LENS REFLECTIONS IN VERTICAL SEISMIC PROFILES AND 3D FINITE DIFFERENCE MODELING FROM FLIN FLON, MANITOBA, CANADA

DAVE MELANSON<sup>1</sup>, DON WHITE<sup>1</sup>, CLAIRE SAMSON<sup>2</sup>, GILLES BELLEFLEUR<sup>1</sup>, ERNST SCHETSelaar<sup>1</sup>, AND DOUG SCHMITT<sup>3</sup>

<sup>1</sup> Geological Survey of Canada, 615 Booth Street, Ottawa, Ontario, K1A 0E9

<sup>2</sup> Department of Earth Sciences, Carleton University, 1125 Colonel By Drive, Ottawa, Ontario, K1S 5B6

<sup>3</sup> Department of Physics, University of Alberta, Edmonton, Alberta, T6G 2E1

## INTRODUCTION

Vertical seismic profiles (VSP) were acquired in 2006 as part of a broader seismic exploration program undertaken in the Flin Flon mining camp in Manitoba, Canada (White *et al.*, 2012). The Flin Flon mining camp provides an excellent test-bed to evaluate the ability of VSP methods to detect known volcanogenic massive sulphide (VMS) ore lenses. Three-component VSP data acquired in an open borehole adjacent to the main orebodies of the camp are analyzed here for this purpose. In this case VSP acquisition was limited to the upper half of the borehole. Thus, here we rely on full elastic seismic simulations (Bohlen *et al.*, 2011) conducted for a detailed 3D geological model to correlate the observed VSP reflections with the expected response

stacked intervals of the Millrock member contain VMS ore lenses with varying grades, textures and composition of ore. The VMS mining camp in Flin Flon provides a suitable locality to test the proposed approach. Sufficient control on the geometry of the ore lenses and the host crystalline geology exists such that detailed 3D geological models have been previously built. This study focuses on data from open borehole 4Q66W3.

## VSP DATA PROCESSING

An initial study of the zero-offset dynamite-source data found correlations between strong reflectors along the borehole and some of the primary lithological boundaries obtained from drill cores (Dieteker *et al.*, 2007). The

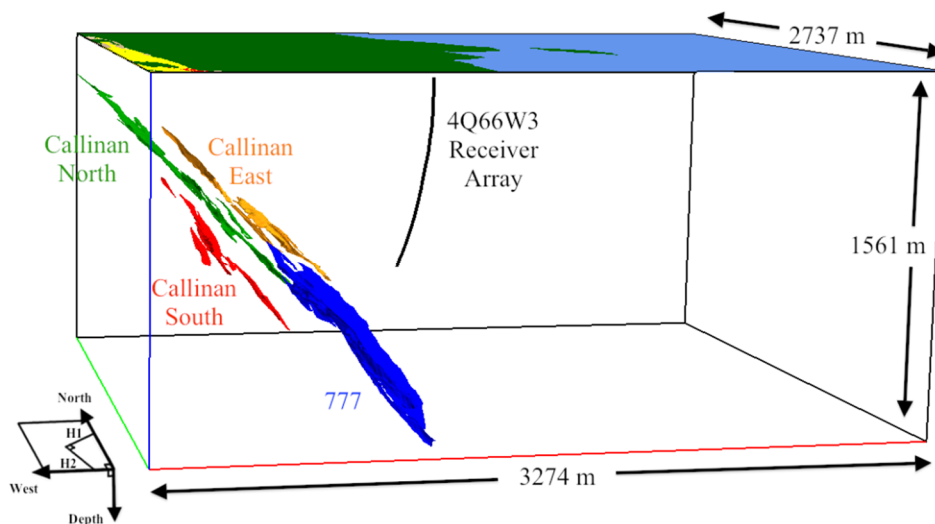


**Figure 19.** Perspective view of the receiver array and ore zones, based on stratigraphic level located in the 3D voxel model. It should be noted that these zones are not the same as those identified by Hudbay Minerals Inc. (e.g. Tessier and O'Donnell, 2001). Ore zones were used together and in individual simulations to further constrain the origins of ore zone reflections (Melanson, 2014).

from the ore lenses. In this project, VSP data was acquired, processed and compared with simulation results of models of increasing complexity to answer the question: Does VSP detect the orebodies?

The Flin Flon Paleoproterozoic greenstone belt is richly endowed with VMS deposits, including the 85.5 Mt Flin Flon-Callinan-777 ore system. Chalcopyrite, pyrrhotite and sphalerite-rich ore lenses are hosted in altered rhyolites of the Millrock member, which lies between the footwall basalts and mafic volcanoclastics of the Flin Flon formation and the hanging wall basalts of the Hidden and Louis formations (Schetselaar *et al.*, 2010). At least three thrust-

azimuthal orientation of the horizontal sensors during acquisition is variable due to the uncontrolled rotation of the geophone sondes as they are moved from level to level. To achieve consistent alignment of the horizontal component data, two raw horizontal components for each depth level were mathematically rotated to maximize and minimize, respectively, the first arrival P-wave energy from a far-offset dynamite source (DiSiena *et al.*, 1984). This resulted in two horizontal components that are aligned to (H1) and perpendicular to (H2) the direction between the borehole and the far-offset source location (Figure 19). Accounting for the location of the far-offset source location, H1 and H2 are aligned at  $\sim N68^\circ E$  and  $N158^\circ E$ . Data rotation was

**Table 7.** Physical rock properties used for modeling in this study. ‘HPL Core’ indicates measurements from core taken at the Dalhousie University High Pressure Laboratory. Other values are based on downhole measurements with the surveyed borehole indicated. All S-wave velocities were calculated using a Vp/Vs ratio from HPL core measurements.

Rock Type	Density (kg/m <sup>3</sup> )	From	P-Wave Velocity (m/s)	From	P-wave Impedance (kg/m <sup>2</sup> s)	S-Wave Velocity (m/s)	From	S-wave Impedance (kg/m <sup>2</sup> s)
coherent rhyolite	2740	HPL Core	6008.9	GSC 4Q66	1.65E+07	3609.2	Core Vp/Vs	9.89E+06
mafic fragmentals	2824	GSC 4Q66	6013.7	GSC 4Q66	1.70E+07	3612.1	Core Vp/Vs	1.02E+07
lapilli tuff	2865	HPL Core	6031.9	GSC 4Q66	1.73E+07	3623.1	Core Vp/Vs	1.04E+07
argillite	2830	HPL Core	6180.8	GSC 4Q66	1.75E+07	3712.5	Core Vp/Vs	1.05E+07
massive sulphide ore	4360	HPL Core	6117.9	DGI T7X074	2.67E+07	3674.7	Core Vp/Vs	1.60E+07
meta-basalt	2955	HPL Core	6058.3	GSC 4Q66	1.79E+07	3638.9	Core Vp/Vs	1.08E+07
meta-sandstone	2745	HPL Core	5696.5	DGI 4Q83	1.56E+07	3421.6	Core Vp/Vs	9.39E+06

performed using public domain DSISoft processing software (Beaty *et al.*, 2002).

Each component of the rotated field data was processed individually using GLOBE Claritas software. The application of notch filters was particularly important in reducing the strong electrical noise (60 Hz and harmonics) that can be clearly observed in the raw data. Electrical noise was particularly strong on the vertical component where the 60 Hz and 180 Hz amplitude peaks were ~ 15 – 20 dB

Since 4Q66W3 does not intersect any of the ore lenses, corresponding reflections will display an apparent velocity in the shot gathers that is controlled by the 3D geometry of the reflectors and the receiver array. In general, reflections in the field VSP data are discontinuous and can be difficult to trace across the shot gather. The processed shot gathers show very little energy from the direct waves, reduced electrical noise and an enhanced reflected wavefield when compared with the raw shot gathers. The horizontal component shot gathers do not show as much reflectivity as

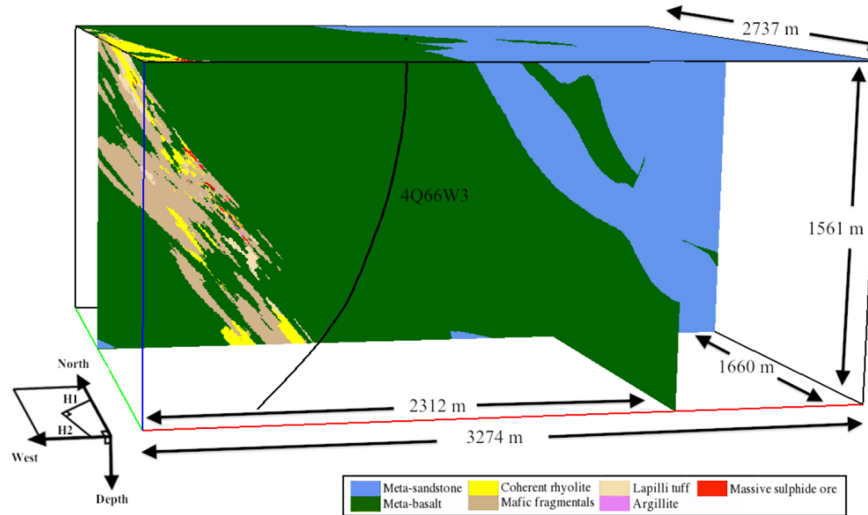


**Figure 20:** Perspective view of the 3D voxel model displaying all geological units. The ore-hosting Millrock member (yellow and tan) is seen on the left, dipping towards the East, borehole 4Q66W3 is included in black and the edge of the Missi metasedimentary basin (blue) is shown on the right.

above the nominal signal level, whereas amplitude peaks of only 10 – 12 dB and 5 – 7 dB were observed for the H1 and H2 horizontal components, respectively. *F-k* filters were used to remove as much of the direct wavefield as possible. A full-trace amplitude balance and *f-x* deconvolution attenuated random noise and sharpened the reflected wavefield. Finally, a 50 ms static shift was applied to correct a known triggering delay and the data were displayed using automatic gain control (AGC). A similar processing sequence was applied to the horizontal component data, except that the mute window in the *t-x* domain included the direct S-waves as well as the direct P-waves.

the vertical component, but the observed events are more distinct.

### 3D FINITE DIFFERENCE MODELING

Computer simulations of the seismic response were conducted for detailed 3D geological models to allow comparison with the seismic events observed in the field VSP data, with a particular focus on reflections from the known ore zones (Figure 19). Several raster-based 3D voxel models were constructed based on geological maps, borehole lithological logs and 2D and 3D seismic data (Schetselaar *et al.*, 2010). For each of the 7 rock types included in the various models, density, P-wave velocity

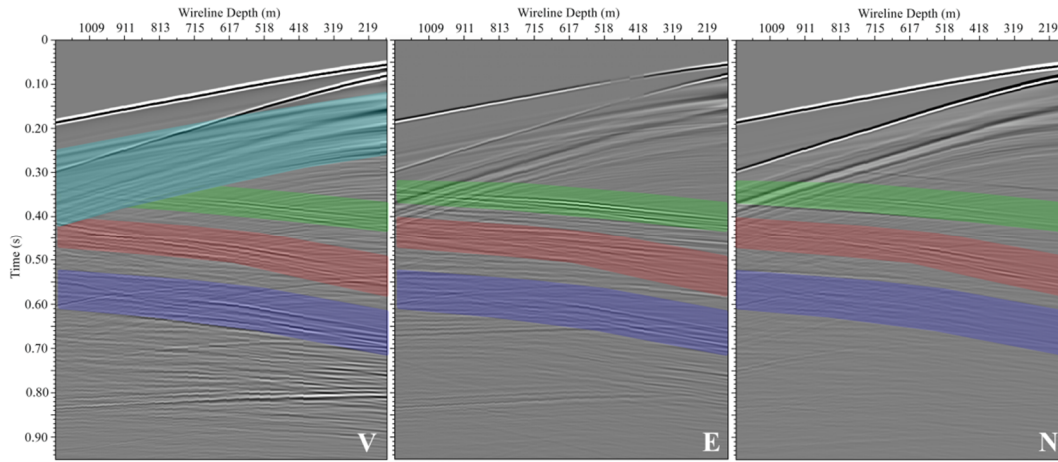


**Figure 21:** a) vertical (left), b) easting (center) and c) northing (right) particle velocity shot gathers from the lithological model, which includes all 7 major geological units. The light blue region represents downgoing reflections from the Missi basin. There are strong early downgoing reflections (annotated light blue) of surface waves associated with the boundary of the Missi metasedimentary basin, but these do not interfere significantly with the ore zone events. These results indicate that the geometry of and physical properties measured by the field VSP survey will potentially produce an ore zone signature in the data. With these modeling observations in mind, we can now attempt to correlate some reflections between the modeled and field VSP data.

and S-wave velocity values needed to be specified for finite difference modeling (Table 7). These values were determined from laboratory measurements of core samples and downhole geophysical logs from several Flin Flon boreholes including 4Q66W3.

Much of the Callinan deposit has been mined out and backfilled with a low-density material. Intense chlorite-carbonate and clay alteration zones exist and strong variability in mineralogy and texture of the ore zones are known (Tessier and O’Donnel, 2001). We assumed that none of these factors would significantly affect the timing, shape or apparent velocity of observed reflections. Thus, the only differences expected in the field data would be a more complex response and an opposite polarity of reflected waves from the mined out lenses when compared to the modeled VSP data.

The modeling software used in this study was SOFI3D (Bohlen *et al.*, 2011), a 3D viscoelastic finite-difference seismic modeling program. The outputs of each simulation are shot gathers displaying divergence (i.e. P-wave propagation), curl/rotation (i.e. S-wave propagation), pressure and 3-component particle velocities and 3D wavefield visualizations displaying divergence or curl. Comparing shot gathers from simulations with different geological units demonstrated specific seismic events associated with those units as well as their anticipated location in the field VSP data. 3D wavefield visualizations allowed tracing of events back to their point of origin and also identified their mode of propagation (i.e. P-P scattering, P-S conversion, etc.). These observations were then compared to the fully processed field VSP data to identify ore zone events based on their timing, shape and apparent velocities.

Simulations were conducted for a set of models covering a range of geological complexity. The initial simulations were conducted for models where only the ore zones were embedded within a uniform background of meta-basalt (Melanson, 2014). The objective was to understand the fundamental orebody response before considering more detailed models. The complexity of the models was increased for each subsequent simulation culminating in a model which included all 7 of the major lithological units, shown in Figure 20.

In Figure 21, three bands of composite ore zone reflections can be identified corresponding to the PP (green), PS (red) and SS (dark blue) reflected phases based on their timing, apparent velocity and particle motion. These bands are comprised of groups of similar ore zone reflected phases. All of the reflected phases can be identified on each of the geophone components. However, the shear-wave reflections (PS and SS) are most prominent on the vertical-component whereas the PP phase is most prominent on the horizontal components. This is a consequence of the sub-vertical attitude of the wavefront as it approaches the borehole. The PP particle motion, which is orthogonal to the wavefront should be mostly horizontal and a vertical-component of shear would be expected.

**DATA COMPARISON AND DISCUSSION**

The data from the field VSP survey is considerably more difficult to interpret due to the generally low signal-to-noise ratio and discontinuity of the observed reflections. The vertical component field VSP data (Figure 22a) shows many discontinuous reflections with similar amplitudes, making correlation and identification of specific events difficult. By comparison, the horizontal component field VSP data (Figure 22b, c) show fewer reflections but they appear much

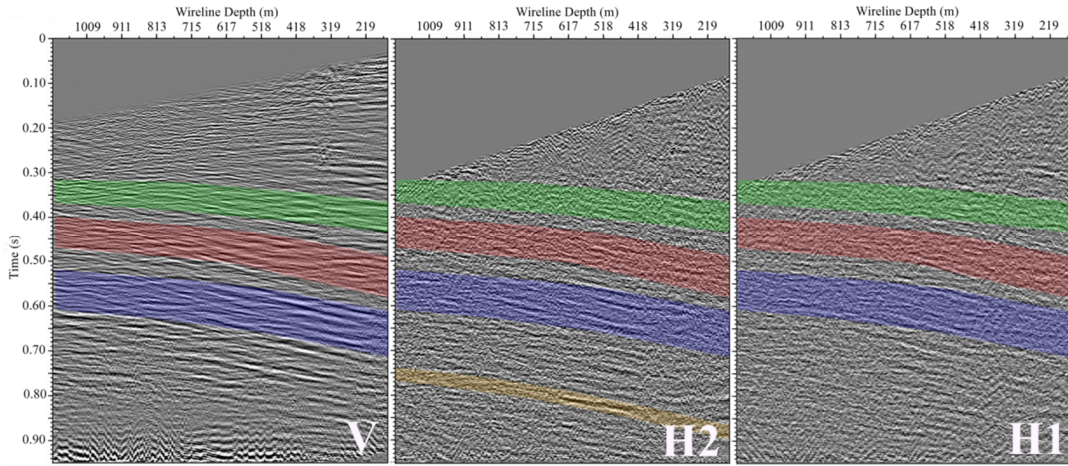


**Figure 22.** a) vertical (left), b) H2 horizontal (center) and c) H1 horizontal (right) component field data. The orange-annotated event does not correlate with any modeled events.

stronger against background noise levels (particularly on the H2 component, Figure 22b). To allow direct comparison of the field VSP data with the synthetic results, travel time curves for the ore zone events determined from the synthetic shot gathers are overlain on the field data (Figure 22). The following observations can be made: 1) The PP phase (highlighted by the green band in Figure 22) is not apparent on either the vertical- or horizontal- components except perhaps for the shallowest receivers. 2) Calculated travel times and apparent velocities for the PS (red band) and SS (dark blue band) phases show the best correlation with prominent reflections observed on all components of the field data, but particularly for the vertical and H2 components. Based on this comparison, the strongest reflections in the field data correspond to the SS phase from the ore zones. 3) There are a few strong reflections observed between the PS and SS phases on the horizontal field data. These are consistent with the increased complexity in this zone observed on the synthetic data for the lithological model. A single strong event, most noticeable in the H2 horizontal component field data (annotated with orange in Figure 22b) is similar to identified ore zone events, could not be correlated with any modeled event and potentially represents a new exploration target.

Surprisingly, the PP phase from the ore zones is not observed in the field data. In contrast, the SS phase and to a lesser extent the PS phase are observed. The modeling results suggest that all three phases should be observed. The simplest explanation for this is that the magnitude of the P-wave impedance contrast incorporated in the model for the “ore zones” is larger relative to that assigned for the S-wave impedance contrast than is the case for the actual subsurface. This would result in the model predicting a larger PP amplitude relative to the PS and SS phases. As noted earlier, there is significant uncertainty in the physical properties of the ore zones as they have been back-filled with an assumed low-impedance material.

In regard to the phases that are well-observed in the field data (SS and to a lesser extent PS) the modeling results suggest that they should be most prominent on the vertical component. Inspection of the field data in Figure 22 indicates that this is not the case. However, we refrain from ascribing too much significance to this observation as the signal-to-noise ratio is variable amongst the different data components. As noted earlier, the raw vertical-component data had a significantly higher level of electrical noise (by as much as 15 dB) as compared to the raw horizontal component data, and although this noise is greatly attenuated during processing, some residual degradation effect remains.

These observations also demonstrate the importance of 3-component geophones in such applications, as the seismic response has strong directivity and all phases (PP, PS, SS) can have particle motion in any direction due to the complex subsurface geometry and the influence of a deviated borehole. For exploration purposes, the receiver array should be made as long as possible. For example, the 777 deposit was not observed in this study as it was too deep and steeply dipping relative to the receiver array. Also, although detection is possible, it is critical to know where (how far, and in which direction) the target is. With a multi-source VSP, this could potentially be determined based on directivity of arrival and may be the focus of further study.

**CONCLUSIONS**

The strongest and most identifiable of the ore zone reflections appear to be shear wave reflections (SS) and mode-converted reflections (PS), present on all three components of the field and modeled VSP data. Because of the number and complex shape of the ore zones and the measured reflection coefficients, strong reflected shear waves were expected from their contacts. Such shear waves are best captured by geophones oriented perpendicularly to the wave propagation direction, which explains the strong

response observed in the horizontal component field VSP data.

This study shows that VSP surveys have the potential to image VMS lenses in a greenstone host assemblage. The environmental challenge of cultural and electrical noise from an active mine and poor coupling of the geophone tool lead to an overall low signal-to-noise ratio. In this case, the VSP response from the ore lenses is not as prominent as initially anticipated. However, reflections originating from some of the VMS lenses were identified and interpreted in each component of the zero-offset dynamite source VSP data. With the significant investment required for drilling deep targets, it is important to extract as much geological information from boreholes as possible. VSP can provide a means to image dense bodies in the subsurface, even in challenging seismic environments.

# ACQUISITION, PROCESSING, AND INTERPRETATION OF GRAVITY DRILL HOLE DATA

ERNST SCHETSelaar<sup>1</sup> AND PEJMAN SHAMSIPOUR<sup>1</sup>

<sup>1</sup> Geological Survey of Canada, 615 Booth Street, Ottawa, Ontario, K1A 0E

## BACKGROUND

A high-precision borehole gravity (BHGM) survey was acquired in five drill holes intersecting the host-rock periphery of the Lalor VMS deposit. The benefits of using borehole gravity for exploration were recognized more than 64 years ago by Smith (1950). Considering that the decay of the gravity field is inversely proportional to the squared distance between an anomalous mass and the gravimeter, it is obvious that the potential for detecting a local anomalous mass at depth is significantly enhanced in comparison to surface or airborne gravity surveys. The first borehole gravity surveys were limited to petroleum applications where gravimeters were deployed in large-diameter and near vertical boreholes (see for example McCulloh *et al.*, 1967; McCulloh 1965; LaFehr 1983; Popta *et al.*, 1990). A new generation of borehole gravimeters (GRAVILOG) has recently been developed that is small enough to be deployed in boreholes with NQ (47.6 mm core) diameter (Nind *et al.*, 2007) which is a commonly-used standard in mineral exploration. This innovation made it possible to conduct the gravity drill hole survey of the Lalor deposit.

In February 2014 borehole gravity data were acquired by Abitibi geophysics in 5 drill holes intersecting the host-rock envelope of the Lalor deposit. These drill holes were selected from a limited subset of surface exploration drill holes that were left open in the periphery of the massive sulphide ore zones (all the other drill holes were cemented to protect the excavation of mine workings at depth from infiltrating surface water). The objectives of the drill hole gravity survey were to interpret the density distributions associated with geological formations in the hanging wall and footwall of the VMS deposit and to identify additional anomalous masses potentially associated with massive sulphide mineralization lying outside the drill-intersected portion of the deposit. The geological significance of the gravity drill hole data was evaluated by comparing the derived apparent density logs with co-located lithofacies and immobile element ratios logs computed from drill hole lithochemistry. In addition, gamma-gamma density logs that were previously acquired in a multi-parameter geophysical log survey, provided a secondary information source for mapping the subsurface density distribution and aided the correlation of apparent density anomalies across larger distances.

Four of the surveyed drill holes (DUB202, DUB280, DUB282 and DUB287) intersect geological formations in the down-plunge extent of the Lalor sulphide ore lenses, while one drill hole (DUB279) intersects the host rocks up-plunge from the known sulphide ore lenses (Figure 1). The GRAVILOG sensor was lowered in each borehole using a cable-winch and left one hour to stabilize. Each borehole

was logged twice in one direction for quality control. At least five readings were taken at each station. More readings were recorded when the difference between them exceeded 3  $\mu$ Gal.

## Corrections and reductions applied to gravity drill hole data

Corrections of the borehole gravity measurements were conducted using routine processing procedures. After obtaining the observed gravity subsequent to the instrument corrections (for drift, tidal, temperature and sensor rotation) the Bouguer anomaly logs were computed from:

$$G_B = G_{obs} - F - BE \quad [1]$$

Where F is the free-air gradient that compensates for the increase in gravity with depth (free-air correction):

$$F = -(0.308769 + 0.0004398 \sin^2 \varphi)h + 7.2125 * 10^{-8}h^2 \quad [2]$$

Where  $\varphi$  is the latitude of the borehole and h is the depth of the stations in m and BE is the Bouguer effect for drill hole gravity data (twice the Bouguer effect of surface gravity data) and defined by:

$$BE = -4\pi G\rho h \quad [3]$$

Where  $\rho$  is the slab Bouguer density and G the universal gravitational constant.

## Computation of apparent density logs

The main application of borehole gravity measurement is to determine the mean bulk density of the geology formations where the borehole is traversed. Smith (1950); Hammer (1950) and LaFehr (1983) provide the theoretical basis for the method of governing bulk densities. Under the assumption of a horizontally-layered earth, the mean bulk density of the rock formations between two stations is proportional to the gravity gradient measured over these stations minus the free-air vertical gradient of the Earth's gravity within a radius of about five times their vertical spacing (Nind *et al.*, 2007):

$$\rho_{n+1|n} = \frac{1}{4\pi G} \left\{ F - \frac{(g_{n+1} - g_n)}{(z_{n+1} - z_n)} \right\} \quad [4]$$

Where  $\rho_{n+1|n}$  is the rock density between depths  $z_n$  and  $z_{n+1}$ , F is the free-air gradient,  $g_{n+1} - g_n$  is the difference in gravity readings at depths  $z_{n+1}$  and  $z_n$  respectively and G is the universal gravitational constant. It should be noted that the

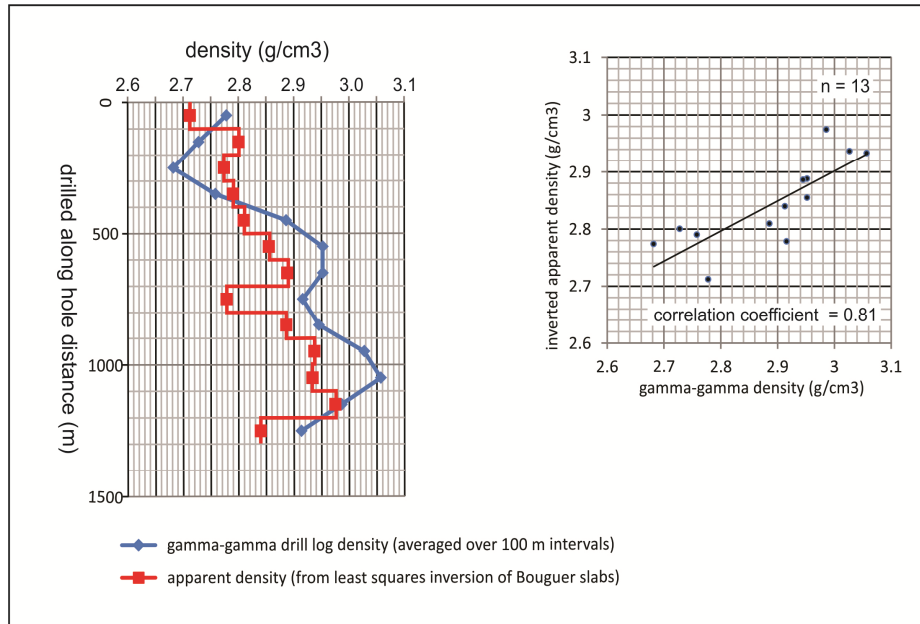


**Figure 23.** Apparent density and gamma-gamma density logs of borehole DUB202. Inset shows scatter plot between apparent and gamma-gamma densities.

density obtained in this calculation is an apparent density because it is based on the assumption of a horizontally-layered earth. As a result in settings with dipping geological formations, the apparent density anomaly can, dependent on the geological structure, be significantly offset from the causative mass intersected in the drill hole. MacQueen and LaCoste (2007) introduce a method to calculate densities using inversion techniques to accommodate for the influence of interval densities above and below the density interval considered. Application of this method can be useful to recover densities at station spacing as small as one meter.

#### INTERPRETATION OF GRAVITY DRILL HOLE DATA

In order to support geological interpretation of the apparent density logs, co-located lithofacies and Zr/TiO<sub>2</sub> immobile element ratio logs were compiled from the industry drill hole database. Detailed lithofacies descriptions of FROM-TO intervals of the industry drill hole database were encoded into 16 lithofacies classes. This classification categorized volcanic and volcanoclastic rocks into felsic, intermediate and mafic classes of volcanic rock composition. The volcanoclastic rocks were further subdivided into coarse tuff breccia and finer-grained lapilli tuff and tuff lithofacies. Intensely hydrothermally-altered and metamorphosed equivalents of these rocks were subdivided into schist and gneiss, while the remainder of rock units intersected in the drill holes were classified into argillite, gabbro, fault rocks, quartz veins and sulphide ore, yielding a total of 16 lithofacies classes. The Zr/TiO<sub>2</sub> immobile element ratio, routinely used as a proxy to differentiate volcanic protoliths of felsic, intermediate and mafic composition (Winchester and Floyd, 1977) was particularly useful to interpret the apparent density logs across drilled intervals of gneiss and schist in the

hydrothermally-altered footwall of the deposit where it is virtually impossible to visually recognize the volcanic/volcanoclastic rock of origin (i.e. protolith).

#### DUB202

Borehole DUB202 is the only drill hole for which a gamma-gamma density log is available. Figure 23 shows the apparent density and gamma-gamma density log, the latter being averaged over 100 meter intervals to facilitate comparison with the apparent density intervals. Note that although the minimum and maximum amplitudes of the averaged gamma-gamma density logs exceed the extremes of the apparent density logs, the log patterns are broadly similar. Moreover, the apparent and averaged gamma-gamma density values appear to be highly-correlated (Figure 23). The difference in amplitude range is obviously due to the much larger rock volume sampled in the drill hole gravity measurements around the drill hole in comparison to the rock volume sampled in the gamma-gamma density log survey. The gamma-gamma density log, in turn, is highly correlated with the densities of 32 rock samples that were co-located within 10 cm from the stations of the geophysical wireline log (Figure 24). The rock density samples show distinctly higher density for sulphide ore samples and a linear increase from felsic to intermediate to mafic volcanic host rock compositions. The gneiss and schist samples span this full range, suggesting that the density variations of their volcanic protoliths from which they were derived were preserved (Figure 24).

A distinct approximately linear trend from 2.72 to 2.98 g/cm<sup>3</sup> can be observed in the apparent density log from surface to 1200 m (Figure 25), which is likely due to a regional background effect, in which density gradually

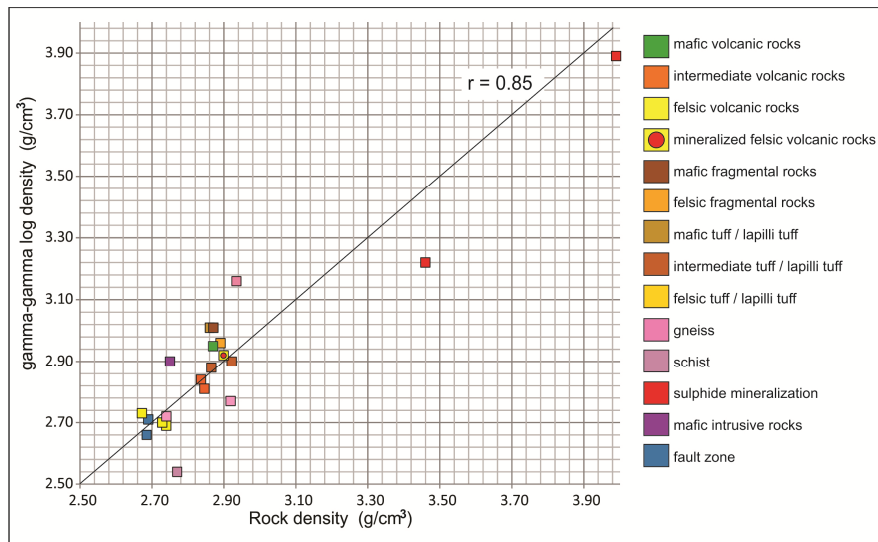


**Figure 24.** Scatterplot of gamma-gamma density logs averaged over 100 m intervals versus drill core sample densities co-located along borehole DUB202 within 0.1 m.

increases with depth. Higher spatial frequency apparent-density variations, superimposed on this trend, approximately correspond to alternating mafic and felsic volcanic and volcanoclastic rock units in the hanging wall of the Lalor VMS ore zones. Apparent density values ranging between 2.72 – 2.82 g/cm<sup>3</sup> correspond to felsic volcanic units (rhyolite and rhyodacite), whereas apparent-density values between 2.82 and 2.98 g/cm<sup>3</sup> correspond to mafic volcanic (basalt, andesite) and mafic volcanoclastic units (mafic tuff breccia). An acute decrease in apparent density at a drilled distance of 1200 m occurs 50 m below the contact between mafic volcanoclastic rocks in the hanging wall of the Lalor deposit and schist and gneiss in its footwall. The significant decrease in apparent-density of approximately 1.0 g/cm<sup>3</sup> across this contact is readily explained by the high Zr/TiO<sub>2</sub> ratio between 1220 and 1340 m (Figure 25), which suggest that the gneisses were derived from a felsic volcanic protolith with preservation of a relatively low density of 2.80 g/cm<sup>3</sup>.

Another local apparent-density low occurs at a depth of 1420 m. This low corresponds to another more localized Zr/TiO<sub>2</sub> peak, suggesting that this relatively thin interval also corresponds to a gneiss with a felsic volcanic protolith. The spatial association between apparent density lows and felsic volcanic rocks are also evident on DUB280 and DUB282. The highest apparent density anomalies between 3.01 and 3.02 g/cm<sup>3</sup> occur at depths of 1450 and 1520 m and correspond to gneisses of mafic composition. Their anomalously high values compared to rock intervals of mafic composition elsewhere along the hole may suggest that they are also due to sulphide ore in the vicinity of the drill path of DUB 202.

#### DUB279

The apparent-density log of DUB279 (Figure 26) shows a significant increase from 2.83 to 2.89 g/cm<sup>3</sup> at 155 m

corresponding to the contact between felsic volcanic and mafic volcanoclastic rocks and an abrupt decrease of the Zr/TiO<sub>2</sub> log. A highly variable interval from 600 to 800 m cannot be unequivocally correlated to the corresponding lithofacies interval of intermediate and felsic volcanic rocks. Also the Zr/TiO<sub>2</sub> log shows peaks that are only locally consistent with volcanic rocks of intermediate composition. The apparent density log shows a variable but a high average density of approximately 3.0 g/cm<sup>3</sup> between 820 and 940 m, corresponding to mafic volcanoclastic and volcanic rocks in the lithofacies log. At 840 m a local anomaly of 3.12 g/cm<sup>3</sup> (Figure 26) which is the highest apparent density value obtained for the gravity drill hole survey, appears to correspond to a 20 m thick weakly mineralized mafic tuff unit and a carbonate-altered pyrrhotite-bearing argillite. These thin lithofacies intervals, exhibiting disseminated mineralization only, however, unlikely explain this significant apparent-density anomaly. Considering the proximity of the ore horizon at this structural level, the alternative interpretation is that the anomaly is due to more massive sulphide ore in the vicinity of the drill hole. To corroborate this interpretation the excess mass was computed from the corresponding peak-to-peak Bouguer anomaly of 0.661 mGal, assuming a spherical causative body not intersected in the drill hole Blakely (1996):

$$M = 0.1A.D^2 \quad \text{with } R = 0.7D \quad [5]$$

Where M is the excess mass in tonnes, A = the peak-peak amplitude (in  $\mu$ Gal), D is the peak-peak distance in meter and R is the radial distance from the center of the anomaly to the center of mass in meters (Nind *et al.*, 2007). Using this formula yields an excess mass of 0.7 mT at a distance of approximately 100 m from the borehole, which would be consistent with the interpretation that the Bouguer anomaly is caused by a nearby mass not intersecting the borehole, potentially representing sulphide mineralization.

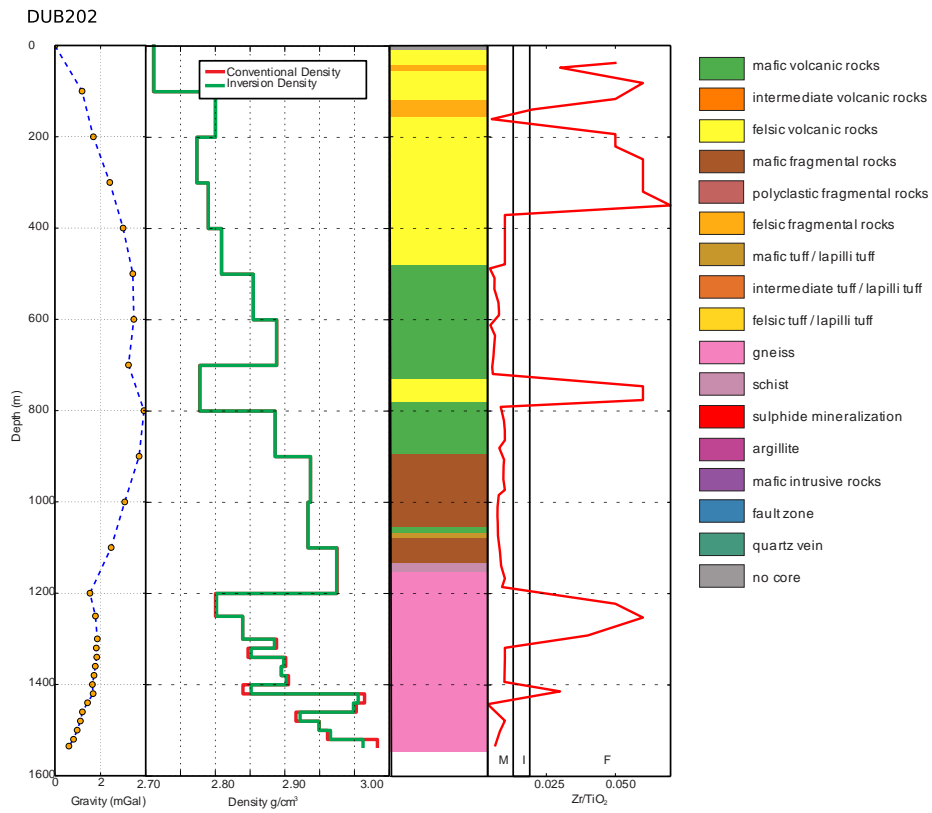


Figure 25. Bouguer, apparent density, lithofacies and Zr/TiO<sub>2</sub> logs of borehole DUB202.

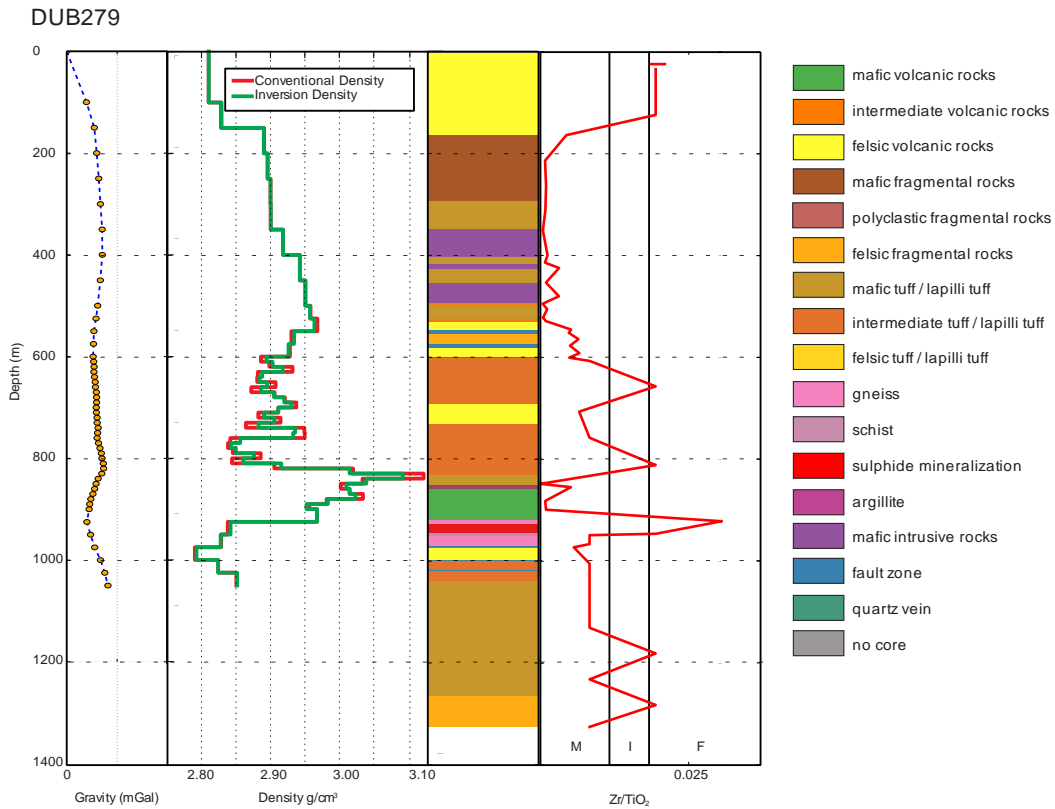
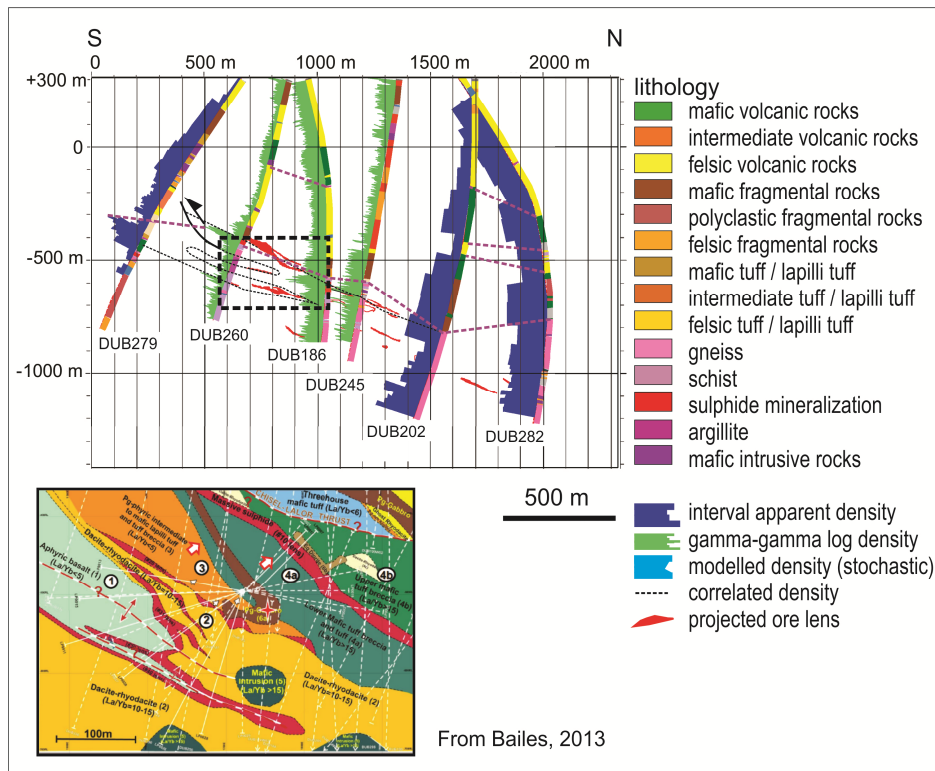


Figure 26. Bouguer, apparent density, lithofacies and Zr/TiO<sub>2</sub> logs of borehole DUB279.



**Figure 27.** NS-oriented section to interpret hole-to-hole correlation of apparent and gamma-gamma density anomalies (purple lines) with projections of lithofacies logs and 3D sulphide ore shell models; Inset shows detailed section of geological interpretation of underground mapping and geological interpretation of drill logs from Bailes (1993). This section shows S-vergent isoclinal syncline of the ore horizon (red colour) enveloping basalt in its core. See text for more details on the interpretation.

**Correlation of apparent density anomalies across the Lalor deposit**

A number of distinct apparent density anomalies of similar geological origin, such as the sharp decrease in density across the hanging wall and footwall of the Lalor ore zone, can be recognized in the gravity boreholes. In an attempt to correlate these anomalous features from hole to hole, the apparent density logs were together with their associated lithofacies logs projected on a NS-oriented vertical section (Figure 27). The projected gamma-gamma density logs of three drill holes and 3D models of the sulphide ore lenses were included on this section to facilitate correlating density signatures over the relative large distance between borehole DUB279 and the other four boreholes. Correlated apparent density anomalies on the sections are marked by purple lines, while associated hole-to-hole correlated lithofacies are marked by yellow lines. The overall conformable pattern and close spacing between these lines on both the NS- and EW-oriented sections shows that, overall, there is a good correlation between apparent density contrasts and geological units.

A distinct decrease in apparent density low between 750 to 1000 m depth can be correlated from borehole DUB282 to DUB202 on the northern extent of the NS-oriented section. This abrupt decrease marks the contact between mafic volcanic and volcanoclastic rocks in the hanging wall and gneiss and schist in the footwall of the massive sulphide

lenses of the Lalor deposit and can be traced along this contact to similar breaks in the gamma-gamma density logs of boreholes DUB186 and DUB245 (Figure 27). The highest peaks in the gamma-gamma density logs, just below the hanging wall - footwall contact, correspond to massive sulphide intersections in boreholes DUB260, DUB186. The spiked gamma-gamma density signature of these two boreholes is tentatively correlated with the highest amplitude in the apparent density log of borehole DUB279 (Figure 27). The apparent offset between this peak in DUB279 and the gamma-gamma density signature of DUB260 is readily explained by a geological structure which after restoration of its apparent displacement would align this peak with the projected massive sulphide ore zones on the section. This structure brings rocks intersected in the drill holes south of DUB279 over rocks intersected in DUB279 along a N-dipping structure with a displacement that is in agreement with the apparent offset between intervals of sulphide mineralization in holes DUB279 and DUB260 (Figure 27).

This structure has been previously recognized in underground geological mapping campaigns in which the ore zone is involved in S-vergent asymmetric isoclinal folds and possibly a N-dipping shear zone abruptly separating intensely hydrothermally-altered from unaltered volcanic rocks (Bailes *et al.*, 2013; Caté *et al.*, 2013). It is interesting to note that if the excess mass of 0.7 mT (spherical body) computed for the Bouguer anomaly at DUB279 is caused by

sulphide mineralization, this could suggest an up-plunge continuation of the main sulphide ore zone towards the S beyond current drilling extent.

### CONCLUSIONS

The gravity borehole data acquired in drill holes in the Lalor VMS mine camp display significant apparent density anomalies that can be correlated across the NS extent of the deposit. An apparent offset between the density anomaly patterns is consistent with fold and fault structures inferred in underground mapping campaigns juxtaposing contrasting intensities of alteration and different geological units. Most of the apparent density anomalies correspond to alternations of mafic and felsic volcanic rocks in the hanging wall and their hydrothermally-altered and metamorphosed equivalents in the footwall. There is a consistent spatial association between apparent density lows and Zr/TiO<sub>2</sub> peaks indicative of felsic volcanic rocks throughout the hanging- and footwall- successions, including rocks affected by intense hydrothermal alteration and metamorphism in the proximal footwall of the VMS ore zones. This is an important result, which suggests that the density contrasts between volcanic protoliths in metamorphosed hydrothermally-altered rocks (e.g. gneiss and schist) remain intact despite their intense hydrothermal alteration and subsequent metamorphic recrystallization. This finding also corroborates the analysis of compressional seismic velocity and density data from drill core samples that supported the interpretation of the 3D seismic cube (see section on physical rock properties) which shows that seismic impedance contrasts between rock units (i.e. gneiss /schist) with protoliths of felsic and mafic composition remain preserved.

# 3D STOCHASTIC INVERSION OF POTENTIAL FIELD DATA USING STRUCTURAL GEOLOGIC CONSTRAINTS

PEJMAN SHAMSIPOUR<sup>1</sup> AND ERNST SCHETSelaar<sup>1</sup>

<sup>1</sup> Geological Survey of Canada, 615 Booth Street, Ottawa, Ontario, K1A 0E9

## BACKGROUND

A variety of techniques have been utilized to invert potential field data (Oldenburg and Pratt, 2007). Most methods are under determined and have non-uniqueness properties, i.e., there are an infinite number of models that fit the geophysical observations. The purpose of any well-founded method is to provide a model that is consistent with all the available geophysical, petrophysical and geological information. Lelièvre and Oldenburg (2009) investigate options for incorporating structural orientation data into under determined inversions.

Herein, we propose a stochastic inversion method that integrates structural information data including bedding and foliation. The idea of this work originates from geostatistical interpolation approaches which add gradient information to the cokriging system (Lajaunie *et al.*, 1997; Chilès and Delfiner, 1999). We adapted this to stochastic inversion of potential field data introduced by Shamsipour *et al.* (2010). The algorithm is tested on a synthetic model consisting of a folded high density layer buried in a homogeneous background. The results illustrate the capability of the method in improving the reconstructed image of the subsurface. The method is applied on a case study in the Lalor area in Manitoba, Canada in order to

characterize the deposit and host environment by integrating seismic information and borehole data.

## SYNTHETIC EXAMPLE

The gravity data produced by a synthetic model consisting of a high density fold which is shown in Figure 28 (a) is calculated. The synthetic geological structure has a placed in a homogeneous background. The 3D domain is divided into  $20 \times 20 \times 15 = 6000$  with edge length of 1 m. We assume there is no noise in the gravity data, meaning  $C_0 = 0$ . We use the gravity data and inversion based on cokriging to estimate the density distribution. The result is shown in Figure 28 (b). The solution appears to be close to the surface rather than at the same depth as the real structure, as expected in unconstrained inversion. In order to improve the inversion result, we can use a few point pairs along an EW-oriented profile across the anticline, defining zero gradients of density. The inversion result using depth weighting and these point pair constraints is shown in Figure 28 (c). Note that the point pairs help to recover to some extent the shape of the anticline. In order to estimate the density values more closely to the actual values, we can assume that we have gradient information between one point in the folded layer and one point in the homogeneous background. The inversion result using point pairs and this known density

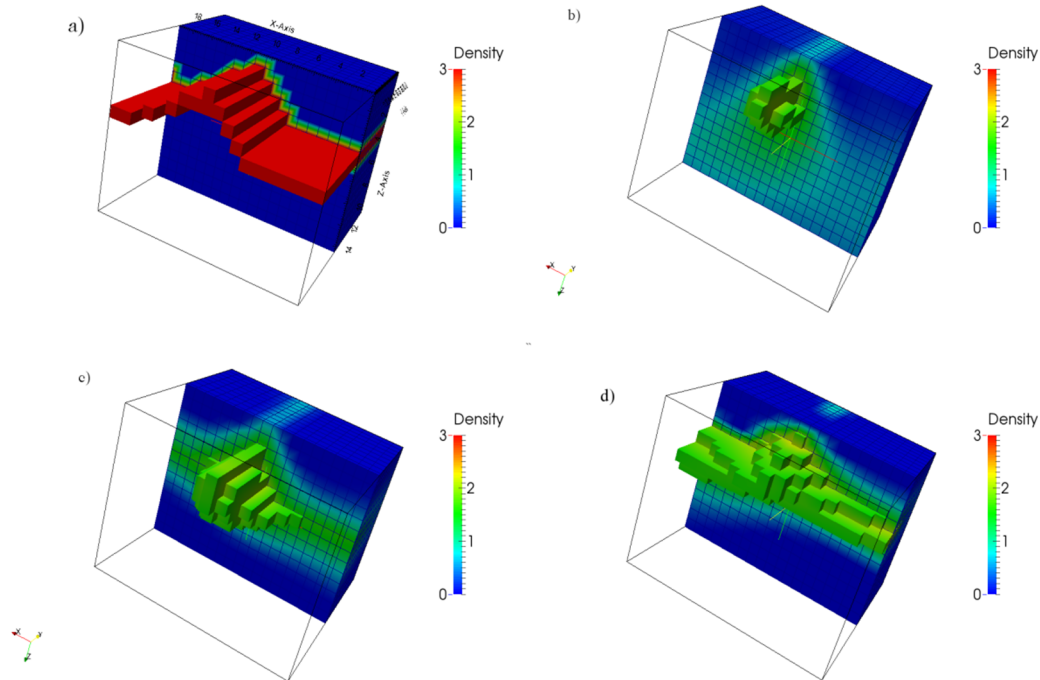


**Figure 28.** (a) Synthetic model, (b) Inverted data without constraints, (c) Inverted data using point pairs and depth weighting with  $b = 0.7$  and (d) Inverted data using point pairs and one known gradient. All the figures are shown at section  $y = 10,5$  m and the threshold is  $r > 1.5 \text{ g-cm}^3$ .

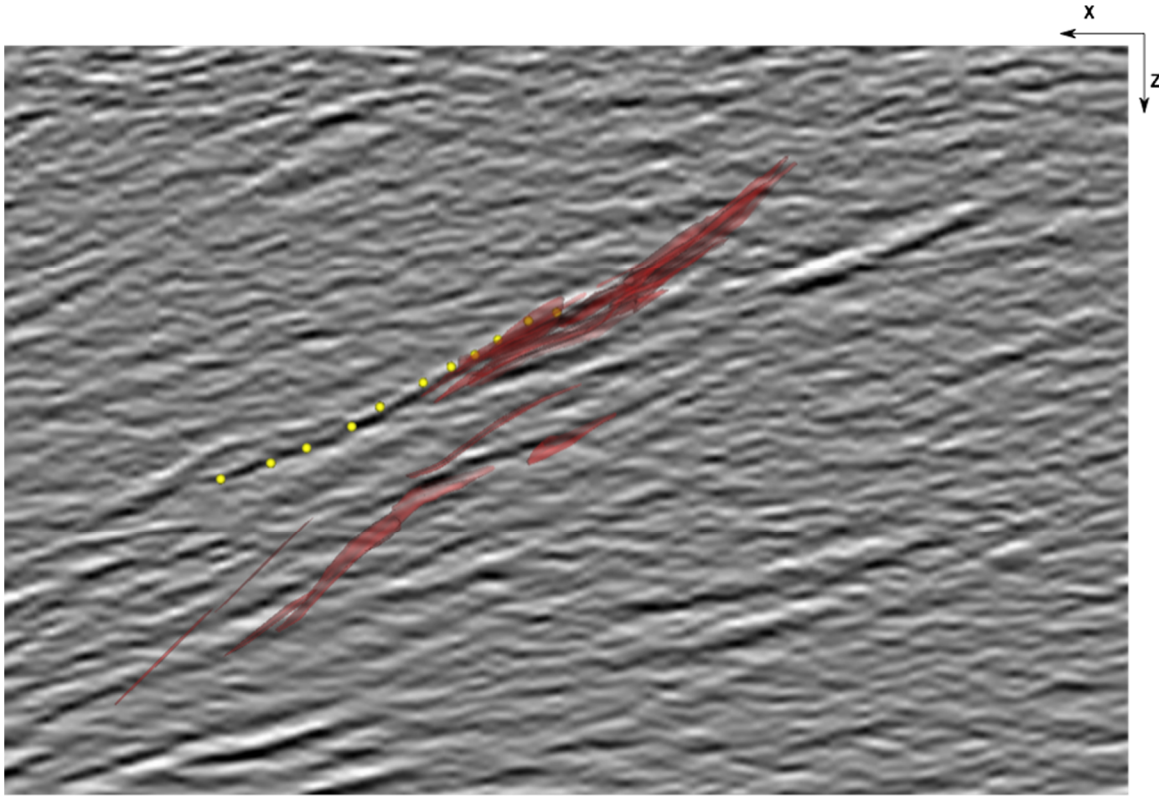


**Figure 29.** Seismic section from which 12 point pairs were extracted. The deposit is shown in red and point pair locations are in yellow.

gradient is shown in Figure 28 (d), the top showing a very clear resemblance to the initial synthetic model. All solutions shown in Figure 28 perfectly reproduce the gravity data as there were no observation errors in the gravity data.

#### CASE STUDY

As part of the TGI-4 program, the Geological Survey of Canada accessed geological, petrophysical, and geophysical data over the Lalor Lake volcanogenic massive sulphide (VMS) deposit at Snow Lake, Manitoba, Canada. The Lalor Lake deposit hosted in the Chisel Basin of the Flin Flon Greenstone Belt, 15 kilometres from the HudBay concentrator in Snow Lake in central Manitoba, Canada. The deposit is the largest volcanogenic massive sulphide (VMS) deposit in this region. In March 2007, an electromagnetic survey identified several large deep targets including the Lalor Lake VMS deposit. An exploration drill program on the Lalor Lake continued between 2007 and 2012. This extensive drilling program has determined three mineralization zones including a zinc zone, a gold zone and a gold-copper zone. The deep high grade gold at the gold-copper zone attracts extended exploration at greater depth (more than 1500 m). One objective of the TGI-4 program is to characterize the deposit and host environment by integrating all the available data including geochemistry, drillhole, lithological descriptions, borehole geophysical logging, electromagnetic data, surface potential field data, and a recently acquired 3D seismic data set. Borehole gravity data was also acquired in the first part of 2014.

The case study presented here is an application of our stochastic inversion approach using point pairs from seismic reflectors as structural constraints. In order to show the efficiency of the algorithm, we consider a simple scenario where only one part of the area is inverted and information from one borehole is used in the inversion.

In order to determine the point pairs, we use seismic reflectors of the VMS ore zone in a 3D seismic cube. Figure 29 shows the seismic section from which 12 point pairs (shown in yellow) were extracted to define structural gradient constraints. These points follow approximately the contact between hanging wall and foot wall rocks.

The inversion result with and without using point pairs is shown in Figure 30. Note that the use of structural constraints helps to recover the orientation of the deposit at depth which is in agreement with the seismic reflectors associated to the ore zone Figure 29. As we can see, using constraints helps to recover the orientation of the deposit at depth which is in agreement with results from 3D seismic.

#### DISCUSSION

The presented inversion algorithm allows adding structural orientation constraints to the stochastic inversion method. The algorithm is successful in recovering the structural orientations, particularly near the surface. At depth where the point pairs are the only constraints, they are not sufficient to recover exact orientations because of the low

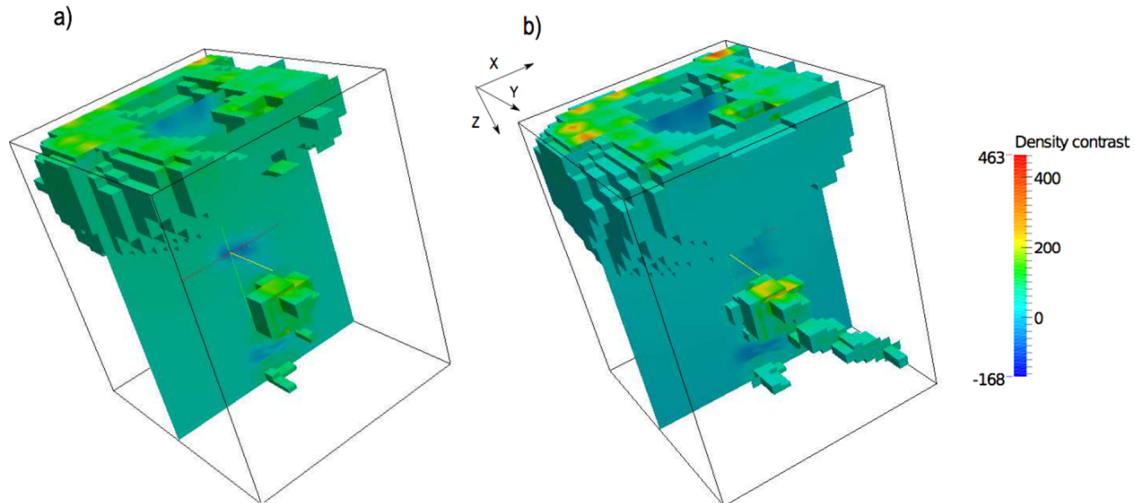


**Figure 30.** a) Inverted results without using point pairs and information of one borehole b) Inverted results data using point pairs obtained from seismic data and information of one borehole. Densities contrasts with threshold  $r > 22 \text{ Kg/m}^3$  are shown.

resolving power of inversion. This issue can be resolved by either adding depth weighting or applying known gradients from drillhole data.

At depth, inverted density contrasts tend to be close to zero. Thus adding point pairs at depth defining zero gradients cannot clearly help to recover the geological structure. However, addition of just a few points with known gradients can surprisingly help to recover the structural orientation. Such known gradients can be deduced from geological information or borehole data. Including the point pairs along the vertical axis (magnetic synthetic example) can also help to decrease the low resolution effect at depth.

Note that a practical difficulty of the method arises when the point pair is located in the immediate vicinity of true density constraints (e.g. from drill hole data) that are in conflict with the zero gradient defined by the point pair. In such situations the inversion produces singularities in the solution. Consequently, the user needs to assure that the point pairs chosen are not in conflict with hard density constraints.

### CONCLUSIONS

Integrating structural geologic constraints into geophysical inversions by incorporating point pairs that define structural gradients notably improves the recovered model and can easily be applied to any linear geophysical problem. This improvement is highlighted in potential field inversion where the recovered model suffers from the lack of resolution at depth. In addition to the synthetic example, promising results were obtained from the inversions of gravity data acquired over the Lalor VMS deposit, Flin Flon greenstone belt, Canada, in which zero-gradient point pairs were extracted from seismic reflectors.

## SUMMARY OF RESULTS AND IMPLICATIONS FOR EXPLORATION

GILLES BELLEFLEUR<sup>1</sup>, ERNST SCHETSELAAR<sup>1</sup>, AND JIM CRAVEN<sup>1</sup>

<sup>1</sup> Geological Survey of Canada, 615 Booth Street, Ottawa, Ontario, K1A 0E9

### GEOPHYSICAL PERSPECTIVE

Analysis of passive seismic data using ambient noise interferometry has received a lot of attention by the geophysical community in recent years, and is recognized as an important new research area (see Wapenaar *et al.*, 2002; Wapenaar 2004; Wapenaar *et al.* 2004, Draganov *et al.* 2007; Draganov *et al.*, 2013). Without the need for any sources, one of the primary benefits of the approach is the cost-effective acquisition of seismic data. However, the applicability of the method to the mining environment and potential difficulties related to the inherent geological complexity found in such environments needed to be determined. The analysis of the ambient noise data acquired over the Lalor Lake mine demonstrated the potential of the interferometry method for mineral exploration by generating geologically meaningful reflections. The underground mining activity and human activity at surface proved to be useful sources of ambient noise that could be used to generate virtual shot gathers and produced 3D seismic volumes with geologically-significant reflections. Comparison of the results with the 3D dynamite survey acquired at Lalor is encouraging even if, in general, results of the passive survey show fewer reflections. Most importantly, the analysis of the data led to new data processing ideas that may significantly improve the final seismic images made from passive recordings in mining areas.

Up to very recently, seismic exploration for mineral exploration utilized only P-wave energy reflected or scattered at mineralized bodies. Results from the analysis of VSP data acquired near the 777 deposit in Flin Flon demonstrate that other wave modes have a higher potential for the detection of massive sulphide orebodies. In particular, the strongest and most identifiable reflections on the VSP data are shear wave reflections (SS) and mode-converted reflections (PS). These waves are present on all three components of the VSP data and are stronger than the P-wave reflections (PP) typically used to generate images of the subsurface. The study also indicates that multi-component geophones are needed to properly measure all wave modes due to complex shape of the ore zones and their geometrical relationship with seismic sources placed at surface and receivers located in deviated boreholes. This work demonstrates that VSP can provide a means to image dense bodies in the subsurface, even in complex seismic environments.

A novel approach for integrating structural geologic constraints into 3D geophysical inversions has been established during this project. Constraints are easily incorporated using point pairs that define structural

gradients and notably improve the recovered model. The approach can be applied not only to potential field data, but to any linear geophysical problem. Improvement from this approach was demonstrated on the inversion of gravity field data acquired over the Lalor VMS deposit. Results from the inversion recovered the contact between the hanging wall and footwall with the addition of a limited number of zero-gradient point pairs extracted from seismic reflection data. The hanging wall-footwall contact, a significant horizon for exploration in the Snow Lake mining camp, cannot be recovered with unconstrained inversion of surface gravity data.

The borehole gravity measurements at Lalor proved to be useful to obtain density estimates at depth away from boreholes in areas where density could not be determined accurately from surface gravity measurements alone. For instance, density changes associated with the main units near the deposit could not be determined from surface gravity data whereas a sharp density decrease obtained from borehole gravity clearly marks the contact between mafic volcanic and volcanoclastic rocks in the hanging wall and gneiss and schist in the footwall of the massive sulphide lenses of the Lalor deposit. Thus, detailed knowledge on the spatial distribution of densities obtained from borehole gravity data can help to map key lithological units at depth in a mining area. In addition, another advantage of the borehole gravity method resides in its capacity to investigate excess of mass that could potentially be associated to mineralized bodies, especially near existing ore zones. At Lalor, an excess mass of 0.7 mT (spherical body) computed for the Bouguer anomaly at DUB279 suggests a possible up-plunge continuation of the main sulphide ore zone towards the South beyond current drilling extent. This density anomaly is located near an unexplained electromagnetic anomaly and has been identified as a potential follow-up drilling target.

### INTEGRATED PERSPECTIVE

One of the key results from the TGI4 method development project is the demonstration that seismic methods can map contacts between volcanic rocks with felsic and mafic protolith compositions near volcanogenic massive sulphide deposits affected by intense hydrothermal alteration and post-volcanic metamorphism. Felsic and mafic host rock lithologies, previously only identifiable through trace element geochemistry in the intensely altered and metamorphosed footwall of the Lalor VMS deposit, were linked to acoustic impedance contrasts and seismic reflections. This provides, in addition to direct detection of ore, a novel approach to map favourable subsurface host rocks using seismic data where visual interpretation of drill

logs would fail to unequivocally distinguish such compositionally-contrasting protoliths and in areas where no drill information exists. It is important to note here that this result could *only* be obtained by integrating geochemical, geological, petrophysical, and seismic data in a spatially collocated 3D common-earth model. In addition, it should be noted that intensely metamorphosed hydrothermal footwall alteration observed at Lalor is typical of most volcanogenic massive sulphide deposits in the Snow Lake mining district and other volcanogenic massive sulphide mining districts elsewhere (Galley *et al.*, 2007).

Knowledge on the location of mafic/felsic contacts in the most altered part of the footwall has implications for the understanding of the geological evolution near the deposit, and can also be used to guide exploration in the Snow Lake mining camp. As shown in this Open File, the shallowest reflection in the footwall corresponding to the contact between mafic-felsic protoliths is close to or at the hanging wall-footwall interface (F4 on Figures 10 and 12). Thus, this reflection is an excellent proxy for the hanging wall-footwall contact which is only partly imaged on the seismic data. The ability to follow the shallowest footwall contact in 3D is of *primary* importance for exploration in this mining camp as most of the deposits are found at or near the hanging wall-footwall contact. Here, the 3D model was key to establish the nature of the shallowest footwall reflection whereas the 3D seismic data allowed its mapping in areas with no borehole information. The location of this proxy reflection to the hanging wall-footwall contact is now

known for the 3D seismic area located north-east of the Lalor deposit.

The integration of densities obtained from borehole gravity data in the 3D geological model allowed to establish a consistent spatial association between apparent density lows and Zr/TiO<sub>2</sub> peaks indicative of felsic volcanic rocks throughout the hanging-wall and footwall successions. Similar to the 3D seismic data, this also includes rocks affected by intense hydrothermal alteration and metamorphism in the proximal footwall of the VMS ore zones. This important result indicates that the density contrasts between volcanic protoliths (e.g. gneiss and schist) remain intact despite their intense hydrothermal alteration and subsequent metamorphic recrystallization. In addition, offsets in the apparent density logs computed from the borehole gravity data supports the presence of a fault structure (see Figure 23). This structure brings rocks intersected in the drill holes south of DUB279 over rocks intersected in DUB279 with a displacement that is in agreement with the apparent offset between intervals of sulphide mineralization in holes DUB279 and DUB260 (Figure 23). The offset between the density anomaly patterns is also consistent with fold and fault structures inferred in underground mapping campaigns juxtaposing contrasting intensities of alteration and different geological units. The presence of this fault and its associated offset both have implication for exploration south of the main more zones at Lalor.

## ACKNOWLEDGMENTS

This project would not have been possible without the support of Hudbay. We thank P. Dueck, C. Taylor, T. Butt, T. Scheres, and all of Hudbay's staff at the Flin Flon exploration office and at the Lalor Mine site. We thank P. Mercier-Langevin, A. Caté, A. Bailes, C. Böhm and S. Gagné for the constructive discussions on the Lalor deposit and geology of the Snow Lake area. The 3C-3D seismic data for this work was acquired by SAExploration, Calgary, under the leadership of J. Mackie. We are grateful to SAExploration for folding our crews into their safety procedures and for retrieving our passive data recorders at the end of their active source survey. A prestack-time migrated volume of the Lalor 3D was processed by Sensor Geophysical. The GSR units used for passive seismic data recording were graciously provided by the Petroleum Technology Resource Center, and SaskPower provided support in Estevan, SK to aid in the harvesting of the data from the recorders. Geospace Technologies Inc. is thanked for their flexibility in accommodating the late return of two geophones. Abitibi Geophysics acquired the borehole gravity data at Lalor. M. Salisbury, R. Enkin, and N. el Goumi carefully measured physical rock properties on core samples. We thank BCGS, MGS, Hudbay, and KEGS for allowing us to present key results from this project at a series of Symposiums on the Lalor deposit. R. Wasylechko (Abitibi Geophysics) is thanked for his presentations on the acquisition of the borehole gravity data at those Symposiums. Data processing was done with Globe Claritas™. Finally, we thank Dave Snyder for thoughtful comments reviewing the manuscript.

## REFERENCES

- Adam, E., Perron, G., Arnold, G., Matthews, L., and Milkereit, B., 2003. 3D seismic imaging for VMS deposit exploration, Matagami, Quebec. In: *Hardrock seismic exploration*, (eds. D.W. Eaton, B. Milkereit, M.H. Salisbury) pp. 229–246, Society of Exploration Geophysicists.
- Bailes, A. H., and Galley, A. G., 1999. Evolution of the Paleoproterozoic Snow Lake arc assemblage and geodynamic setting for associated volcanic-hosted massive sulphide deposits, Flin Flon Belt, Manitoba, Canada. *Canadian Journal of Earth Science* 36, 1789–1805.
- Bailes, A. H. and Galley, A. G., 2007. Geology of the Chisel-Anderson lakes area, Snow Lake, Manitoba (NTS areas 63K16SW and west half of 63J13SE); Manitoba Science, Technology, Energy and Mines Manitoba Geological Survey, MAP Geoscientific map 2007-1, 1 colour map with accompanying notes, scale 1: 20 000.
- Bailes, A. 2012 Stratigraphic and structural controls on VMS mineralization in the Chisel-Ghost Lake Area: consulting Report for HudBay minerals Inc., November 2012, 62 p.
- Bailes, A., Rubingh, K., Gagné, S., Taylor, G., Galley, A., Bernauer, S., and Simms, D., 2013. Volcanological and structural setting of Paleoproterozoic VMS and gold deposit at Snow Lake, Manitoba. Geological Association of Canada-Mineralogical Association of Canada Joint Annual Meeting, Field Trip Guidebook FT-A2, Manitoba Innovation, Energy and Mines, Manitoba Geological Survey, Open File OF2013-3, 63 p.
- Bailes, A.H., 2013b. Logging notes for the 17 Lalor drill holes (unpublished report).
- Bailes, A. 2014a. Results from work in 2013-14 on the Lalor Lale Mine, unpublished powerpoint presentation, Geological Survey of Canada TGI progress meeting, 14 May 2014, Quebec, Canada.
- Bailes, A. 2014b. Regional geological setting of the Zn- and Au-rich Lalor VMS deposit, Snow Lake, Manitoba, Canada *in* Exploration for Deep VMS Ore bodies: the HudBay Lalor Case Study, 2014 Fall Symposium British Columbia Geophysical Society, 16-17 October, 2014, Vancouver. Program with Abstracts.
- Beaty, K.S., Perron, G., Kay, I., and Adam, E., 2002. DSISoft - A MATLAB VSP data processing package. *Computers & Geosciences* 28, 501–511.
- Bellefleur, G. and White, D., 2014. 3D-3C Seismic acquisition and data processing at the Lalor VMS deposit, Manitoba. Geological Survey of Canada, Open File 7548, 18 p., doi:10.4095/293613.
- Bellefleur, G., Schetselaar, E., White, D., Miah, K., and Dueck, P., 2015. 3D seismic imaging of the Lalor volcanogenic deposit, Manitoba, Canada. *Geophysical Prospecting* (in press).
- Blakely, R.J., 1996. *Potential Theory in Gravity and Magnetic Applications*, Cambridge University Press.
- Bohlen, T., De Nil, D., Köhn, D., and Jetschny, S., 2011. SOFI3D - seismic modeling with finite differences 3D - acoustic and viscoelastic version: users guide. Department of Physics, Geophysical Institute. Karlsruhe Institute of Technology, Karlsruhe, 72 pp.
- Boltz, M.S., Pankow, K.L. and McCarter, M.K, 2014. Fine Details of Mining-Induced Seismicity at the Trail Mountain Coal Mine Using Modified Hypocentral Relocation Techniques, *Bulletin of the Seismological Society of America*, 104, 193–203, doi: 10.1785/0120130011
- Carter, R., Schwartz, T., West, S., and Hoover, K., 2012. Pre-feasibility study technical report, on the Lalor deposit, Snow Lake, Manitoba, Canada. Hudbay Minerals internal report, 292 p.
- Caté, A., Mercier-Langevin, P., Ross, P.S., Duff, S., Hannington, M., Dubé, B., and Gagné, S., 2013. The Paleoproterozoic Lalor VMS deposit, Snow Lake, Manitoba: Observations on the nature and architecture of the gold and base metal-rich ore zones and associated alteration. Geological Survey of Canada, Open File Report 7483, 19 p., doi:10.4095/293116.
- Caté, A., Mercier-Langevin, P., Ross, P.S., Duff, S., Hannington, M., Gagné, S., and Dubé, B., 2014. Insight on the chemostratigraphy of the volcanic and intrusive rocks of the Lalor auriferous volcanogenic massive-sulphide deposit host succession, Snow Lake, Manitoba. Geological Survey of Canada, Current Research 2014-6, 19 p., doi:10.4095/295080.
- Caté, A, Mercier Langevin, P., Ross, P.-S. and Simms, D. 2014b. Structural controls on geometry and ore distribution in the Lalor auriferous VMS deposit, Snow Lake, west-central Manitoba (part of NTS 63K16): preliminary results from underground mapping *in* Report of Activities 2014, Manitoba

## REFERENCES

- mineral Resources, Manitoba geological Survey, p. 104-115.
- Caté, A., Mercier-Langevin, P., Ross, P.-S., Duff, S., Hannington, M., Dubé, B., and Gagné, S., 2015. Geology and gold enrichment processes at the Paleoproterozoic Lalor auriferous volcanogenic massive sulphide deposit, Snow Lake, Manitoba, *In: Targeted Geoscience Initiative 4: Contributions to the Understanding of Volcanogenic Massive Sulphide Deposits Genesis and Exploration Methods Development*, (eds) J.M. Peter and P. Mercier-Langevin; Geological Survey of Canada Open File
- Cheraghi, S., Malehmir, A., Bellefleur, G., 2012, 3D imaging challenges in steeply dipping mining structures: new lights on acquisition geometry and processing from the Brunswick No. 6 seismic data, Canada. *Geophysics*, 77 (5), WC109–WC122.
- Cheraghi, S., Craven, J.A., and Bellefleur, G., 2015. Feasibility of virtual source reflection seismology using interferometry for mineral exploration: A test study in the Lalor Lake VMS mining area, Manitoba, Canada. *Geophysical Prospecting*.
- Chilès, J. and Delfiner, P., 1999. *Geostatistics: modeling spatial uncertainty*. Wiley.
- Claerbout, J. F., 1968, Synthesis of a layered medium from its acoustic transmission response: *Geophysics*, 33, 264–269.
- Craven, J.A., Cheraghi, S., Roberts, B.J., Bellefleur, G., Schetselaar, E., Melanson, D., Bancroft, B. and Miah, K., 2014. Details and Preliminary Positive Evaluation of a Test Seismic Interferometry Survey at an Active VMS Mine Near Snow Lake, Manitoba, Geological Survey of Canada, Open File 7590, 30 p. doi:10.4095/293669
- David, J., Bailes, A.H., and Machado, N., 1996. Evolution of the Snow Lake portion of the Palaeoproterozoic Flin Flon and Kisseynew belts, Trans-Hudson Orogen, Manitoba, Canada. *Precambrian Research* 80, 107–124.
- Dieteker, B., and White, D.J., 2007. Flin Flon, Manitoba vertical seismic profile (VSP) survey 2006/2007: first processing of VSP near offset dynamite data. Internal Report: Seismology and Electromagnetism Section, Geological Survey of Canada, Ottawa, 216 pp.
- DiSiena, J.P., Gaiser, J.E., and Corrigan, D., 1984. Horizontal components and shear-wave analysis of three-component VSP data. In: *Vertical seismic profiling, part B: Advanced concepts*, (Eds. M.N. Toksoz, R.R. Stewart) pp. 177–189, Geophysical Press.
- Draganov, D., Campman, X., Thorbecke, J., Verdel, A., and Wapenaar, K., 2013. Seismic exploration-scale velocities and structure from ambient seismic noise (>1 Hz), *Journal of Geophysical Research B: Solid Earth*, 118, 4345 - 4360, doi: 10.1002/jgrb.50339.
- Draganov, D., Campman, X., Thorbecke, J., Verdel, A., and Wapenaar, K., 2009. Reflection images from ambient seismic noise, *Geophysics*, 74, 63–67.
- Draganov, D., Wapenaar, K., Mulder, W., Singer, J., and Verdel, A., 2007. Retrieval of reflections from seismic background-noise measurements, *Geophys. Res. Lett.*, 34, L04305, doi:10.1029/2006GL028735.
- Duff, S., Hannington, M., Caté, A., Mercier-Langevin, P., and Kjarsgaard, I.J., 2015. Major ore types of the Lalor auriferous volcanogenic massive sulphide deposit, Snow Lake, Manitoba, *In: Targeted Geoscience Initiative 4: Contributions to the Understanding of Volcanogenic Massive Sulphide Deposits Genesis and Exploration Methods Development*, (eds) J.M. Peter and P. Mercier-Langevin; Geological Survey of Canada Open File.
- Engelbert, M.S., Friesen, V., Gibson, H., Lafrance, B. 2014a. Volcanic reconstruction of the productive VMS ore interval in the Paleoproterozoic Chisel sequence. Snow Lake, Manitoba, Geological Association of Canada-Mineralogical Association of Canada, Joint Annual Meeting, Fredericton, May 20-22, 2014. Program with Abstracts, p. 83-84.
- Engelbert, M.S., Lafrance, B. and Gibson, H. 2014b. Structural and stratigraphic characterization of the Chisel Basin, Snow Lake Manitoba *in* Exploration for Deep VMS Ore bodies: the HudBay Lalor Case Study, 2014 Fall Symposium British Columbia Geophysical Society, 16-17 October, 2014, Vancouver. Program with Abstracts.
- Fowler, C.M.R., Stead, D., Pandit, B.I., Janser, B.W., Nisbet, E.G., and Nover, G., 2005. A database of physical properties of rocks from the Trans-Hudson Orogen, Canada. *Canadian Journal of Earth Sciences* 42, 555–572.
- Galley, A.G., Bailes, A.H. and Kitzler, G. 1993. Geological setting and hydrothermal evolution of the Chisel Lake and North Chisel Zn-Pb-Cu-Ag-Au massive sulfide deposits, Snow Lake, Manitoba; *Exploration and Mining Geology*, v. 2, no. 4, p. 271–295.

## REFERENCES

- Galley, A., Syme, E., and Bailes, A., 2007. Metallogeny of the Paleoproterozoic Flin Flon belt, Manitoba and Saskatchewan. In: *Mineral deposits of Canada: A synthesis of major deposit types, district metallogeny, the evolution of geological provinces, and exploration methods* (ed. W. Goodfellow) pp. 509-531, Geological Association of Canada, Mineral Deposits Division, Special Publication No. 5.
- Górszczyk, A., Malinowski, M., and Bellefleur, G., 2015. Application of 2D curvelet transform for denoising 3D seismic data acquired in hardrock environment. *Geophysical Prospecting*.
- Hammer, S., 1950. Density determinations by underground gravity measurements: *Geophysics*, 15, 637–652.
- Heinonen, S., Imaña, M., Snyder, D.B., Kukkonen, I.T., and Heikkinen, P.J., 2012. Seismic reflection profiling of the Pyhäsalmi VHMS-deposit: A complementary approach to the deep base metal exploration in Finland. *Geophysics* 77, WC15–WC23.
- Kraus, J., and Williams, P.F., 2000. Structural development of the Snow Lake allochthon and its role in the evolution of the southeastern Trans-Hudson Orogen in Manitoba, central Canada. *Canadian Journal of Earth Sciences* 36, 1881–1899.
- Lajaunie, C., Courrioux, G., and Manuel, L., 1997. Foliation fields and 3d cartography in geology: principles of a method based on potential interpolation. *Mathematical Geology*, 29(4), 571–584.
- LaFehr, T., 1983. Rock density from borehole gravity surveys: *Geophysics*, 48, 341–356.
- Lelièvre, P., and Oldenburg, D., 2009. A comprehensive study of including structural orientation information in geophysical inversions. *Geophysical Journal International*, 178 (2), 623–637.
- MacQueen, J. D., and LaCoste, M.G., 2007. High-resolution density from borehole gravity data: *SEG Technical Program Expanded Abstracts*, 1, 23–27.
- Malehmir, A., and Bellefleur, G., 2009. 3D seismic reflection imaging of VHMS deposits, Insights from reprocessing of the Halfmile Lake data, New Brunswick, Canada. *Geophysics* 74, B209–B219, doi: [10.1190/1.3230495](https://doi.org/10.1190/1.3230495).
- Malehmir, A., Durrheim, R., Bellefleur, G., Urosevic, M., Juhlin, C, White, D.J., Milkereit, B., and Campbell, G., 2012. Seismic methods in mineral exploration and mine planning: A general overview of past and present case histories and a look into the future. *Geophysics* 77, WC173–WC190.
- Malehmir, A., Andersson, M., Lebedev, M., Urosevic, M., and Mikhaltsevitch, V., 2013. Experimental estimation of velocities and anisotropy of a series of Swedish crystalline rocks and ore. *Geophysical Prospecting* 61, 153–167.
- Mallet, J. L., 2004. Space-time mathematical framework for sedimentary geology *Mathematical Geology*, 36, 1–32.
- Marcotte, D., and Chouteau, M., 1993. Gravity data transformation by kriging. In: *Geostatistics Troia92*. Springer, 249–260.
- McCulloh, T. H., 1965. A confirmation by gravity measure measurements of an underground density profile based on core densities: *Geophysics*, 30, 1108–1132.
- McCulloh, T., Lacoste, L.J.B., Schoellhamer, J.E., Pampeyan, E.H., 1967. The US geological survey Lacoste and Romberg precise borehole gravimeter system instrumentation and support equipment. U.S. Geological Survey professional paper, D92–D100.
- Mercier-Langevin, P., Caté, A., and Ross, P.-S., 2014. GS-7 Whole-rock oxygen-isotope mapping of the footwall alteration zones at the Lalor auriferous VMS deposit, Snow Lake, west-central Manitoba (NTS 63K16), In: *Report of Activities 2014; Manitoba Mineral Resources, Manitoba Geological Survey*, p. 94–103.
- Melanson, D.M., 2014. Identification of VMS ore lens reflections using vertical seismic profiling and 3D finite difference modeling in Flin Flon, Manitoba, Canada. M.Sc thesis, Carleton University, Ottawa, Ontario.
- Milkereit, B., Berrer, E.K., King, A.R., Watts, A.H., Roberts, B., Adam, E., Eaton, D.W., Wu, J., and Salisbury, M.H., 2000. Development of 3-D seismic exploration technology for deep nickel-copper deposits— A case history from the Sudbury basin, Canada. *Geophysics* 65, 1890–1899, doi:10.1190/1.1444873.
- Nind, C., Seigel, H.O., Chouteau, M., and B. Giroux, B., 2007. Development of a borehole gravimeter for mining applications: *First Break*, 25.
- Oldenburg, D., and Pratt, D., 2007. Geophysical inversion for mineral exploration: A decade of progress in

## REFERENCES

- theory and practice. *Proceedings of Exploration*, 5, 61–95.
- Popta, J. V., Heywood, J.M.T., Adams, S.J., and Bostock, D.R., 1990. Use of borehole gravimetry for reservoir characterization and fluid saturation monitoring. Presented at the European Petroleum Conference, Society of Petroleum Engineers. SPE 20896.
- Ramsay, J.G., 1967. *Folding and Fracturing of Rocks*. McGraw-Hill, New York (1967).
- Salisbury, M. H., Harvey, C.W., and Matthews, L., 2003. The acoustic properties of ores and host rocks in hardrock terranes. In: *Hardrock seismic exploration*, (eds. D.W. Eaton, B. Milkereit, M.H. Salisbury) pp. 9–19, Society of Exploration Geophysicists.
- Shamsipour, P., Marcotte, D., Chouteau, M. and Keating, P., 2010. 3D stochastic inversion of gravity data using cokriging and cosimulation. *Geophysics* 75, 11.
- Schetselaar, E., Pehrsson, S., Devine, C., Currie, M., White, D.J., and Malinowski, M., 2010. The Flin Flon 3D Knowledge Cube. Geological Survey of Canada Open File 6313, 35 pp.
- Schetselaar, E.M., 2013. Mapping the 3D lithofacies architecture of a VMS ore system on a curvilinear-faulted grid: A case study from the Flin Flon mining camp, Canada. *Ore Geology Review* 53, 261–275.
- Schetselaar, E., and Shamsipour, P., 2015. Interpretation of borehole gravity data of the Lalor volcanogenic massive sulphide deposit, Snow Lake, Manitoba. Interpretation (submitted).
- Skirrow, R.G., and Franklin, J.M., 1994. Silicification and metal leaching in subconcordant alteration zones beneath the Chisel Lake massive sulphide deposit, Snow Lake, Manitoba. *Economic Geology* 89, 31–50.
- Smith, N. J., 1950. The case for gravity data from boreholes: *Geophysics*, 15, 605–636.
- Snelling, P.E., Godin, L., and McKinnon, S.D., 2013. The role of geologic structure and stress in triggering remote seismicity in Creighton Mine, Sudbury, Canada, *International Journal of Rock Mechanics & Mining Sciences*, 58, 166–179.
- Tessier, A.C., and O'Donnell, J.J., 2001. Callinan / 777 deposit: compilation and target generation project. Internal Report: Hudson Bay Mining and Smelting Co, A.C. Tessier Consulting Geologist, Kingston, 154 pp.
- Valley, B., Milkereit, B., Pun, W., Pilz, M., Hutchinson, J., Delaloye, D., Madjdabadi, B. M., Dusseault, M., Thibodeau, D., Forsythe, A., 2012. Rock mass change monitoring in a sill pillar at Vale's Coleman mine (Sudbury, Canada). *Proceedings of the CMI*, 8p.
- White, D.J., Secord, D., and Malinowski, M., 2012. 3D seismic imaging of volcanogenic massive sulfide deposits in the Flin Flon mining camp, Canada: Part 1 - seismic results. *Geophysics* 77(5), WC47–WC58.
- Winchester, J.A., and Floyd, P.A., 1977. Geochemical discrimination of different magma series and their differentiation products using immobile elements. *Chemical Geology* 20, 325–343.